A NUCLEAR MAGNETIC RESONANCE SPECTROSCOPY STUDY OF THE SOLVENT DEPENDENCE OF THE BARRIER TO ROTATION IN N,N,N',N'-TETRAMETHYLTHIODICARBONIC DIAMIDE

A thesis presented in partial fulfilment of the
requirements for the degree of
Master of Science in Chemistry
at
Massey University

Lesley Marion Hughes

1977

ABSTRACT

Barriers to rotation were determined from variable-temperature nuclear magnetic resonance spectra. The computer program used to calculate the rotational rates was validated by obtaining results in good agreement with the literature values from studies carried out on neat N,N-dimethylcarbamic chloride. The barrier to rotation for N,N,N',N'-tetramethylthiodicarbonic diamide was measured in a variety of solvents and large variations in activation energy were observed (more than 40 kJ mol^{-1}). The free energies could be correlated with the dielectric constant, the dipole moment, the Hildebrand solubility parameter and the empirical polarity parameters E_T and Z. A linear plot of $\Delta H^{\neq}_{298}$ versus $\Delta S^{\neq}_{298}$ for different solvents was obtained.

Attempts to obtain other systems suitable for NMR study are reported.

ACKNOWLEDGEMENTS

I wish to thank my supervisors Dr. P.D. Buckley and Dr. K.W. Jolley for their help and advice during the study herein summarised. I also wish to thank Alan R. Furness for encouragement and advice and Mrs. J.R. Parry for typing this thesis and thus greatly easing its preparation.

TABLE OF CONTENTS

LIST OF TABLES

LIST OF FIGURES

LIST OF SYMBOLS

A,B	Sites which are not equivalent
$\underline{B},\underline{B}_o$	Constant magnetic fields
B_o	Magnitude of $\underline{B}_o$ along the z-axis
$\underline{B}_1$	Oscillating magnetic field
B_x,B_y,B_z	Components of $\underline{B}$ along the x, y, z axes
G	Complex magnetization
G_T	Defined as $\sum_n G_n$
G_n	Magnetization at site n
h	Plancks constant
$\hbar$	$h/2\pi$
I	Spin quantum number
$\underline{i},\underline{j},\underline{k}$	Unit vectors along the x, y, z axes
i	$\sqrt{-1}$
$\mathcal{I}m(G)$	The imaginary part of G
J_{nm}	The coupling constant between groups n and m
k_B	Boltzmann constant
k_n	Defined as $1/\tau_n$
$\underline{M}$	Magnetization of a collection of nuclei
M_o	The component of $\underline{M}_o$ along the z-axis
$M_x\ M_y\ M_z$	The components of $\underline{M}$ along the x, y, z axes
M_{zn}	M_z at site n
m_I	Momentum quantum number
m_{I-x}	A value of m_I
N_n	The number of nuclei at the nth energy level
$\underline{P}$	Angular momentum
P_z	The component of $\underline{P}$ along the z-axis
p_n	The mole fractional population at site n
T	Absolute temperature
T_1	Longitudinal relaxation time

T_2	Transverse relaxation time
T_{2n}	T_2 at site n
U	Energy
u,v	Components of $\underline{M}$ along x', y'
x', y'	Axes perpendicular to the z-axis and rotation at $-\omega$ rad s^{-1}
α	$1/T_2 + i(\omega_o - \omega)$
γ	Magnetogyric ratio
δ	$10^6 (\nu_i - \nu_{TMS})/\nu_{TMS}$; Hildebrand solubility parameter
ε	Dielectric constant
η	Viscosity
θ	Angle between $\underline{B}_o$ and $\underline{\mu}$
$\underline{\mu}$	Magnetic moment of a nucleus
μ_z	z component of $\underline{\mu}$
ν	Frequency of radiation in Hz
ν_o	Operating frequency of the spectrometer
ν_n	Resonance frequency of the nuclei at position n
ν_{obs}	Observed resonance frequency for a time-averaged peak
ν_{TMS}	Resonance frequency for TMS
σ_n	Shielding constant for the nth group of nuclei
σ_{TMS}	Shielding constant for TMS
$\underline{\tau}$	Torque
τ	Defined as $p_A \tau_B$ or $p_B \tau_A$
ω	Angular frequency in rad s^{-1}
ω_o	Defined as $\gamma B_o = 2\pi \nu_o$
ω_1	Defined as γB_1

SECTION 1

INTRODUCTION

1.1 DESCRIPTION OF NUCLEAR MAGNETIC RESONANCE

The first attempts to observe nuclear magnetic resonance (NMR) were made in 1942[1] but it was not until 1946 that resonance signals were actually seen[2,3]. Once the equipment used had become more sophisticated the theory behind the observed phenomena could be elaborated[4,5,6,7,8].

1.1.1 Angular Momentum

Amongst the properties of some isotopes is that of spin which is associated with angular momentum, $\underline{P}$. Angular momentum is a vector quantity with magnitude, $(h/2\pi)\sqrt{I(I+1)}$, and with a component in the z direction given by the expression

$$P_z = m_I \, h/2\pi \qquad 1\text{-}1$$

where I is the spin quantum number which may have values 0, $\frac{1}{2}$, 1, $\frac{3}{2}$, 2 ... and m_I can have values I, I-1, ... 0, ... -(I - 1), - I. Each isotope has a fixed value of I; for the proton, $I = \frac{1}{2}$.

1.1.2 The Resonance Frequency

Nuclei are charged and a spinning charge has an associated magnetic moment, $\underline{\mu}$, related to the angular momentum by the equation

$$\underline{\mu} = \gamma \underline{P}$$

where γ is called the magnetogyric ratio. In a constant uniform magnetic field, $\underline{B}_o$, aligned along the + z direction, the possible orientations of $\underline{\mu}$ (and hence of $\underline{P}$) become non-degenerate (Fig. 1-1) with energies given by

$$U = - \underline{\mu} \cdot \underline{B}_o = - \mu_z B_o \qquad 1\text{-}2$$

where μ_z is the component of $\underline{\mu}$ along the z axis and B_o is the magnitude

Figure 1-1:

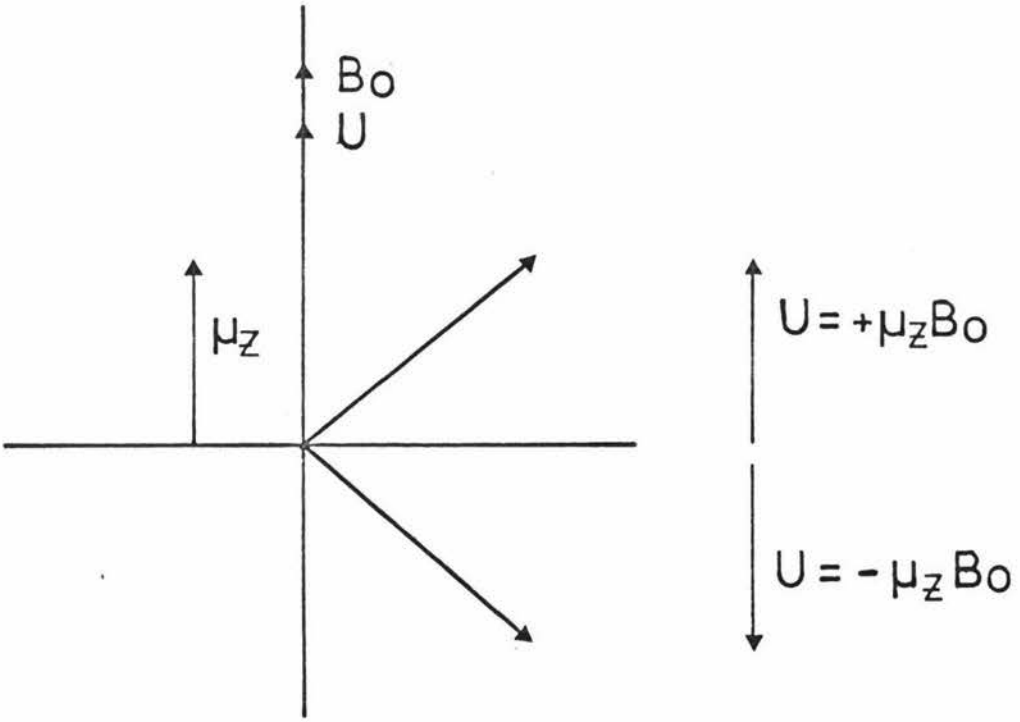

For $I = \frac{1}{2}$, there are two possible orientations of μ with an energy difference

$$\Delta U = 2 \mu_z B_o = \gamma \hbar B_o$$

of $\underline{B}_o$.

Since, for an isotope with even atomic and mass numbers, I = 0, this nucleus does not have spin and is unaffected by the applied magnetic field, it cannot be detected in the nuclear magnetic resonance experiment. Such nuclei include ^{12}C, ^{16}O, ^{28}Si and ^{32}S.

The energy difference, ΔU, between the nth and mth orientations in the magnetic field is

$$\Delta U = U_n - U_m = - (\mu_{zn} - \mu_{zm}) B_o$$

but $\mu_z = \gamma h m_I$

so $U = |\gamma h B_o \Delta m_I|$

where $\Delta m_I = m_n - m_m$

Only transitions between m_n and either m_{n-1} or m_{n+1} are allowed so

$$\Delta m_I = \pm 1$$

and if ν is the frequency of the radiation for such a transition then

$$\Delta U = h\nu = |\gamma h B_o| \qquad 1\text{-}3$$

or

$$\nu = |\gamma/2\pi| B_o \qquad 1\text{-}4$$

1.1.3 Chemical Shifts

If the magnetic environment of a nucleus is not exactly B_o, the applied field, then the frequency which induces resonance will not be $\nu_o = \left|\frac{\gamma}{2\pi}\right| B_o$ but $\nu = \nu_o \pm \Delta$. Such a variation in the local field of a nucleus occurs when neighbouring electrons shield the nucleus from the applied field B_o. Since the electronic environment differs for each group of similar nuclei it is found that for example the resonance signal of a methyl group (CH_3-) is at a different position from that of a methylene group (-CH_2-). This variation is usually expressed as

$$\nu_j = |\gamma/2\pi| B_o (1 - \sigma_j)$$

where σ_j is the shielding constant for the jth group of nuclei.

Since the separation of resonance signals varies with the strength of B_o, the absorption peaks are usually expressed in parts per million (ppm) as $\sigma_j = {}^{\nu_j}/_{\nu_o}$ where ν_o is the operating frequency of the

spectrometer. Unfortunately ν_0 cannot usually be measured accurately because of difficulty in measuring B_0 so often a standard sample is selected and ν_j is measured in ppm from the standard signal. The usual standard in proton NMR is tetramethyl silane (TMS) which contains a single environment for all its protons and resonates at high field from most other proton signals. The values in ppm referenced to TMS are said to be on the δ scale and are defined as

$$\delta = 10^6 \, (\nu_j - \nu_{TMS})/\nu_{TMS} \text{ at constant } B_0 \qquad 1\text{-}5$$

or $$\delta \simeq 10^6 \, (\delta_{TMS} - \delta_j)$$

1.1.4 Internuclear Coupling

The electronic environment, and hence the shielding of the proton, is affected not only by the nature of the group of which it is a part but by neighbouring groups. If the neighbouring group has n protons and as each proton has two possible orientations in the applied magnetic field, the number of possible combinations of spins is n + 1. In the simplest case (referred to as a first order spectrum) the proton may experience a magnetic field due to any one of these combinations and so, for the whole sample, the total absorption peak is split into n + 1 lines with equal separation. The relative intensities of the lines are given by the binomial coefficients (as found in Pascal's triangle).

This interaction is known as spin-spin coupling. Its magnitude is determined by a spin-spin coupling constant (simply referred to as a coupling constant) written as J_{nm} for interaction between spins n and m.

This type of spectral analysis can only be used if $\Delta\nu_{nm} \gg J_{nm}$; in any other case a full quantum mechanical analysis is required to determine chemical shifts and coupling constants.

1.1.5 Exchange-induced Variations in Spectra

Once multiple peaks for a group had been observed[7,8], it was found that the expected splitting in absorption signals was not always apparent.[9]

The lack of coupling was explained by postulating that fast exchange was occurring between several non-equivalent sites so the exchanging nuclei were decoupled from their neighbours whose resonance signals were therefore unsplit.

In most cases the rate of exchange was so fast that only a time-averaged peak was seen at a position ν_{obs} which can be related to the peak positions ν_A and ν_B of the separate sites A and B thus:

$$\nu_{obs} = p_A \nu_A + (1 - p_A)\nu_B = \nu_B + p_A(\nu_B - \nu_A) \qquad 1\text{-}6$$

where p_A is the mole fraction of nuclei at site A.

In some cases at room temperature the peaks at positions ν_A and ν_B are apparent but for intermediate rates of exchange between the two sites the spectrum changes in a regular manner from the slow exchange spectrum with peaks at ν_A and ν_B (for lower temperatures) to the time-averaged peak at ν_{obs} for higher temperatures[10].

1.2 QUANTITATIVE APPROACH TO NMR

The first step in quantitatively describing the observed temperature dependence of the NMR spectrum was to develop a set of equations which would fit the line-shape for a temperature-independent spectrum. These equations were developed, for a simple system, from classical physics but are consistent with quantum mechanical descriptions.

1.2.1 Classical Derivation of the Bloch Equations

If a spinning particle has a magnetic moment $\underline{\mu}$ then, in a uniform external magnetic field $\underline{B}$, a torque $\underline{\tau}$ is exerted on the particle, tending to align $\underline{\mu}$ with $\underline{B}$.

$$\underline{\tau} = \underline{\mu} \wedge \underline{B}$$

Such a torque, combined with the spin, results in the precession of $\underline{\mu}$ about $\underline{B}$ (Fig. 1-2) which can be analysed in terms of angular momentum $\underline{P}$:

Figure 1-2 :

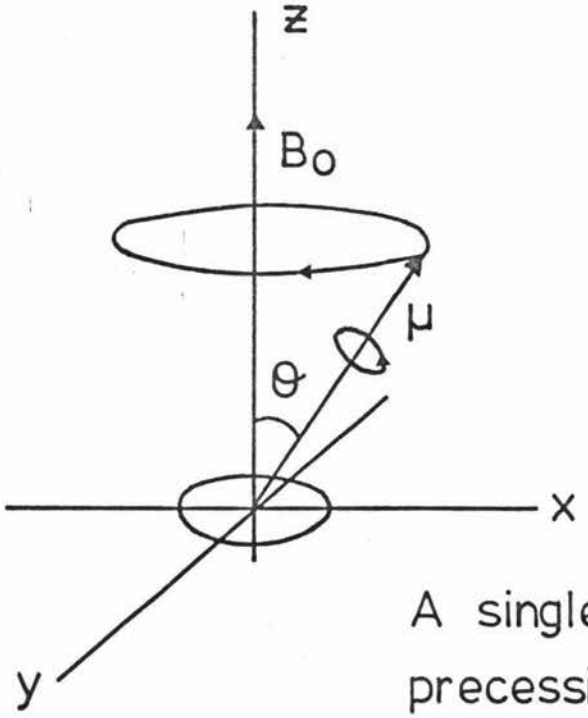

A single dipole precessing about B_o

Figure 1-3:

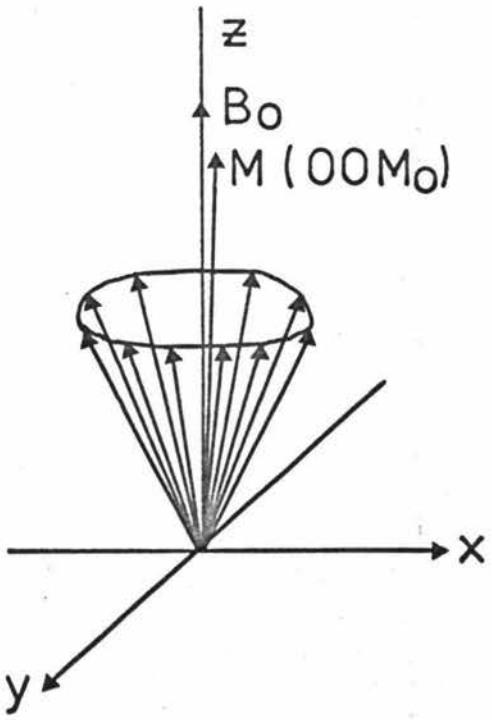

A random collection of nuclei precessing about an external magnetic field B_o along the +z axis

$$\frac{d}{dt}\underline{P} = \underline{\tau} = \underline{\mu} \wedge \underline{B}$$

But $$\underline{\mu} = \gamma \underline{P}$$

So $$\frac{d}{dt}\underline{\mu} = \gamma \frac{d}{dt}\underline{P} = \gamma (\underline{\mu} \wedge \underline{B}) = -\gamma (\underline{B} \wedge \underline{\mu})$$

Since ω_o, the angular velocity of precession, is given by

$$\frac{d}{dt}\underline{P} = \underline{P}\,\omega_o$$

$$\underline{\mu}\,\omega_o = -\gamma (\underline{B} \wedge \mu)$$

or $$\omega_o = |\gamma B|$$

Since $\omega_o = 2\pi\,\nu_o$ this becomes

$$\nu_o = |\gamma/2\pi|\ B$$

This equation was developed from a quantum mechanical basis earlier (see equation 1-4).

In a random collection of nuclei precessing at the same angle, each nucleus has a different phase so that the total magnetic moment (or magnetisation) of the collection, $\underline{M}$, has only a component in the z direction when the collection is in a constant magnetic field $\underline{B}_o$ aligned along the z direction (Fig. 1-3). If the external field varies then $\underline{M}$ will also have components in the xy plane. In the usual continuous wave NMR experiment an oscillating field, 2B, cos t, is applied along the x-axis. Such a field can be regarded as being the sum of two fields, ($B_1 \cos\omega t$, $-B_1 \sin\omega t$, 0) and $B_1 \cos\omega t$, $B_1 \sin\omega t$, 0), counter-rotating about the z axis in the xy plane (Fig. 1-4). Only one of these fields is rotating in the same direction as the precessing moments so only this field ($B_1 \cos\omega t$, $-B_1 \sin\omega t$, 0) can affect the magnetisation $\underline{M}$. The frequency of the applied field, ω , must be that of the precessing moments or the torsional effects at $\omega_o - \omega$ will cancel out those effects at $180 + \omega_o - \omega$ (Fig. 1-5).

The general equations for $\underline{M}$ are

$$\underline{M} = M_x\,\underline{i} + M_y\,\underline{j} + M_z\,\underline{k} \qquad 1\text{-}7a$$

$$\frac{d}{dt}\underline{M} = \left(\frac{d}{dt}M_x\right)\underline{i} + \left(\frac{d}{dt}M_y\right)\underline{j} + \left(\frac{d}{dt}M_z\right)\underline{k} \qquad 1\text{-}7b$$

Figure 1-4:

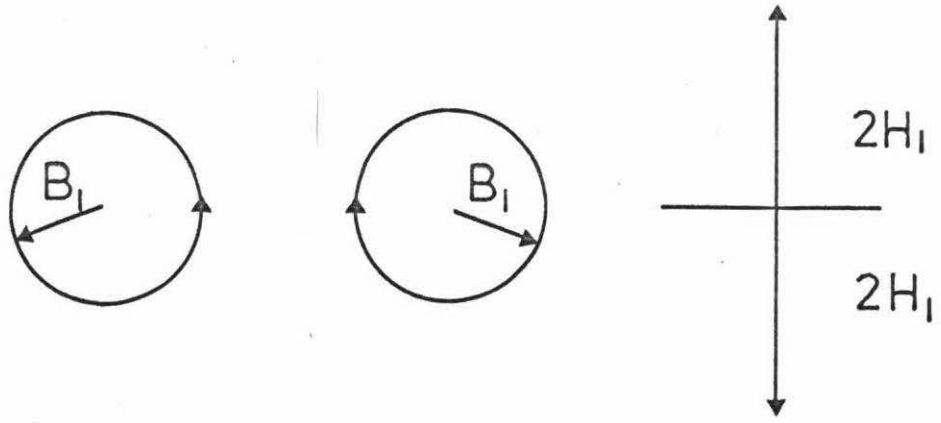

The oscillating magnetic field separated into rotational components

Figure 1-5:

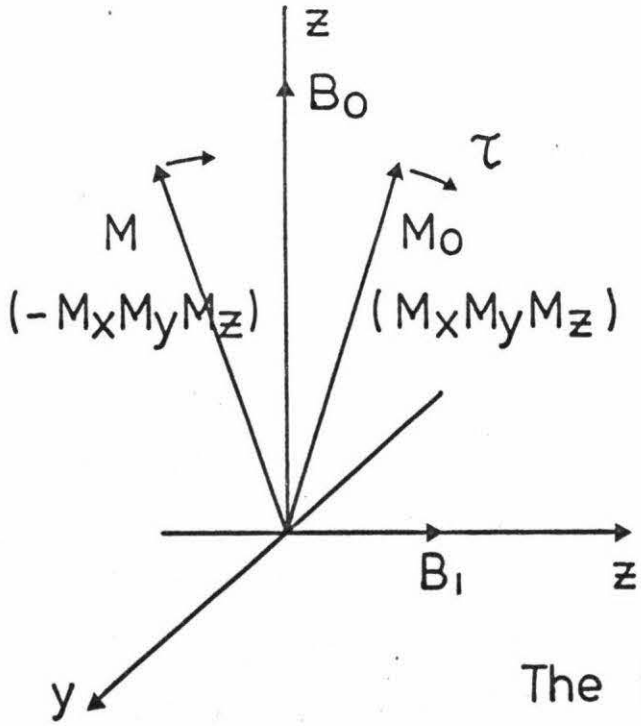

The torque exerted on a dipole by a magnetic field B_1 along the +x axis

If the oscillating field $2B_1 \cos \omega t$ is suddenly switched off then the components (M_x, M_y, M_z) of $\underline{M}$, which are non-zero in the field $\underline{B}$ ($B_1 \cos \omega t$, $-B_1 \sin \omega t$, B_o) will revert to the equilibrium values found in the field $\underline{B}$ ($0,0,B_o$) which were earlier given as $\underline{M}(0, 0, M_o)$. The time constants which govern the exponential decay of M_x, M_y and M_z to their equilibrium values are known as relaxation times. The time constants for the decay of M_x and M_y are assumed to be the same and are called the transverse relaxation time or the spin-spin relaxation time (since the interactions between nuclear spins can relax M_x and M_y without transferring energy to the lattice) and are given the symbol T_2. The time constant for M_z is called the longitudinal relaxation time (since M_z is parallel to the constant field B_o) or the spin-lattice relaxation time (since the energy flow associated with relaxation of M_z is from the nuclear spin system to the lattice) and given the symbol T_1.

The equations governing relaxation are:

$$\frac{d}{dt} M_x = - M_x/T_2 \qquad 1\text{-}8a$$

$$\frac{d}{dt} M_y = - M_y/T_2 \qquad 1\text{-}8b$$

$$\frac{d}{dt} M_z = - (M_z - M_o)/T_1 \qquad 1\text{-}8c$$

Since $\underline{M}$ is the resultant of the collection of magnetic moments it must obey the same type of equation for variation with time as $\underline{\mu}$. Hence

$$\frac{d}{dt} \underline{M} = - \gamma (\underline{B} \wedge \underline{M})$$

$$= - \begin{vmatrix} B_x & M_x & \underline{i} \\ B_y & M_y & \underline{j} \\ B_z & M_z & \underline{k} \end{vmatrix}$$

$$= - \gamma (B_y M_z - B_z M_y) \underline{i} - \gamma (-B_x M_z - B_z M_x) \underline{j} - \gamma (B_x M_y - B_y M_x) \underline{k}$$

When both the oscillating field in the xy plane and the constant field in the z direction are applied

$$\underline{B} = (B_1 \cos \omega t, - B_1 \sin \omega t, B_o)$$

so if the decay terms are also included, the equations controlling the variation of the x, y and z components of the magnetisation with respect to time are given by:

$$\frac{d}{dt} M_x = -\gamma(- B_1 \sin\omega t\, M_z - B_o M_y) - M_x/T_2 \qquad 1\text{-}9a$$

$$\frac{d}{dt} M_y = -\gamma(B_o M_x - B_1 \cos\omega t\, M_z) - M_y/T_2 \qquad 1\text{-}9b$$

$$\frac{d}{dt} M_z = -\gamma(B_1 \cos\omega t\, M_y + B_1 \sin\omega t\, M_x) - (M_z - M_o)/T_1 \qquad 1\text{-}9c$$

These equations can be simplified by transferring to axes x^1, y^1, z which rotate at an angular frequency $-\omega$ in the xy plane. u, the component of $\underline{M}$ along x^1 and v, the component of $\underline{M}$ along y^1, can be related to the components of the magnetisation along the stationary axes thus:

$$u = M_x \cos(-\omega t) + M_y \sin(-\omega t) = M_x \cos\omega t - M_y \sin\omega t$$

$$v = -M_x \sin(-\omega t) + M_y \cos(-\omega t) = M_x \sin\omega t + M_y \cos\omega t$$

Equation 1-9 then becomes, in the new coordinate system (if $\gamma B_o = \omega_o$)

$$\frac{d}{dt} u = -(\omega - \omega_o) v - u/T_2 \qquad 1\text{-}10a$$

$$\frac{d}{dt} v = (\omega - \omega_o) u + B_1 M_z - v/T_2 \qquad 1\text{-}10b$$

$$\frac{d}{dt} M_z = -\gamma B_1 v - (M_z - M_o)/T_1 \qquad 1\text{-}10c$$

These are the Bloch equations[11,12].

The NMR spectrometer can be set up to observe either the in-phase component of the magnetisation, u (this is called the dispersion mode), or the out-of-phase component of the magnetisation, v (this is called the absorption mode).

1.2.2 Line Shapes and Saturation

For the usual continuous wave NMR experiment it can be assumed that to a close approximation

$$\frac{d}{dt} u = 0 \qquad \frac{d}{dt} v = 0 \qquad \frac{d}{dt} M_z = 0$$

With these conditions the Bloch equations can be solved to give the following expressions for u and v:

$$u = \gamma B_1 M_o T_2^2 (\omega_o - \omega) / [T_2^2 (\omega_o - \omega)^2 + \gamma^2 B_1^2 T_2 T_1 + 1] \qquad 1\text{-}11a$$

$$v = \gamma B_1 M_o T_2 / [T_2^2 (\omega_o - \omega)^2 + \gamma^2 B_1^2 T_2 T_1 + 1] \qquad 1\text{-}11b$$

$$M_z = M_o [T_2^2 (\omega_o - \omega)^2 + 1] / [T_2^2 (\omega_o - \omega)^2 + \gamma^2 B_1^2 T_2 T_1 + 1] \qquad 1\text{-}11c$$

The NMR experiment depends on the unequal populations of the two spin states available, the low energy state being more populated. For a thermally equilibrated Boltzmann distribution of nuclei in the two energy states:

$$N_2/N_1 = \exp(-\Delta U/k_B T)$$

where N_1 and N_2 are the populations of the low and high energy levels respectively

k_B is the Boltzmann constant

T is the absolute temperature

and ΔU is the energy level separation given by

$$\Delta U = 2\mu B_o$$

so $$N_2/N_1 = \exp(-2\mu B_o/k_B T) \qquad 1\text{-}12$$

and since $2\mu B_o/k_B T$ is small

$$N_2/N_1 = 1 - (2\mu B_o/k_B T)$$

The excess population in the lower state is

$$(N_1 - N_2)/N_1 = 2\mu B_o/k_B T$$

so when T = 291 K and B_o = 1 T then

$$(N_1 - N_2)/N_1 = 7 \times 10^{-6}$$

For every million nuclei in the lower energy level there are seven less nuclei in the upper energy level.

This excess population in the lower energy level absorbs energy from the radiofrequency field which excites some nuclei sufficiently to transfer them to the higher level. A strong radiofrequency field can

rapidly equalise the populations of the two levels thus reducing the height of the observed peak to zero. The reduction of the excess population by intense applied magnetic fields is called saturation and is one of the main operational problems in obtaining spectra suitable for lineshape analysis.

From the equation 1-12, the larger the magnetic field the greater is the excess population and the more widely spaced are the energy levels so, if the field is increased, saturation becomes less of a problem. The problem arises because the relaxation rate of nuclei is governed by the longitudinal relaxation time T_1 which may be of the order of 10^{-3} sec to 10 sec for liquids so, if the field B_1 is of sufficient intensity, the excess population of the lower level quickly reaches zero and the absorption signal is diminished or absent. In terms of the absorption line shape (equation 1-11) B_1 is sufficiently large that the term $\gamma^2 B_1^2 T_2 T_1$ is no longer much less than one so the height of the absorption peak decreases while the width of the peak increases[10].

1.2.3 Exchange Between Two Sites and the Absorption Lineshape

The equations for u and v (or for M_x and M_y) may be combined to give G, the complex magnetisation, which is defined as

$$G = u + iv \qquad 1\text{-}13a$$

Hence
$$\frac{d}{dt} G = \frac{d}{dt} u + i \frac{d}{dt} v \qquad 1\text{-}13b$$

Substituting from equation 1-10

$$\frac{d}{dt} G = -i(\omega_o - \omega)(u + iv) - (u + iv)/T_2 - i\omega_1 M_z$$

$$= -\alpha G + i \omega_1 M_z$$

where $\omega_1 = \gamma B_1$

and $\alpha = 1/T_2 + i(\omega_o - \omega)$.

Under steady state conditions $\frac{d}{dt} G = 0$

so $G = i\omega M_z/\alpha$ but since $M_z \simeq M_o$

$$G = i\omega M_o/\alpha$$

therefore $v = \mathcal{J}_m(G) = \omega_1 M_o T_2/(1 + T_2^2(\omega_o - \omega)^2)$

where $\mathcal{J}_m(G)$ is the imaginary part of G.

In a series of papers, Gutowsky and co-workers[9,13,14] and other groups[15,16] developed complete lineshape equations for the exchange of nuclei between two non-equivalent sites (with and without coupling) from the Bloch equations. The following treatment, however, is that of McConnell[17].

The jump of a nucleus from site A to site B and back again if τ_n (n = A, B) is the lifetime in site n and k_n the rate constant for exchange from site n, is equal to $1/\tau_n$ has the following effects on M, the magnetisation:

it decreases M at site A by $k_A G_A$

it increases M at site B by $k_A G_A$

it decreases M at site B by $k_B G_B$

it increases M at site A by $k_B G_B$

The magnetisation at sites A and B will therefore change according to equation 1-13B which, with the appropriate additional terms included gives the following equations:

$$\frac{d}{dt} G_A + \alpha_A G_A = i\omega_1 M_{zA} + k_B G_B - k_A G_A \qquad 1\text{-}14a$$

$$\frac{d}{dt} G_B + \alpha_B G_B = i\omega_1 M_{zB} + k_A G_A - k_B G_B \qquad 1\text{-}14b$$

Under steady state conditions

$$M_{zn} \simeq M_{on} = p_n M_o \quad \text{and} \quad \frac{d}{dt} G_n = 0 \quad \text{for} \quad n = A, B$$

If equations 1-14a and 1-14b are solved with the appropriate substitutions for M_{zn} then the total complex magnetisation G_T (defined as $G_A + B_B$) is given by the expression

$$G_T = \frac{i\omega_1 M_o \{\tau_A + \tau_B + \tau_A\tau_B(p_A\alpha_B + p_B\alpha_A)\}}{\{(\alpha_A\tau_A + 1)(\alpha_B\tau_B + 1) - 1\}} \qquad 1\text{-}15$$

where $$\alpha_n = + \frac{1}{T_{2n}} + i(\omega_o - \omega)$$

Since this exchange is between two sites the population at each site is related to the lifetime of the nuclei at that site of equilibrium:

i.e. $k_A p_A = k_B p_B$ or $p_A \tau_B = p_B \tau_A = \tau$ 1-16

Hence the absorption signal can be calculated from the imaginary parts of G according to the equation

$$v = \mathcal{J}_m(G) = \mathcal{J}_m \frac{i\omega_1 M_o\{\tau_A + \tau_B + \tau_A\tau_B(p_A\alpha_B + p_B\alpha_A)\}}{\{(\alpha_A\tau_A - 1)(\alpha_B\tau_B - 1) - 1\}} \qquad 1\text{-}17$$

if the quantities τ, p_A, p_B, T_{2A}, T_{2B}, ν_A, ν_B are given. It is also possible to specify set values for all parameters but τ and to vary τ by increments to obtain the closest possible match to an experimental spectrum. The quantities T_{2A}, T_{2B}, ν_A and ν_B are usually determined in the slow exchange limit when $\tau = \infty$.

This equation for the absorption lineshape has been derived by assuming that the signals in the low temperature limit are from a first order spectrum. If the spectrum is not first order then a density matrix approach should be used if a rigorous treatment is required[18].

1.2.4 Use of the Rate Constant

Once τ at each temperature is known then the Arrhenius equation can be used to find the activation energy E_a since

$$1/\tau = k = A \exp(-E_a/k_T) \qquad 1\text{-}18$$

where R is the gas constant

T is the absolute temperature

or the equation derived from transition state theory can be used.

$$1/\tau = k = k_B T/h \exp - (\Delta G^{\neq}/RT) \qquad 1\text{-}19$$

where k_B is the Boltzmann constant

T is the absolute temperature

h is Planck's constant

$\Delta G^{\neq}$ is the free energy difference of the transition state from the ground state

R is the gas constant

and $$\Delta G^{\neq} = \Delta H^{\neq} - T \Delta S^{\neq} \qquad 1\text{-}20$$

Since the full lineshape equation was very tedious to apply, the equation has at times been simplified to use such parameters as the intensity ratio of a maximum to the central minimum[19], the width of the peaks at half height both above[20] and below[21,22] the temperature at which the peaks coalesce, and the peak separation[14] to find a value for k at a specific temperature. The results obtained depended on the careful use of the simplified equations in the regions where the approximations made in their derivations are valid. If the equations were used outside this region the results were unreliable and led to discrepancies between the values quoted by different research groups.

By the time such disagreements in the magnitude of thermodynamic parameters had been well documented high speed computers were widely available so the full lineshape treatment could be used on systems such as the amides and selectively deuterated analogues which fulfilled the requirements of the Bloch lineshape equation that the spectrum in the slow exchange limit be first-order. As the number of total lineshape studies increased the agreement between the data from different research groups improved to the stage where external limitations on the accuracy of temperature, T_2 and position measurements were of greater importance in the determination of errors than the approximations used. Some approximations were made in cases such as formamide and acetamide[23] where coupling between the carbon-methyl group or proton and the nitrogen methyl groups could affect the relative intensity of the peaks, but in other cases such coupling is incorporated into the computer program[24].

The limitations of the absorption lineshape for two site exchange led to the generalization for first order exchange spectra of the Kubo Sack matrix approach[25] but for more complex spectra the most accurate possible description is given by the density matrix method[26,27]. At present lineshapes are analysed by the simplest possible method which will accurately describe the system so all three lineshape descriptions may be considered depending on the complexity of the spin system being studied.

1.2.5 Thermodynamic Parameters for Amide Systems

Many amides have been extensively studied by lineshape analysis in various solvents. In Table 1-1, data for N,N-dimethyl acetamide (DMA) has been collected from several papers which used complete lineshape analysis so the reported thermodynamic parameters should be accurate. The solvents used in these studies vary widely in polarity and reactivity (in the sense of associating with the solute) but unfortunately the parameters other than $\Delta G^{\neq}$ (the free energy of activation) vary, even for the same solvent, if analysed by different research groups.

When $\Delta G^{\neq}$ is considered the solvent has a marked effect on the magnitude of the free energy change. Changes in solvent alter the micro-environment of the solute so variations in $\Delta G^{\neq}$ with solvent can be expected. In the only study where the concentration of the DMA was varied purposefully on a large scale, $\Delta G^{\neq}$ does appear to change for the initial two dilutions but then seems to approach a limit. In this table, both deuterated and undeuterated DMA have been presented as though the thermodynamic parameters for rotation in these two compounds are the same. The data for DMA in formamide and neat DMA would seem to confirm this assumption; the discrepancies in thermodynamic parameters for DMA in D_2O and CCl_4 could be due to the differing concentrations of DMA used in these analyses and this would confirm the results for DMA

Table 1-1

N,N-Dimethylacetamide in Various Solvents

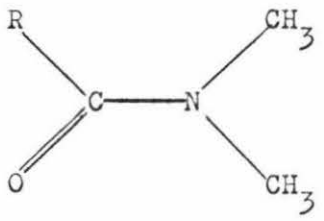

R	E_a[a] kJ mol^{-1}	$G^{\neq}_{298}$ kJ mol^{-1}	$S^{\neq}_{298}$ JK^{-1} mol^{-1}	Solvent	Conc.
CD_3[28]	82.0 ± 1.3	76.1	+ 11.3	neat	
CH_3[24]	79.5 ± 0.4	75.7 ± 0.4	+ 2.9 ± 4.1	neat	
CH_3[24]	82.8 ± 0.4	80.8 ± 0.4	+ 3.3 ± 4.1	D_2O	10 mol%
CD_3[23]	87.9 ± 3.8	80.8 ± 3.8	+ 11.3	D_2O	1.04M
CD_3[29]	84.9 ± 1.3	77.4	+ 17.2 ± 3.3	DMSO-d_6	9.5 mol%
CH_3[24]	82.0 ± 1.3	75.3	+ 13.0 ± 8.4	$(CD_3)_2CO$	10 mol%
CH_3[30]	70.5 ± 1.7	72.5	- 15.0 ± 5.1	CCl_4	14.9 mol%
CD_3[31]	76.6 ± 0.8	72.8	+ 4.6	CCl_4	1.7 mol%
CD_3[31]	75.3 ± 1.3	72.4	+ 2.1	Isooctane	2.6 mol%
CH_3[32]		77.4[b]		o-dichlorobenzene	20g l^{-1}
CD_3[33]	89.1 ± 2.5	81.2		Formamide	90.2 mol%
CH_3[33]	87.4 ± 1.7	80.8		Formamide	90.1 mol%
	82.0 ± 2.1	79.5			80.5 mol%
	81.6 ± 2.5	78.7			70.9 mol%
	81.6 ± 1.3	78.2			47.7 mol%

a $H^{\neq}_{298} = E_a - 2.5$ kJ mol^{-1}

b $G^{\neq}$ at 318K

in formamide.

Another way to change the environment of the solute is to use only one solvent but change its properties by adding salts of various kinds (Table 1-2). Very little work on this type of effect has been done so a coalescence temperature study by Egan[34] has been included. The two salt-free solutes at the head of the table are listed as controls on the reported parameters.

Temussi[23] attributes the large entropy change, $\Delta S^{\neq}$, for the DMA/Ag^{+}/D_2O solution to inaccurate T_2 values used to compensate for carbon-methyl coupling to the N-methyl groups. Such coupling was not explicitly included in the lineshape program but was treated as an extra broadening effect of the N-methyl peaks. To test whether $\Delta S^{\neq}$ was affected by T_2, analyses of N,N-dimethyltrideuteroacetamide in D_2O with and without the silver ion Ag^{+} were done at various temperatures. As the Table shows, attributing large values of $\Delta S^{\neq}$ to inaccurate T_2 values is probably correct for this molecule.

Unfortunately there are no systematic studies of salt effects on rotational barriers. The data in Table 1-2 show a marked change in $\Delta G^{\neq}_{298}$ in the presence of monovalent salts but more studies of ions in similar solvents are needed before theories about the interactions involved can be formulated.

Table 1-2

Salt Effects on Rotational Barriers in N,N-Dimethylacetamide

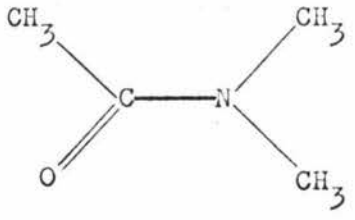

Ref	E_a kJ mol^{-1}	$G^{\neq}_{298}$ kJ mol^{-1}	$^{\neq}_{298}$ JK^{-1} mol^{-1}	Solvent
24	82.0 ± 1.3	75.3 ± 0.4	+ 13.0 ± 8.0	10 mol% $(CD_3)_3CO$
24	82.8 ± 1.3	80.6 ± 0.4	+ 3.3 ± 4.2	10 mol% D_2O
23	105.4 ± 2.1	74.1 ± 2.1	+ 85.4	1M D_2O + $4MAG^+$
23	79.5 ± 2.9	74.9 ± 2.9	± 5.9	1M DMA-d_3 in D_2O + $4MAG^+$
23	87.9 ± 3.8	80.8 ± 3.8	± 11.3	1M DMA-d_3 in D_2O
34		74.1[a]		1M dioxan
34		83.7[b]		1M dioxan + 1M Li^+

a $G^{\neq}$ at 333K

b $G^{\neq}$ at 374K

SECTION 2

INSTRUMENTAL AND EXPERIMENTAL PROCEDURES

In this section the instruments and procedures in dealing with the samples prepared for variable temperature NMR spectroscopy are given in some detail so that particular problems may be mentioned in lesser detail as they arise.

For all experiments described the spectrometer, a JEOL JNM-C-60HL high resolution NMR spectrometer, was used in combination with a JES-VT-3 variable temperature controller and a Marconi TF-2414 counter timer.

2.1 THE NMR HIGH RESOLUTION SPECTROMETER

2.1.1 Internal Lock and the Spectrometer[35]

The magnet for providing the main magnetic field is an electromagnet producing a field of 1.4092 Tesla at 60MHz. The magnet is excited by a stabilized AC power supply which is stable to 1 part in 10^7. Since this field is affected by temperature variation; magnetic fields associated with power switches, transformers and motors; and magnetic fields due to magnetic materials in and around the magnet, a super-stabiliser is incorporated in the instrument to reduce fluctuations in the magnetic field to 1 part in 10^8 but this cannot compensate for overall drift of the magnetic field caused by changes in the resistivity characteristics of components.

To deal with this drift a reference sample positioned near the detector coil or one of the peaks in the spectrum is used as a lock i.e. the drift is controlled using this sample or peak as a standardised value. In internal lock, which was the mode generally used in obtaining spectra reported in this thesis, the signal of tetramethylsilane (TMS),

which had been added to the sample tube, was used as an internal reference for drift control.

Tetramethylsilane has twelve protons in identical environments so the single signal is much stronger than for most other compounds used in NMR and a correspondingly small amount (usually 1%) can be added to an NMR tube. Since the TMS signal is at higher field (lower frequency) than most compounds used in NMR, only a low field sweep is usually needed.

Two modulation frequencies are used and the TMS signal is detected as a dispersion curve, so that variations from the null point provide feedback to reverse any drift, while the rest of the spectrum is recorded as a set of absorption peaks. If the main field varies by ΔB

Figure 2-1:

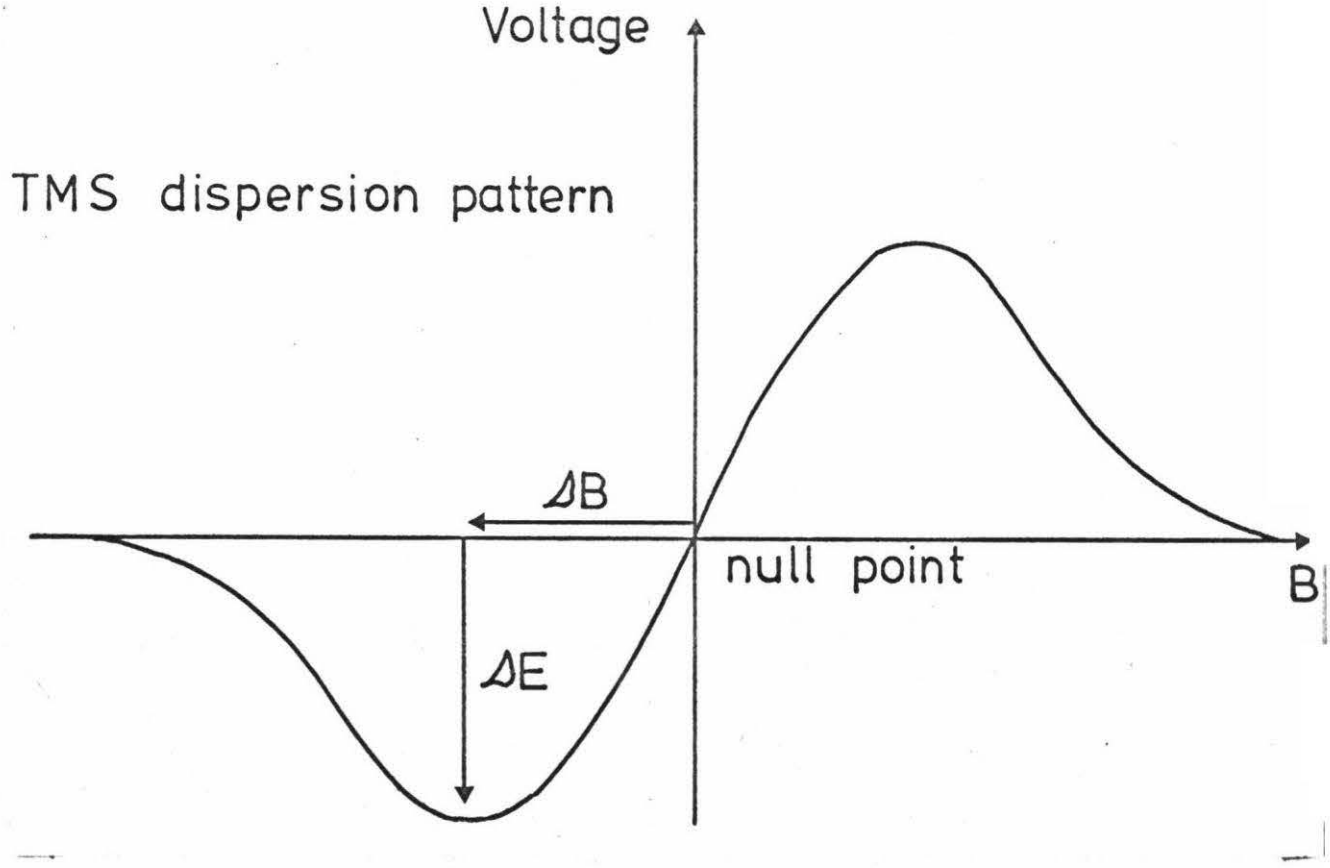

from the field at the null position B, the disperions signal instead of being zero will correspond to - E. By feeding this voltage to the super stabiliser a voltage + E is produced which will return the

applied field to the field value at the null position.

This lock system improves the stability to 1 part in 10^9 but restricts the possible sweep methods to those which vary the frequency or the field/frequency ratio. From the resonance equation 1-4

$$\upsilon/B = |\gamma/2\pi|$$

so both field and frequency can be altered at the same time to sweep the spectrum.

The use of two closely related modulation frequencies for lock and spectral observation results in interaction between these two channels. As the resolving power increases so does the signal stability causing absorption peaks to become sharper. The major advantage of internal lock methods is the small volume over which field homogeneity must be maintained. Since both reference and measured samples are in the same tube the total sample volume is at a minimum when compared to external lock in which a separate reference is provided, simplifying the circuitry but enlarging the volume over which the field must be stable.

The stability in the internal lock mode given in the specifications is $\pm$0.4 Hz for five successive five minute sweeps. The claimed resolution is 5×10^{-9} or 0.3 Hz.

2.1.2 The Frequency Counter

A Marconi TF-2414 counter timer was linked to the NMR spectrometer. At the centre of the beat pattern resulting when the reference and observation signals have nearly the same frequency the counter, when applied to the lock signal, read 4000.2 Hz. All spectral positions were calculated from this reference signal. The recorded frequency readings were the average of three or more successive determinations for a given peak position. The claimed accuracy of the countertimer is $\pm$0.1 Hz.

Frequency measurements for spectra were made by putting two or

more vertical markers of known frequency (as read from the frequency counter) on a spectrum and interpolating between them to any given position.

2.2 VARIABLE TEMPERATURE MEASUREMENTS

2.2.1 Control of Probe Temperature[36]

The variable-temperature controller alters the probe temperature from ambient temperature (usually 300.0K) by surrounding the sample tube in the probe with a stream of gas which will warm or cool the sample to the required temperature. For low temperature control, the bas evaporating off liquid air in a 10 litre dewar is piped into the probe. The evaporation rate in the dewar is automatically controlled by a heating coil immersed in the liquid air to give the required sample temperature.

To reach temperatures above ambient temperature, compressed air is fed into the temperature controller which heats the air to the level needed, before the air is sent into the probe.

The stability claimed for the temperature controller in the specifications is $\pm 0.5^{\circ}C$.

2.2.2 Temperature Gradients

In an effort to find a more accurate means of measuring the temperature than was possible with a thermometer, a pair of thermocouples were set up in the NMR machine. One thermocouple was placed in the probe as near as possible to the receiver coil while the other thermocouple was suspended in a spinning tube in an attempt to simulate the usual operating conditions. Unfortunately the electromagnet had to be turned off during these measurements so the actual operating conditions were not reproduced.

The other ends of the copper-constantan thermocouples were immersed in a deionised ice/deionised water mixture during measurements.

At room temperature under these conditions both thermocouples gave a voltage difference of 774μV as measured by a potentiometer bridge (W.G. Pye and Co.). From standard tables[37] this corresponds to a temperature of 20°C.

The thermocouple in the probe is labelled B (with the corresponding potential difference E_B) while the thermocouple in the spinning tube was labelled A (with potential difference E_A). Thermocouple A was marked on its stem to indicate when the tip was at the base of the tube (0cm) and at 1.0, 1.5, 2.0, 3.0 and 4.0cm above the base. The receiver coil is 1.5cm above the base of the probe.

The variables in the following experiments were the air pressure to the spinner, the temperature in the probe and the height of the thermocouple above the base of the NMR tube. When the air pressure was altered from 40 to 30 g cm^{-3} there was no significant change in the potential difference between the two thermocouples, ΔE (defined as $E_A - E_B$), but when the temperature and the height above the base of the probe were varied the potential difference altered dramatically (Table 2-1). Though the relationship between changes in ΔE and height above the base of the probe appear linear at lower temperatures (Fig. 2-2), as the temperature rises the linearity disappears. The relationship between E_B (a measure of the probe temperature) and E is curvilinear at all positions in the NMR tube (Fig. 2-3). Since the field homogeneity should be greatest at and near the receiver coil, the optimum conditions for future work were the thermocouple at 1.5cm from the base of the probe with a spinning air pressure of 30 g cm^{-3}.

Although the difference in potential between the two thermocouples at room temperature was necessarily zero, as the temperature each day varied so did the room temperature potential difference E_B for which $\Delta E = 0$. The curves of ΔE versus E_B obtained on two days when the initial room temperatures were 25.5°C and 20.5°C are shown in Fig. 2-4.

Table 2-1

Temperature Gradients in the NMR Probe

T	A in μV					B	ΔE	$\Delta(\Delta E)$
K	Height above base of tube in cm					in	(E_A-E_B)	
	0	1	2	3	4	μV	μV	μV
303	1454					1416	38	-
		1449				1409	40	2
			1485			1431	54	16
				1495		1435	60	22
					1465	1400	65	27
313	1945					1878	67	-
		1951				1876	75	8
			1951			1865	86	19
				1965		1871	94	27
					1971	1866	105	38
323	2402					2296	106	-
		2410				2295	115	9
			2442			2317	125	19
				2426		2285	141	35
					2441	2288	153	47
333	2806					2660	146	-
		2814				2653	161	15
			2825			2647	178	32
				2872		2672	200	54
					2889	2665	224	78
343	3228					3041	187	-
		3253				3048	205	18
			3279			3051	228	41
				3302		3047	255	68
					3354	3064	290	103

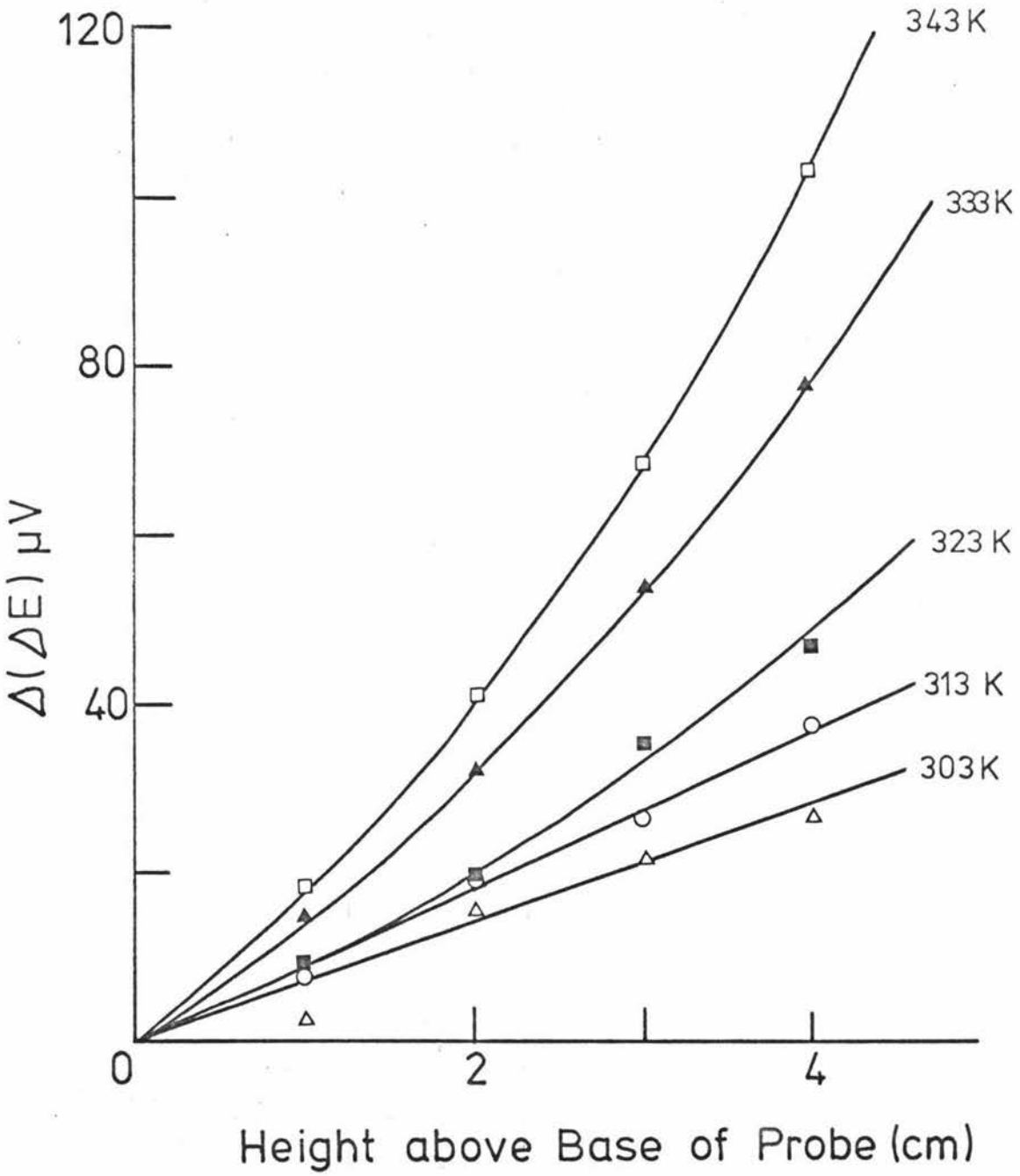

Figure 2-2 : Difference in potential difference between the two thermocouples at different positions in the pole

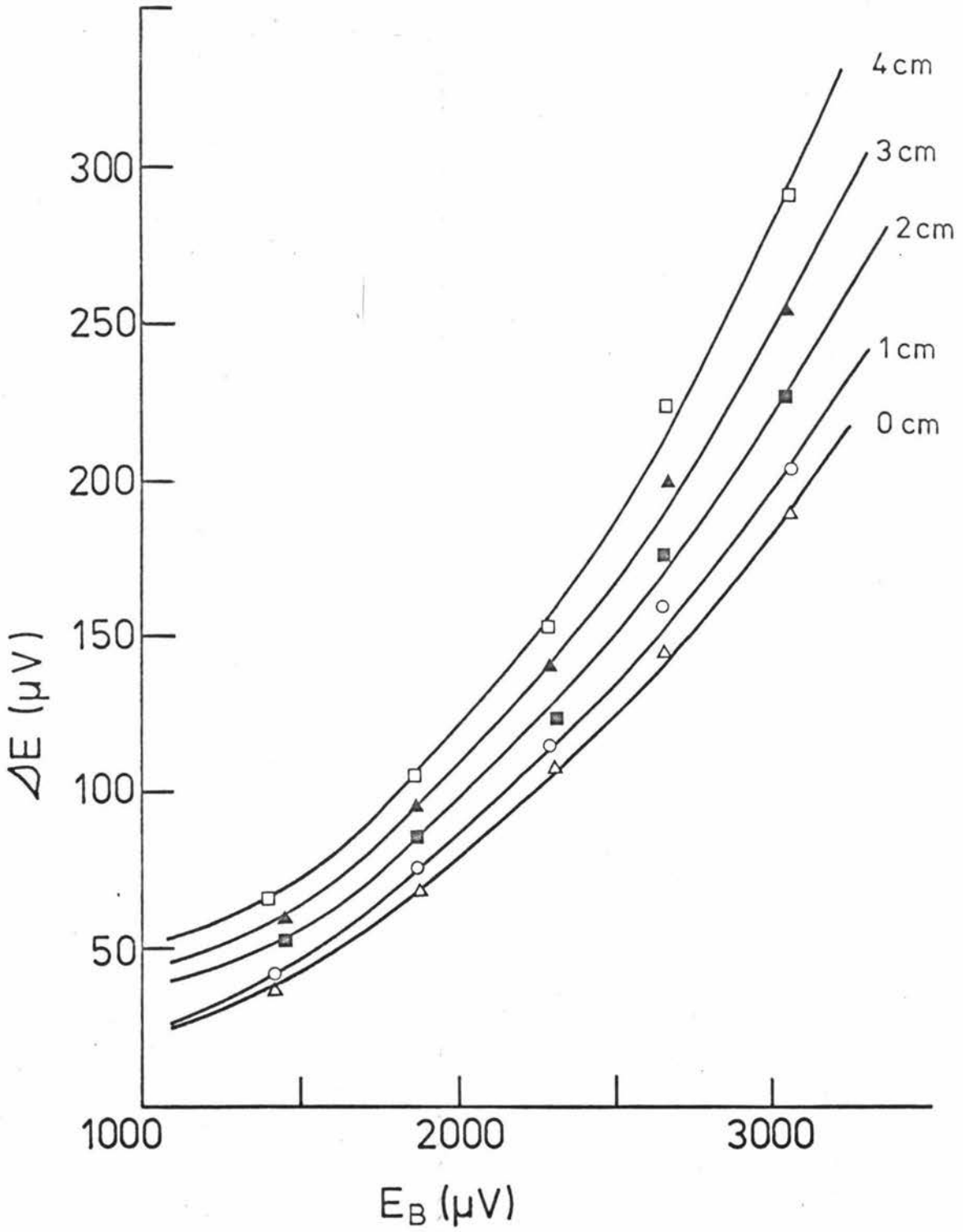

Figure 2-3: Potential difference between the two thermocouples versus the potential of the probe thermocouple

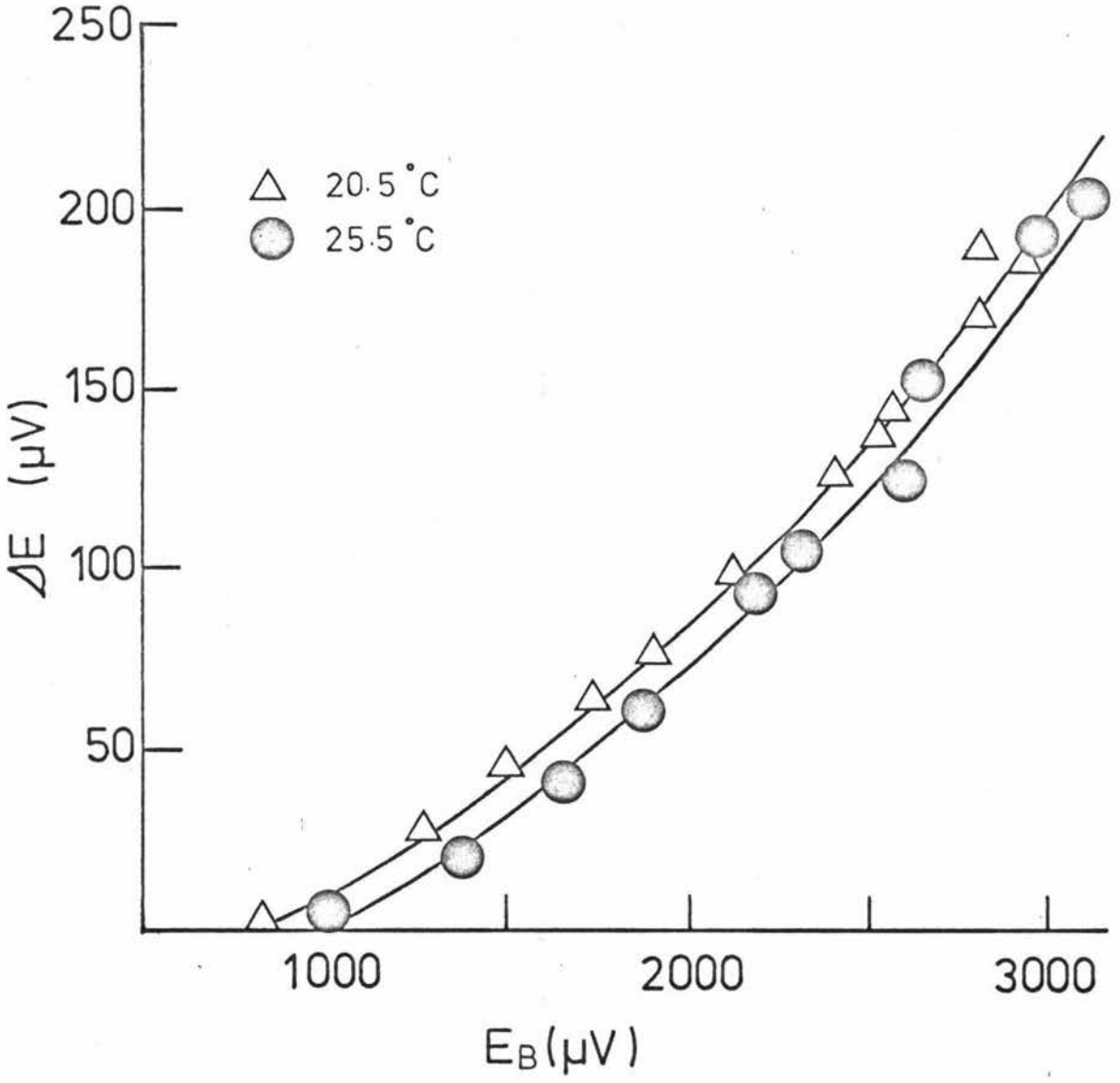

Figure 2-4: Potential difference between the two thermocouples versus the probe thermocouple at varying ambient temperature and 30 gm cm^{-3} pressure

Because of the different initial temperatures (and hence values of E_B) at which ΔE is zero the curves are not super-imposable.

Since these measurements of E_A and E_B could not be made when the probe was thermostatted by the operating magnet and its water cooling, a unique calibration curve which would allow measurements of the emf of thermocouple B to be used to determine the temperature in the NMR tube can not be determined.

At this stage the papers by Van Geet[38,39] on the temperature dependence of the peak separation in methanol and ethylene glycol were discovered. To check the method both the peak separations of these two samples and the corresponding value of E_B were determined. The plot of $\Delta\nu$ versus E_B was linear but rather than calibrate E_B from $\Delta\nu$ which had, in turn, been calibrated from a thermistor, $\Delta\nu$ only was used.

2.2.3 Methods of Temperature Measurement

Early attempts to measure the temperature in the probe were made using a thermometer inserted into the probe under the same air flow conditions as for recording a spectrum but this was thought to be too inaccurate since the error was $\pm$ 1°C.

Later measurements made with methanol or ethylene glycol samples and, using the temperature-dependent separation, $\Delta\nu$, of the hydroxyl and methyl or methylene peaks in combination with the equations developed by Van Geet (Table 2-2), were accurate to between 0.3 and 0.8 degrees. The temperature-measuring samples were distilled methanol or ethylene glycol to which had been added .03% concentrated hydrochloric acid to sharpen the hydroxyl peak. Since the methyl or methylene peaks were sharp enough to act as lock signals, no TMS was added and $\Delta\nu$, the peak separation, could be read directly from the frequency counter by locking on to these peaks and then observing the hydroxyl peak. In a few cases the temperature determined from the equations was checked by

Table 2-2

Van Geet's Equations[38,39]

Methanol	220-270 K	T = 498.4 - 2.083	± .7 K
	260-320 K	T = 464.0 - 1.775	± .4 K
Ethylene Glycol	310-410 K	T = 466.0 - 1.694	± .3 K

measuring the temperature directly using a thermometer.

2.3 PREPARATIVE PROCEDURES

2.3.1 The Glove Box

The glove box was fitted with new gloves of the required small hand size. All ports were checked to ensure that they were air-tight. Initially the glove box was flushed with dry nitrogen directly from the cylinder. To keep the glove box dry and clean after the initial flushing, the nitrogen from the cylinder was passed through two traps, the first containing concentrated sulphuric acid to remove any traces of water and the second containing sodium hydroxide pellets to trap any acid entrained in the gas. Before use, the glove box was always flushed overnight with nitrogen. Thereafter the glove box was kept at slightly positive pressure with respect to the laboratory so any gas flows were out of the glove box.

Equipment was usually left overnight in the dry box before use. Before being placed in the box, bottles were uncapped and flushed with dry nitrogen to remove any moist air that might remain after oven drying.

2.3.2 The Cleansing of Glassware

NMR tubes were first soaked in chromic acid for at least an hour (more usually for twenty-four hours) before being rinsed three or four times with tap water and four times with distilled water. Glassware was washed with detergent or soaked in chromic acid, rinsed with tap water and again with distilled water.

All glassware (including the NMR tubes) was dried in the oven and cooled either in the dry box itself or in a desiccator.

2.3.3 Sample Preparation

The samples were usually made up in a glove box under nitrogen.

Precalibrated 2cm^3 flasks were prepared as above (Section 2.3.1 and 2.3.2). These flasks were stoppered in the glove box, removed (using tissues for handling the clean glassware) and weighed on a four-figure Mettler balance. They were returned to the glove box where solids were added then the flasks were reweighed, returned and the amount of solid was adjusted until the approximately correct weight of solid was present. The solvent was added via Pasteur pipettes to the flask up to the 2cm^3 mark then 4 drops of TMS were added. The flask was stoppered and shaken. About 0.5 - 0.7cm^3 of the solution was put in an NMR tube with a quick fit joint sealed to the top and capped. The NMR tube was then degassed on the vacuum line by the freeze-thaw technique (see Section 2.3.4) then sealed under vacuum.

2.3.4 The Freeze Thaw Technique for Sealing NMR Tubes

The NMR tubes had quick fit joints sealed to their tops which matched the joints on the vacuum line. The NMR tubes were put on the vacuum line, the tube and its contents were frozen in a dewar of liquid air and while the solution was frozen the tap to the vacuum line was opened to remove air above the frozen solution. The vacuum line tap was shut, the dewar was removed and the solution thawed releasing dissolved gases into the vacuum above the solution. This freeze-thaw cycle was repeated at least twice more or until gases were no longer expelled from the solution.

2.3.5 Sample Spectra

Once the NMR tubes containing the samples had been sealed a room temperature spectrum was run to verify the preliminary spectra and to

ensure the solution contained enough TMS to give a good lock/reference signal. The next step was to run a few high and low temperature spectra to examine qualitatively how the spectrum changed with temperature and whether the slow exchange region was accessible in the particular solvent being used.

All spectra at temperatures other than ambient temperature had the temperature determined before and after the running of the spectrum either with a thermometer or with a methanol or glycol sample tube in the probe, under the same conditions of power and air flow as the sample tube. The spectra were usually run on an expanded scale since the standard scale for a spectrum is 9 ppm (540 Hz) wide.

2.3.6 Digitizing a Spectrum

Once a spectrum had been run with good phasing at a known temperature the spectrum was digitized. With an expanding ruler, which was adjusted to the vertical markers, intervals of 0.1, 0.2, 0.4 or 0.8 H_z were marked off depending on the rate of change of intensity. Once the intervals had been marked they were extended at right angles to the baseline until they met the absorption line shape. The intensity at each frequency was then measured in cm from the baseline and the frequency and intensity were recorded.

The interpolation between the vertical markers was rarely more than 0.1 Hz in disagreement with the next section. The scale used to measure the intensities is arbitrary since the theoretical spectrum will be adjusted to match the experimental spectrum.

2.4 THE COMPUTER PROGRAM

2.4.1 The Equation on which the Program is Based

The equation used in the program was developed from equation 1-15 for two-site exchange without coupling

$$G = \frac{i\omega_1 M_o \left\{ \tau_A + \tau_B + \tau_A \tau_B (\rho_A \alpha_B + \rho_B \alpha_A) \right\}}{\left\{ (\alpha_A \tau_A + 1)(\alpha_B \tau_B + 1) - 1 \right\}}$$

where $\alpha_n = + \frac{1}{T_{2n}} + i(\omega_o - \omega)$

The absorption signal is given by $v = \mathcal{J}_m(G)$

$$V = \frac{\omega_1 M_o \left\{ \left[1 + \tau \left(\frac{P_B}{T_{2A}} + \frac{P_A}{T_{2B}} \right) \right] P + QR \right\}}{P^2 + R^2} \qquad 2\text{-}4$$

where $\tau = \tau_A \rho_B = \tau_B \rho_A S$

$$\Delta\omega_{AB} = \omega_A - \omega_B$$

$$\Delta\omega = \frac{1}{2}(\omega_A + \omega_B) - \omega \text{ rad s}^{-1}$$

$$P = \tau \left[\frac{1}{T_{2A} T_{2B}} - \Delta\omega^2 + \frac{1}{4}(\Delta\omega_{AB})^2 \right] + \frac{P_B}{T_{2B}} + \frac{P_A}{T_{2A}}$$

$$Q = \tau \left[\Delta\omega - \frac{1}{2}\Delta\omega_{AB}(\rho_A - \rho_B) \right]$$

$$R = \Delta\omega \left[1 + \tau \left(\frac{1}{T_{2A}} + \frac{1}{T_{2B}} \right) \right] + \frac{1}{2}\Delta\omega_{AB}\tau \left(\frac{1}{T_{2B}} - \frac{1}{T_{2A}} \right) + \frac{1}{2}\Delta\omega_{AB}(\rho_A - \rho_B)$$

Since all frequency measurements are in Hz the original equation must be substituted with quantities having these units.

If $\omega = 2\pi\nu$

$$\tau = \frac{1}{2\pi}\tau^1$$

$$T_{2n} = \frac{1}{2\pi} T_{2n}^1$$

then

$$V = \frac{\nu_1 M_o 2\pi \left[1 + \tau^1 \left(\frac{P_B}{T_{2A}^1} + \frac{P_A}{T_{2B}^1} \right) \right] P^1 + Q^1 R^1}{P^{12} + R^{12}} \qquad 2\text{-}5$$

where $P^1 = \tau^1 \left[\frac{1}{T_{2A}^1 T_{2B}^1} - \Delta\nu^2 + \frac{1}{4}\Delta\nu_{AB}^2 \right] + \frac{P_B}{T_{2B}^1} + \frac{P_A}{T_{2A}^1} = \frac{1}{2\pi} P$

$$Q^1 = \tau^1 \left[\Delta\nu - \frac{1}{2}\Delta\nu_{AB}(\rho_A - \rho_B) \right] = Q$$

$$R^1 = \Delta\nu \left\{ 1 + \tau^1 \left[\frac{1}{T_{2A}} + \frac{1}{T_{2B}} \right] \right\} + \frac{1}{2}\Delta\nu_{AB}\tau^1 \left(\frac{1}{T_{2B}^1} - \frac{1}{T_{2A}^1} \right) + \frac{1}{2}\Delta\nu_{AB}(\rho_A - \rho_B)$$

$$= \frac{1}{2\pi} R$$

Hence for a given value of τ^1 the lineshape of the absorption peak can readily be calculated, if $\nu_1 M_o$ is used as a scaling factor since all other quantities are measurable.

2.4.2 The Best Fit Parameters

The experimental spectrum a given temperature (TEMP) is digitised to give a list of frequencies (W(I), I = 1, 2 ...) and the corresponding intensities (WINT (I)). The rest of the input provides the necessary information from which to calculate v = $\mathcal{J}_m(G)$; WA, WB are the slow exchange peak positions; T_{2A}', T_{2B}' are the transverse relaxation times; PA, PB are the populations at sites A and B and TOR is the value selected for τ^1.

A flow diagram for the initial computations in the program LMH is shown in Figure 2-5 and the important operations can be summarised as follows:

The first step is to calculate v = $\mathcal{J}_m(G)$ at each frequency W(I). To get the theoretical lineshape to the correct height, the subprogram NMAX finds the frequency corresponding to the largest value for WINT(I) and multiplies all theoretical intensities by CONS = WINT(NMAX)/V(NMAX) ensuring that WINT(I) and W(I) are on the same scale. The differing intensities of the theoretical and experimental lineshapes (at the same frequency) are compared, DIFF(I) = V(I) - WINT(I) and the difference is squared and summed to give DIF. This quantity is divided by the sum of WINT(I) squared to give SIGM (the normalised sum of squares), the square root of which is SIGMA and is printed as RESIDUALS. The larger the value of RESIDUALS, the worse the fit between the theoretical and the experimental spectrum.

2.4.3 Varying τ^1 so the Value of τ^1 Converges to a Limit

To improve the fit between the calculated spectrum V(I) and that actually observed WINT(I) the value of τ^1 must be altered so that

Figure 2-5

FLOW DIAGRAM 1

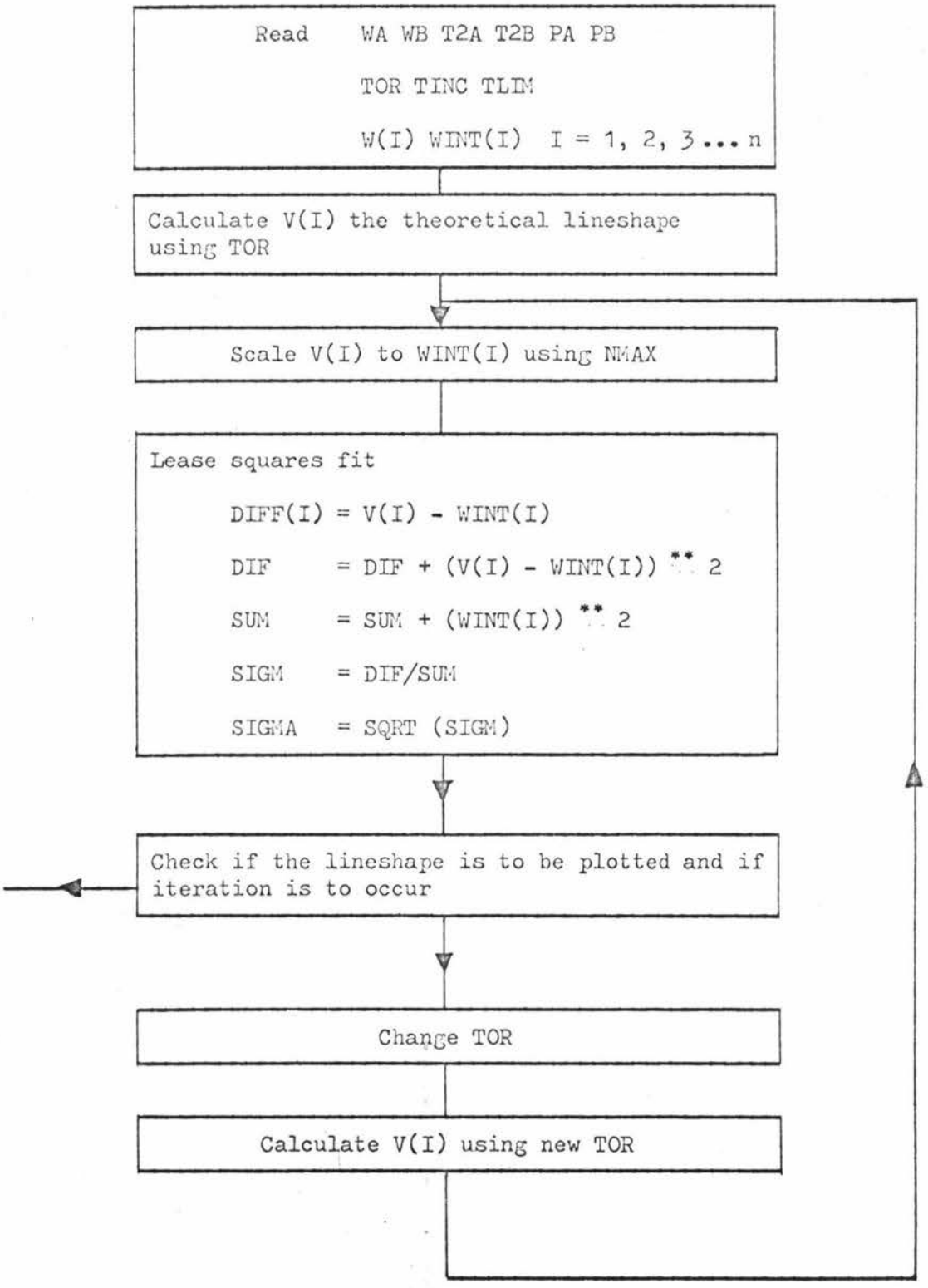

$v = \mathcal{J}_m(G)$ can be recalculated. The logical steps involved are summarised in Fig. 2-6 and are part of Fig. 2-7 . The method used in this program is to add TINC to TOR so that now τ_2^1 = TOR + TINC and recalculate $v = \mathcal{J}_m(G)$ and RESIDUALS. The RESIDUALS for τ^1 and τ_2^1 are compared. If the RESIDUALS have increased then the next value of τ^1 is τ_3^1 = TOR - $\frac{1}{2}$ TINC but if the RESIDUALS has decreased then τ_3^1 = TOR + TINC.

Error limits in TOR can be estimated, for best fit values of TOR less than 3.0, by initially setting TOR to 0.003 units below the best fit (lowest RESIDUALS) value of TOR and setting TINC (the increment) and TLIM at 0.002 units. Then, with NCON set at zero, the program will print out each iteration but will only iterate until the value of RESIDUALS beings to increase and will then stop. To find the RESIDUALS at any value of TOR set TLIM < TINC then only one iteration will occur. The settings, when the best-fit value of TOR is greater than 3.0, are an initial value for TOR which is 0.999 of the best fit value of TOR and TINC and TLIM given as 0.0007 of the best fit value of TOR. The program will then proceed as above.

To avoid any possibility of an infinite loop this variation of τ^1 is limited by incrementing a counter NIT by 1 each time up to a limit of NIT = 21. This counter will shut the program down after 21 iterations and a new value for TOR must then be read in. The reduction in the magnitude of TINC cannot continue indefinitely unless TLIM was zero; usually TLIM was set at .001 or higher so it was hoped that a good fit for τ^1 was found such that $|\text{TINC}|$ - TLIM < 0 before NIT = 21.

Figure 2-6:

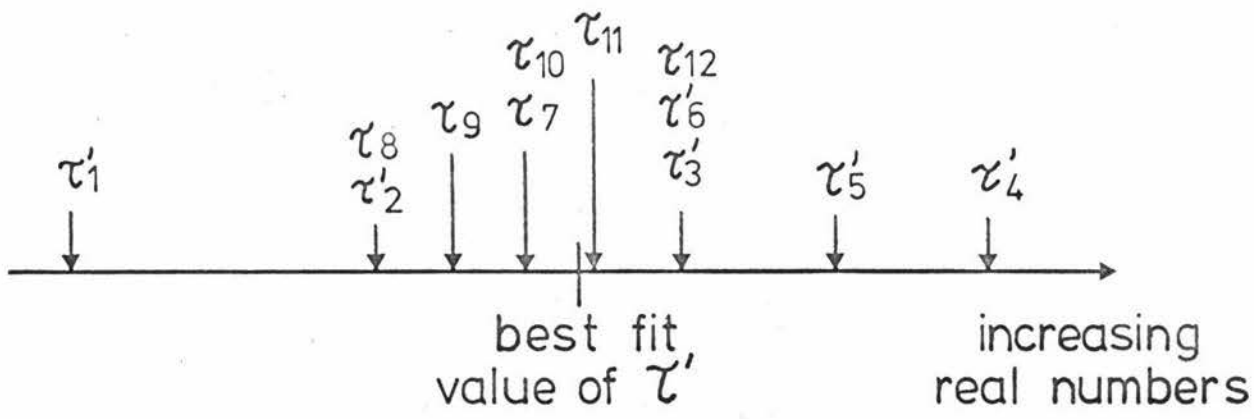
τ_{11}
τ_{10}
τ_{12}
τ_9
τ_7
τ'_6
τ_8
τ'_1
τ'_2
τ'_3
τ'_5
τ'_4
best fit
value of τ'
increasing
real numbers

Figure 2-7: FLOW DIAGRAM 2

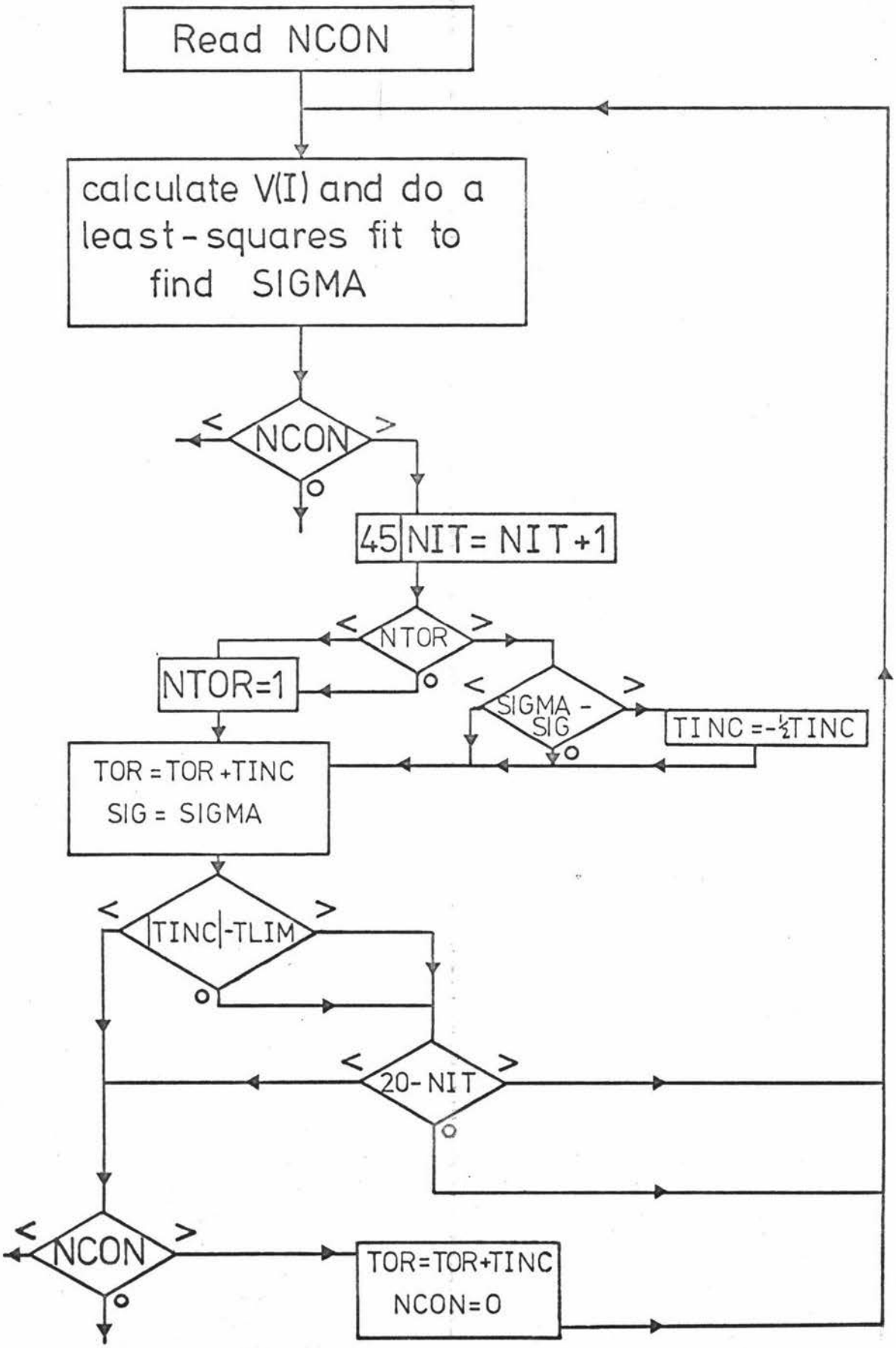

SECTION 3

NMR STUDY OF THE SOLVENT DEPENDENCE OF THE BARRIER TO ROTATION IN N,N,N',N'-TETRAMETHYLTHIODICARBONIC DIAMIDE

3.1 INTRODUCTION

Amides have been extensively studied and are relatively soluble in a wide range of solvents. In Table 3-1 a variety of substituents on N,N-dimethylacetamide and N,N-dimethylacetothioamide are listed with their thermodynamic parameters for chloro-substituted solvents which are commonly thought to be inert. Since sulphur is commonly regarded as less reactive than oxygen in most situations, we felt that a thioamide should give more reproducible results (particularly if the same solvent was not available) and it was decided to study the effect of solvent on the barrier to rotation in N,N,N',N'-tetramethylthiodicarbonic diamide (TTD).

3.2 THE CHOICE OF SOLVENTS

The solubility of N,N,N',N'-tetramethylthiodicarbonic diamide in a range of possible solvents was tested and the results are summarised in Table 3-2.

Chloroform, pyridine and acetone were chosen as the first set of solvents because of the high solubility of TTD in them. In addition since the previous NMR lineshape study of TTD had been carried out in chloroform, further work in this solvent should prove a useful check on the consistency of the NMR data.

After the acetone sample had been sealed for about a day, a colour change from yellow to orange was noticed. Over the next few days the colour darkened to brown despite the sample being kept in a refrigerator. No noticeable change in the NMR spectrum was observed. Another sample in which the concentration of TTD was reduced was prepared and this

Table 3-1

Substituent Effects on the Rotational Barrier in N,N-Dimethylamides

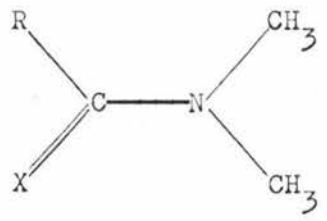

Ref	R	X	E_a [a] kJ mol^{-1}	$\Delta G^{\neq}_{298}$ kJ mol^{-1}	$\Delta S^{\neq}_{298}$ JK^{-1} mol^{-1}	Solvent
30	CH_3	O	70.5 ± 1.7	72.5	- 15.0	CCl_4
32	CH_3	O		77.4[b]		o-dichlorobenzene
40	CH_3S	O	69.5 ± 4.2	60.7 ± 2.1	+ 21.3 ± 16.7	$CDCl_3$
41	CH_3S	O	67.4	70.7	- 19.6	
32	CH_3	S		91.2[c]		
42	CH_3S	S	54.4 ± 2.5	61.5	- 31.0	n-hexane
43	CH_3S	S	43.1 ± 1.3	61.5	- 69.0	n-hexane
41	CH_3S	S	58.2	62.8	- 23.4	
43	CH_3CH_2S	S	50.6 ± 0.8	61.1		n-hexane
44	$(CH_3NC(S))_2$	S	69.0 ± 1.7	66.9	- 1.7 ± 8.4	$CDCl_3$
44	$(CH_3NC(S)S)_2$		65.3 ± 1.7	64.0	- 3.8 ± 8.4	$CDCl_3$

a $\Delta H^{\neq}_{298} = E_a - 2.5$ kJ mol^{-1}

b $\Delta G^{\neq}$ at 318 K

c $\Delta G^{\neq}$ at 409 K

Table 3-2

Solubility of N,N,N',N'-Tetramethylthiodicarbonic Diamide

Solvent	Solubility w/v%	Temperature Range °C	Dielectric Constant
Acetic acid	very soluble	+ 16.7 - 118.0	6.17
Acetone	7.8	- 94.0 - 56.5	20.7
Acetonitrile	3.0	- 45.7 - 81.6	36.2
Carbon Tetrachloride	insoluble	- 23.0 - 76.8	2.22
Chloroform	very soluble	- 63.5 - 61.5	4.64
Dimethyl sulphoxide	5.0	+ 18.5 - 189	46.6
DMSO-H_2O (80:20 v/v)	3.4		65.5
1,4-Dioxan	1.7	+ 11.8 - 101	2.21
Ethanol-H_2O (95:5 v/v)	.5		
n-Hexane	insoluble	- 95 - 68	1.88
Methanol	1.5	- 97.8 - 64.7	32.6
Pyridine	very soluble	- 41.8 - 115.6	12.3
Toluene	1.1	- 95 - 110.6	2.4

also darkened to an orange colour although it was kept in a refrigerator except when spectra were being run.

It was hoped that dimethylsulphoxide (DMSO) could be used as a solvent since it would provide an interesting comparison with acetone but DMSO freezes at 18°C which is in the medium-exchange region for a solution of DMSO and TTD. Mixtures of DMSO-water have freezing points below 0°C (a 1 : 1 mixture of these solvents freezes at -190°C). A mixture of DMSO-water with a ratio of 4 : 1 was used since this combined a low freezing point with reasonable solubility for TTD (which is insoluble in water alone). In the DMSO-water samples the salt which was being used as reference was not satisfactory so the tubes containing DMSO-water were opened, and, in the glove box, the contents were transferred to two other tubes to each of which was added a sealed capillary half-filled with TMS before the tubes were sealed without being again degassed.

Acetic acid was proposed as one of the solvents but in this solvent there was only one peak at 27°C so since the solvent freezes at 18°C even to reach the medium exchange region was impossible.

Although the range of solvents was now varied we had neither a benzenoid nor a nonpolar solvent so we combined these qualities and chose toluene as another solvent. A solution in toluene as solvent was prepared (1.17 w/v%) but it was some weeks before the variable temperature spectra could be run and in this time several anomalous peaks appeared so a new sample was made up and spectra were run immediately, i.e. within 48 hours. Except when spectra were being run this sample was kept in a refrigerator.

To round off the solvent study the last solvent selected was acetonitrile which can be contrasted with chloroform, a protic polar solvent, while acetonitrile is an aprotic polar solvent.

3.2.1 Possible Salt Effects

Since we were also interested in studying the effect of added salts on a rotational barrier we tried dissolving various ions in acetone. Some ions were soluble but when TTD was added precipitates separated out. For a while a cobalt (II) salt $CoCl_2$ seemed to give a stable blue solution but unfortunately this salt was hydrated and when anhydrous $CoCl_2$ was added to TTD in acetone a blue green precipitate appeared which was only slightly soluble in $CHCl_3$ and was insoluble in 1,4-dioxan, methanol cyclohexane and carbon tetrachloride. Since one of the solvents for TTD was Dimethylsulphoxide-water which needed a sodium salt as reference, sufficient sodium perchlorate was added to a solution of TTD in this solvent for the solution to be .24M in Na^+ (disregarding the contribution of the reference sample).

3.2.2 Sample Preparation

Acetone-d_6 (BDH), toluene-d_8 (Stohler Isotope Chemicals), acetonitrile-d_3 (Uvasol), chloroform-d_1 (BDH), pyridine-d_5 (BDH) and TMS (BDH) were obtained from commercial sources and were used without further purification. The N,N,N',N'-tetramethylthiodicarbonic diamide (BDH) was dissolved in hot ethanol, filtered to remove impurities and allowed to cool slowly, enabling the crystals to attain maximum size. The crystals were filtered off and washed with distilled water.

The sample solutions were made up in a glove box by weighing the TTD into $2cm^3$ flasks which were then made up to the mark. Once the tubes had been sealed the room temperature spectrum was run for each sample to ensure sufficient TMS was present and that residual proton peaks in the solvents, particularly toluene, would not overlap or otherwise interfere with the N-methyl peaks. The sample concentrations are given below (neglecting in each case the four drops of TMS):

Table 3-3

Solvent	Concentration of TTD (w/v%)
Acetone	7.0
Acetone	3.6
Chloroform	7.5
Pyridine	5.0
DMSO-water (86 v/v% DMSO)	2.5
DMSO-water (86 v/v% DMSO)	2.5 + .24M $NaClO_4$
Acetonitrile	2.3
Toluene	1.1
DMSO	4.8

The salt sodium 3-(trimethylsilyl)-propanesulfonate (Uvasol) was at first used as reference in the DMSO-water solutions but when this was found to be unsatisfactory, TMS capillaries were added to the NMR tubes (Section 3.2).

3.3 DATA COLLECTION

3.3.1 General Problems and Procedures

All spectra at any temperature other than ambient temperature had the temperature determined, both before and after spectra were run, with either the methanol or the glycol sample in conjunction with the Van Geet equations, Table 2-2. In a very few cases the value of $\Delta\nu$ varied by more than .2 Hz but such spectra had to be repeated since the temperature change would alter the phasing of the methyl peaks.

The usual expansion of sweep width was from the standard width of 9 ppm (540 Hz) to .45 ppm (28 Hz) for the full width of the recorder paper (37.5cm). At such an expansion (.75 Hz/cm) a difference of .1 Hz was about 1mm so high machine stability was required which was only achieved if the NMR spectrometer had been turned on for at least three days. Any change in temperature would shift the N-methyl peaks by a few tenths of a hertz in either direction so spectra could only be recorded after the sample tube had been in the probe for at least 7 minutes depending on the difference in temperature between the probe and its surroundings. This restriction on the speed of recording spectra also applied to the methanol and glycol samples so each spectrum would take between 30 and 60 minutes to complete.

The phasing of the lineshape was extremely sensitive, at this expansion, to small temperature changes, so the phasing altered significantly if the temperature controller was unable to maintain the temperature at the claimed stability.

The spectra were recorded at 3.6 or 2.8 Hz per min. Under such slow

passage conditions saturation is a major problem (as discussed in section 1.2.2) so the lowest possible power levels were used for both lock and observation channels. To determine if saturation was affecting the lineshape, the power levels on the observation channel were increased. If the signal was saturated increased power levels did not increase signal height and either showed no effect or decreased the signal intensity. Because the power levels were low the recorded spectra show a lowered signal/noise ratio.

The main operational problem beside machine stability and phase sensitivity, was the difficulty in holding the lock signal at the low power levels required for avoiding saturation. Unfortunately this particular instrument had, before these experiments started, developed interference which markedly decreased the signal/noise ratio on the channel which usually carried the lock signal in the internal lock field-frequency mode. Attempts to record spectra with the channels reversed i.e. in frequency internal-lock mode produced spectra with impossibly low signal/noise ratios. Unfortunately once the lock was lost on internal-lock mode the machine had to be set up again from the beginning so the lack of reliability in the lock meant that much more time than should have been required was spent on running spectra.

An external limitation on the length of continuous low-temperature runs was the trap used to remove water vapour from the compressed air supply for the spinner. Depending on the humidity and the probe temperature the trap would be full of ice and become blocked after $3\frac{1}{2}$ to $4\frac{1}{2}$ hours. If the trap was defrosted for an hour another 2-$2\frac{1}{2}$ hours running time would be available before the trap was again full.

3.3.2 Slow Exchange Spectra

For a peak separation of 2 Hz, to reach the upper limit of the slow exchange region the probe temperature should be 20-25° below the coalescence temperature (which could usually be determined with the trial

sample). For determining if the peak separation is temperature dependant four or more spectra spread over a temperature range of at least 15° must be recorded. For large peak separations the lowest slow exchange spectrum may have to be 60° below the coalescence temperature.

Liquids which have relatively high melting points will therefore be unsuitable as solvents for most rotameric compounds. Viscous solvents may also prove unsuitable for such studies since in these solvents the peak width may vary significantly with temperature (due to solvent effects) and affect the value of T_2 and hence the calculated best fit value of τ^1.

To determine T_2^1 the width of each peak at half-height, $\nu_{\frac{1}{2}}$, is measured either in Hz using an adjustable scale or in cm then converted into Hz. The following equation is then used to find T_2^1 in seconds.

$$T_2^1 = 2/\nu_{\frac{1}{2}} \qquad 3\text{-}1$$

Narrow peaks mean that the percentage error in $\nu_{\frac{1}{2}}$ and hence T_2^1 is high. To minimise the errors in T_2^1 and $\Delta\nu$ all measurements were treated statistically with the following equations

$$\overline{\Delta\nu} = \Sigma\Delta\nu/n \pm s \qquad 3\text{-}2$$

where s is the standard deviation and is given by

$$s^2 = [\Sigma(\Delta\nu)^2 - (\Sigma\Delta\nu)^2/n]/(n-1)$$

and n is the number of measurements. The width at half height $\nu_{\frac{1}{2}}(X)$ (X = A,B) is calculated for each peak separately

$$\overline{\nu_{\frac{1}{2}}(X)} = [\Sigma\nu_{\frac{1}{2}}(X)]/n \pm s \qquad 3\text{-}3$$

where $s^2 = [\Sigma(\nu_{\frac{1}{2}}(X))^2 - (\Sigma\nu_{\frac{1}{2}}(X))^2/n]/(n-1)$

Providing that $\overline{\nu_{\frac{1}{2}}(A)}$ and $\overline{\nu_{\frac{1}{2}}(B)}$ were the same within one standard deviation (which happened in all cases) they were then treated as 2n measurements of $\nu_{\frac{1}{2}}$ for the system, and $\nu_{\frac{1}{2}}$ and s were recalculated.

In the cases where $\Delta\nu$ appeared to be temperature dependent, regression line analysis was used to extrapolate to the values for $\Delta\nu$ in the medium exchange rate region. The frequency measurements for the peak separation, $\Delta\nu$ and for $\nu_{\frac{1}{2}}$ were interpolated from a minimum of three vertical frequency markers per spectrum.

3.3.3 Medium Exchange Rate Spectra

Once the low temperature parameters were known the spectra at and about the coalescence temperature were recorded. The temperature range for these spectra was experimentally determined by running a spectrum at the lowest temperature at which peak broadening could be seen, then running more spectra at 3-5° intervals on the temperature controller's scale, throughout the coalescent range until the single remaining peak had ceased to narrow. The accessible temperature range was determined by the peak separation.

3.3.4 Low Temperature TTD Spectra in Acetone

The expansion used for these spectra was the maximum possible of .75 Hz/cm although, due to the small separation between the peaks in the slow exchange region, even on this expansion problems arose because of the machine errors in individual measurements as well as the fact that data could be collected only over a narrow temperature range.

The width at half height for the 7.8 w/v% solution in acetone was (from Table 3-4) $\nu_{\frac{1}{2}}(1) = .9 \pm .1$cm; $\nu_{\frac{1}{2}}(2) = .9 \pm .1$cm; $\nu_{\frac{1}{2}} = .9 \pm .1$cm while the width at half-height for the 3.6 w/v% solution was $\nu_{\frac{1}{2}}(1) = .99 \pm .08$cm; $\nu_{\frac{1}{2}}(2) = .91 \pm .09$cm; $\nu_{\frac{1}{2}} = .95 \pm .09$cm. Since the values for the 3.6 w/v% solution were from fewer points, the two values of $\nu_{\frac{1}{2}}$ were combined to give $\nu_{\frac{1}{2}} = .9 \pm .1$cm so converting to the frequency scale $\nu_{\frac{1}{2}} = .68 \pm .07$ Hz and $T_2^1 = 2.9 \pm .3$ s.

The peak separation appears to be constant over the temperature range (see Table 3- 4) for the 7.8 w/v% solution $\Delta\nu = 1.38 \pm .08$ Hz so combined with the 3.6 w/v% solution where $\Delta\nu = 1.4 \pm .1$ Hz, the

Table 3-4

Data used to Determine the Low Temperature Parameters in Acetone

A. 3.6 w/v% TTD in Acetone

T	ν_1	$\nu_{\frac{1}{2}}(1)$	ν_2	$\nu_{\frac{1}{2}}(2)$	$\Delta\nu$
K	Hz	$\frac{1}{2}$ cm	Hz	$\frac{1}{2}$ cm	Hz
240.1	207.4	1.00	208.8	0.90	1.4
246.1	207.3	1.10	208.6	1.00	1.3
265.4	207.0	0.90	208.4	0.80	1.4
	207.0	0.95	208.5	0.95	1.5
278.5	207.2		208.8		1.6
	206.9		208.3		1.4

B. 7.8 w/v% TTD in Acetone

T	ν_1	$\nu_{\frac{1}{2}}(1)$	ν_2	$\nu_{\frac{1}{2}}(2)$	$\Delta\nu$
K	Hz	$\frac{1}{2}$ cm	Hz	$\frac{1}{2}$ cm	Hz
240.1	207.2	0.95	208.5	1.00	1.3
246.1	207.4	0.80	208.7	0.80	1.3
255.3	207.2	1.10	208.5	0.90	1.3
260.9	207.0	0.95	208.5	0.85	1.5
	207.1	1.10	208.4	1.10	1.3
262.2	207.1	0.85	208.6	0.80	1.5
	207.1	0.80	208.5	0.80	1.4
279.9	207.1		208.5		1.4
283.5	207.0		208.4		1.4
287.9	207.0		208.4		1.4

resulting value for $\Delta\nu$ is 1.40 $\pm$ .09 Hz.

3.3.5 Low Temperature TTD Spectra in Acetonitrile

For all spectra of acetonitrile solutions, the expansion used was .75 Hz/cm and the data obtained are shown in Table 3-5. When the peak separation was plotted against temperature, although there was a good deal of scatter in the data, there seemed to be a significant increase in $\Delta\nu$ as the temperature increased (Fig. 3-1). To allow for this variation the regression line for the data was calculated to be

$$\Delta\nu = .724 + .011\ (\pm .002)\ T$$

At the .2% confidence level the test value is $t_{.001,17} = 3.646$ while the test statistic for acetonitrile is $t_0 = 5.569$ so in the acetonitrile solution $\Delta\nu$ has a probability greater than 99.8% of being temperature-dependent (from the given data).

The value of $\Delta\nu$ above the coalescence temperature was calculated from this equation. The relaxation time T_2^{-1} was 3.4 $\pm$ 2 s from $\nu_{\frac{1}{2}}$ of .58 $\pm$ .03 Hz.

3.3.6 Low Temperature TTD Spectra in Chloroform

The spectra for chloroform as solvent were recorded at the expansion of .75 Hz/cm. The low temperature spectra were analysed to find the width at half height of each peak and the separation of the peaks. The mean values of $\nu_{\frac{1}{2}}$ (1) and $\nu_{\frac{1}{2}}$ (2) were determined from Table 3-6 to be .9 $\pm$ .1cm and .91 $\pm$ .09cm. When these values were combined the value for $\nu_{\frac{1}{2}}$ .92 $\pm$ .09cm which, when converted to Hz by using the scale conversion provided by the frequency markers on the chart paper, corresponds to .69 $\pm$ .07 Hz. So $T_2^{-1} = 2/\nu_{\frac{1}{2}} = 2.9 \pm .3$ s.

When determining the peak separation, the values of ν_1 and ν_2 from lineshape analysis of exchange spectra below the coalescence temperature were included. The value for the peak separation was 5.1 $\pm$ .1 Hz over a 63° temperature range (240 - 303K).

Table 3-5

Data Used to Determine

Low Temperature Parameters in Acetonitrile

T	ν_1	$\nu_{\frac{1}{2}}(1)$	ν_2	$\nu_{\frac{1}{2}}(2)$	$\Delta\nu$
Hz	Hz	$\frac{1}{2}$ cm	Hz	$\frac{1}{2}$ cm	Hz
252.0	202.8	.7	206.4	.7	3.6
	203.0	.8	206.3	.8	3.3
259.2	202.9	.8	206.3	.75	3.4
266.8	202.8	.7	206.4	.8	3.6
271.9	202.8	.75	206.5	.8	3.7
	202.7	.8	206.2	.8	3.5
278.5	202.6		206.4		3.8
	202.8		206.5		3.7
283.8	202.9		206.7		3.8
284.0	202.6		206.3		3.7
	202.7		206.4		3.7
289.2	202.9		206.7		3.8
293.6	202.8		206.6		3.8
296.1	202.9		206.8		3.9
300.3	202.9		206.7		3.8
	202.8		206.6		3.8
302.1	202.9		206.9		4.0
303.5	202.8		207.1		4.3
	203.0		206.9		3.9

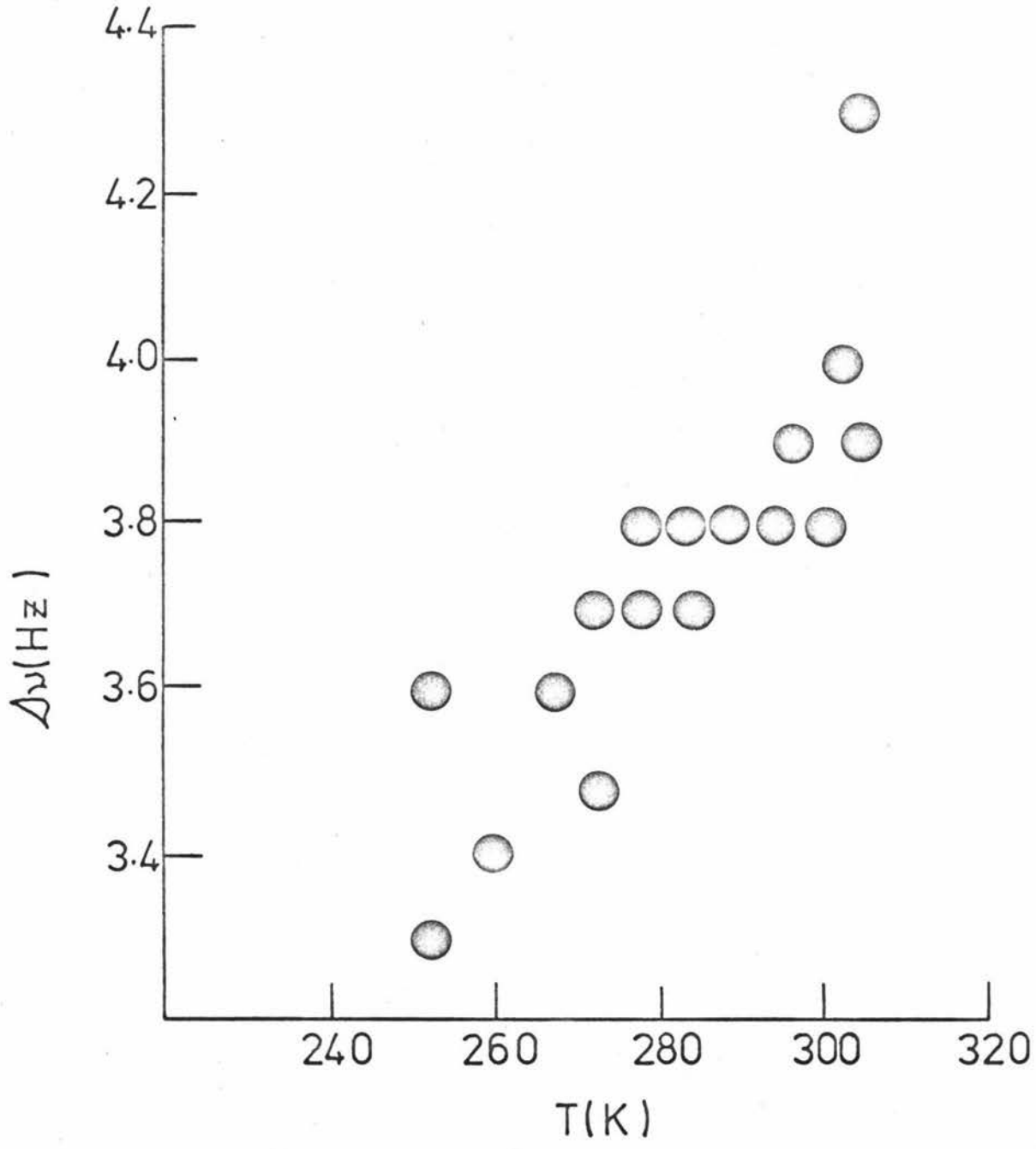

Figure 3-1: Temperature dependence of $\Delta\nu$ for TTD in Acetonitrile

Table 3-6

Data used to Determine the

Low Temperature Parameters in Chloroform

$T \pm .7$ K	ν_1 Hz	$\nu_{\frac{1}{2}}(1) \pm 0.5$ cm	ν_2	$\nu_{\frac{1}{2}}(2) \pm .05$ cm	$\Delta\nu$ Hz
240.1	208.5	1.0	213.6	1.1	5.1
	208.6	0.9	213.5	0.9	4.9
246.1	208.4	0.8	213.4	0.85	5.0
255.3	208.1	0.9	213.1	0.85	5.0
262.2	207.7	0.85	212.8	0.85	5.1
279.9	206.7	1.10	212.0	0.95	5.3
	206.9	0.95	212.1	0.90	5.2
287.6	206.7		211.8		5.1
	206.8		211.8		5.0
293.8	206.6		211.6		5.0
	206.5		211.5		5.0
288.1	206.7		211.9		5.2
294.1	206.5		211.7		5.2
	206.6		211.7		5.1
300.0	206.1		211.1		5.0
	206.3		211.3		5.0
303.7	206.4		211.3		4.9

3.3.7 Low Temperature TTD Spectra in Dimethyl Sulphoxide-Water

The solutions with dimethyl sulphoxide-water as solvent show viscosity broadening in the methyl peaks below 260K so the data from lower temperatures is used only to determine the peak separation. When the peak separation is plotted against temperature no discernible trend was observed so the values obtained at the different temperatures were averaged. The peak separations determined from lineshape analysis of spectra below the coalescence temperature are not included in the analysis of $\Delta\nu$ but would not affect the averages or errors. The values for $\nu_{\frac{1}{2}}$ are somewhat smaller than for the other solvents because these samples were not degassed before being sealed, and presumably contained some dissolved oxygen. The data for determining the peak separation and T_2^{-1} values are given in Tables 3-7 and 3-8 while the experimental values for $\Delta\nu$ and T_2^{-1} are given in Table 3-9.

3.3.8 Low Temperature TTD Spectra in Pyridine

Although the peak separation for pyridine as solvent is much greater than for acetone and chloroform the expansion used was still .75 Hz/cm, though any further increase in peak separation would have required a smaller expansion. The relaxation time T_2^{-1} was determined as usual from $\nu_{\frac{1}{2}}(1)=1.0 \pm .1$cm, $\nu_{\frac{1}{2}}(2) = 1.0 \pm .1$cm, and $\nu_{\frac{1}{2}} = 1.0 \pm .1$cm so $\nu_{\frac{1}{2}} = .75 \pm .08$ Hz and $T_2^{-1} = 2/\nu_{\frac{1}{2}} = 2.7 \pm .3$ s.

From Table 3-10 it is apparent that $\Delta\nu$ decreases with temperature at .03 Hz/K. In Fig. 3-2 the peak separation is plotted against temperature and the data are fitted by a straight line. To find the most accurate equation to fit this line, regression analysis of the data was done and yielded the following equation

$$\Delta\nu = 20.242 - .0345\ (\pm .0009)\ T$$

The values for $\Delta\nu$ at temperatures above coalescence were calculated using this equation.

Table 3-7

Data used to Determine the

Low Temperature Parameters in DMSO - D_2O

T	ν_1	$\nu_{\frac{1}{2}}(1)$	ν_2	$\nu_{\frac{1}{2}}(2)$	$\Delta\nu$
K	Hz	cm	Hz	cm	Hz
261.7	230.2	1.7	232.9	1.6	2.7
263.4	229.8	1.6	232.4	1.6	2.6
264.0	229.8	1.9	232.2	1.9	2.4
267.3	230.0	1.9	232.5	1.9	2.5
	230.0	1.7	232.5	1.8	2.5
273.5	229.8	1.5	232.3	1.6	2.5
	229.8	1.6	232.4	1.5	2.6
280.8	229.9	1.4	232.5	1.45	2.6
283.3	230.1	1.3	232.7	1.1	2.6
	230.0	1.4	232.7	1.5	2.7
290.4	230.1	1.8	233.0	1.7	2.9
	230.2	1.8	232.9	1.6	2.7
255.6	229.6		231.9		2.3
256.7	229.8		232.1		2.3
258.3	229.7		232.1		2.4
	229.7		232.0		2.3
261.3	229.4		231.8		2.4

Table 3-8

Data used to Determine the

Low Temperature Parameters in DMSO-D_2O with $NaClO_4$

T	ν_1	$\nu_{\frac{1}{2}}(1)$	ν_2	$\nu_{\frac{1}{2}}(2)$	$\Delta\nu$
K	Hz	cm	Hz	cm	Hz
261.7	228.5	1.7	230.9	1.8	2.4
	228.5	1.8	230.9	1.8	2.4
263.4	228.6	1.6	231.0	1.6	2.4
264.1	228.8	1.7	231.3	1.7	2.5
228.6	1.7	231.1	1.7	2.5	
267.1	228.7	1.6	231.0	1.7	2.3
	228.5	1.6	231.1	1.6	2.6
273.4	229.1	1.4	231.6	1.5	2.5
	229.1	1.3	231.6	1.4	2.5
280.5	229.3	1.3	231.8	1.3	2.5
280.8	229.0	1.4	231.6	1.4	2.4
283.1	229.4	1.6	231.8	1.5	2.4
283.3	230.2	1.2	233.0	1.2	2.8
255.8	228.4		230.8		2.4
	228.4		230.8		2.4
	228.5		230.8		2.3
258.3	228.5		231.0		2.5
261.5	228.5		231.1		2.6
	228.3		230.8		2.5

Table 3-9

The Low Temperature Parameters for DMSO-D_2O Solutions

		DMSO-D_2O	DMSO-D_2O + $NaClO_4$
$\nu_{\frac{1}{2}}(1)$	cm	1.6 ± .2	1.6 ± .2
$\nu_{\frac{1}{2}}(2)$	cm	1.6 ± .2	1.5 ± .2
$\nu_{\frac{1}{2}}$	cm	1.6 ± .2	1.5 ± .2
	Hz	1.2 ± .2	1.1 ± .1
T_2	s	1.7 ± .2	1.8 ± .2
$\Delta\nu$	Hz	2.5 ± .2	2.5 ± .1

Table 3-10

Data used to Determine the

Low Temperature Parameters in Pyridine

T	ν_1	$\nu_{\frac{1}{2}}(1)$	ν_2	$\nu_{\frac{1}{2}}(2)$	$\Delta\nu$
K	Hz	$\frac{1}{2}$ cm	Hz	$\frac{1}{2}$ cm	Hz
240.1	194.3	1.0	206.4	1.0	12.1
	194.4	0.95	206.4	1.15	12.0
246.1	194.3	0.95	206.1	0.95	11.8
255.3	194.4	1.20	205.8	1.15	11.4
265.4	194.4	0.90	205.4	0.90	11.0
	194.4	0.90	205.4	1.00	11.0
278.9	194.4	1.05	205.0	1.00	10.6
	194.5		205.0		10.5
288.1	194.8		205.0		10.2
300.0	194.7		204.6		9.9
	194.8		204.7		9.9
303.7	194.8		204.7		9.9
310.1	194.9		204.5		9.6
315.1	195.1		204.5		9.4

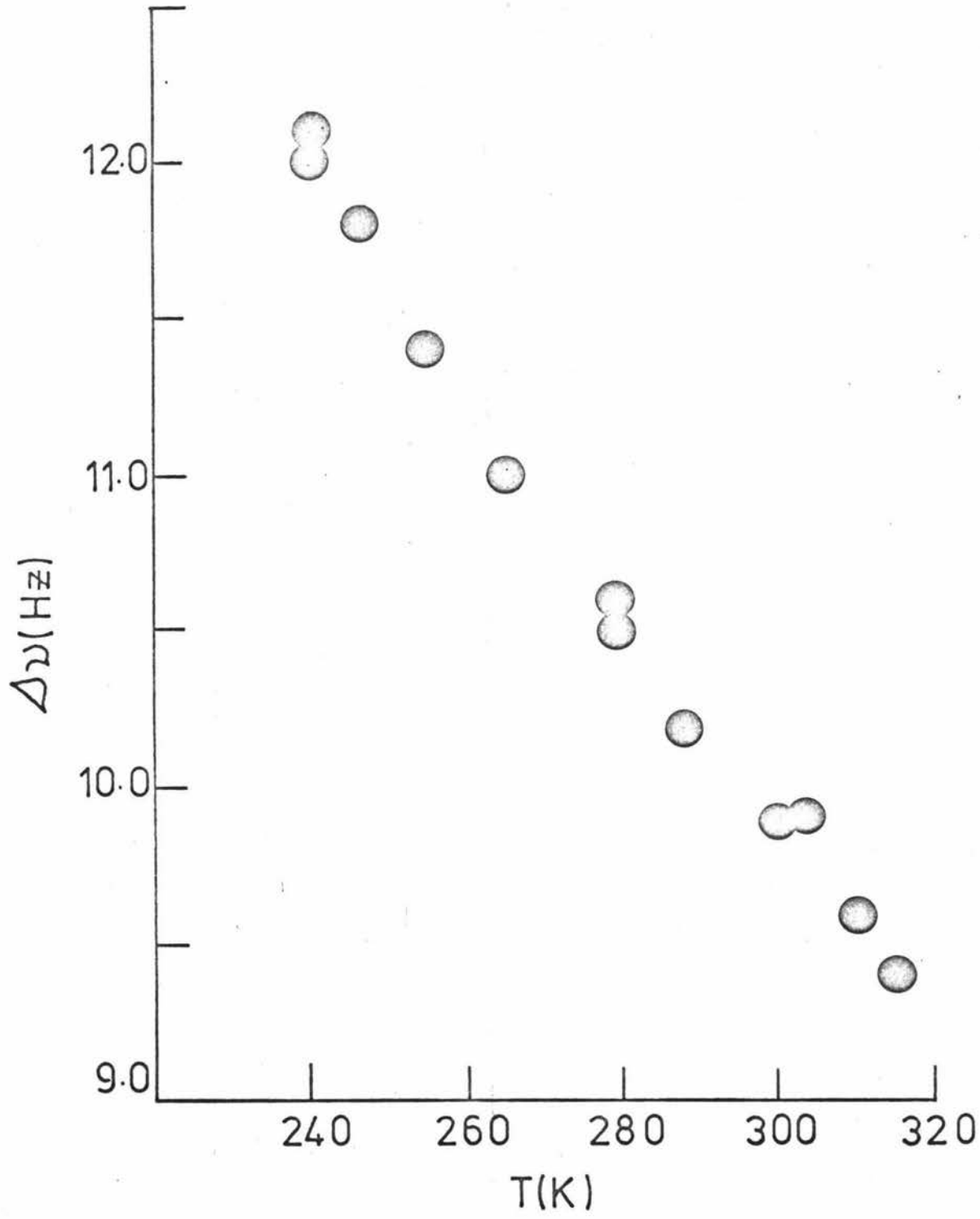

Figure 3-2: Temperature dependence of $\Delta\nu$ for TTD in Pyridine

3.3.9 Low Temperature Spectra for TTD in Toluene

Since the peak separation was too great to allow maximum expansion and satisfactory phasing, the expansion used for all toluene solutions was 1.50 Hz/cm. At very low temperatures the width at half height was consistently .4cm for both peaks (Table 3-11) so this was taken as the optimum value. The resulting relaxation time was $T_2^{-1} = 6.67$ s.

The peak separation decreased with increasing temperature so as described for the spectra obtained from pyridine and acetonitrile solutions regression analysis was used to predict $\Delta\nu$ above the coalescence temperature. The regression line so obtained was

$$\Delta\nu = 41.490 - .084\ (\pm .003)\ T$$

3.4 ANALYSIS OF SPECTRA

3.4.1 Introduction

When a spectrum was digitized, the midpoint of the two peaks was noted and used to find the peak positions, WA and WB which are used as input for the computer. This method of finding WA and WB allows for slight variations in machine stability which is stated to be .4 Hz. At first this was thought to be sufficient to get a reasonable value for τ^{-1} and the relaxation rate $k = \pi/\tau^{-1}$ rad s^{-1}.

Thus with deuterochloroform as solvent, at a temperature of 294.1K when PA = PB = 0.5 and T2A = T2B = 3.0 s. Using values of WA = 206.6 Hz, WB = 211.6 Hz (derived from the spectral mid point, 209.1 Hz, by adding and subtracting 2.5 Hz) the program gave as output a best fit value of $\tau^{-1} = 1.291$ s (i.e. $k = 2.4339\ s^{-1}$) and with residuals of .118335. This output was soon regarded as inadequate since the limits within which the residuals were unchanged were unknown.

The next step was to iterate about the "best-fit" τ^{-1} (as described in Section 2.5.3) so the output became for the same spectrum:

Table 3-11

Data used to Determine the

Low Temperature Parameters in Toluene

T	ν_1	$\nu_{\frac{1}{2}}(1)$	ν_2	$\nu_{\frac{1}{2}}(2)$	$\Delta\nu$
K	Hz	$\frac{1}{2}$cm	Hz	$\frac{1}{2}$cm	Hz
239.3	150.0	.4	171.5	.4	21.5
243.5	151.1	.4	172.0	.4	20.9
249.4	152.3	.4	172.8	.4	20.5
	152.5	.4	172.9	.4	20.4
256.1	153.8	.45	173.8	.47	20.0
	153.9	.43	173.7	.5	19.8
268.8	156.1	.5	174.8	.6	18.7
	156.1		175.0		18.9
273.5	157.1		175.5		18.4
288.8	160.0		177.2		17.2

$\tau^1(s)$	$k(s^{-1})$	Residuals
1.285	2.4458	.118358
1.287	2.4420	.118346
1.289	2.4382	.118338
1.291	2.4344	.118335
1.293	2.4306	.118336

and now the verified best-fit values became $\tau^1 = 1.291 \pm .002$ s, $k = 2.434 \pm .004\ s^{-1}$.

Unfortunately the NMR spectrometer has a specified resolution of .3 Hz so the possible error in $\Delta\nu$, the peak separation, could be $\pm$ .6 Hz. When this error is combined with errors in the midpoint measurement (.2 Hz minimum error) the errors in WA and WB could be highly significant. To counteract these accumulated errors we decided to vary WA, WB and hence WB-WA until the residuals from the theoretical spectrum were at a minimum.

3.4.2 Variation of $\Delta\nu$

Initially the policy of varying $\Delta\nu$ was (in the light of later experience) carried out rather haphazardly by varying WA or WB by 0.1 Hz at a time. The final procedure was to vary WA and WB systematically e.g. if the values determined from the experimental spectrum were WA = 206.8 Hz and WB = 211.9 Hz then the following values of WA and WB will be tried:

WA = 206.7 Hz	WB = 211.8, 211.9, 212.0 Hz
WA = 206.8 Hz	WB = 211.8, 211.9, 212.0 Hz
WA = 206.9 Hz	WB = 211.8, 211.9, 212.0 Hz

When this system is pursued for each variation in WA and WB which leads to lower residuals then the following results were obtained.

Chloroform-d_1 T = 294.1K T2A = T2B = 2.9 s. PA = PB = 0.5

W_A(Hz)	W_B(Hz)	τ^1(s)	k(s^{-1})	Residuals
206.4	211.6	1.218	2.579	.137847
	211.7	1.151	2.730	.114710
	211.8	1.109	2.831	.122557
206.5	211.6	1.273	2.469	.114548
	211.7	1.200	2.619	.081715
	211.8	1.162	2.704	.091982
206.6	211.6	1.319	2.381	.115874
	211.7	1.244	2.524	.084792
	211.8	1.211	2.595	.094047

Once the block method of checking WA, WB and WB-WA had been set up it was used for all variation in $\Delta\omega$. Such a method involves a large amount of computing but it is comprehensive and ensures the best possible values for WA and WB and hence, it is presumed, the best estimate of the parameter of interest, τ^1.

Iteration about τ^1 for error determination did not always give residual differences from which the error could readily be estimated so in some cases graphical methods were needed. Both methods are demonstrated for the following spectrum (see Fig. 3-3).

Chloroform-d_1 T = 294.1AK T2A = T2B = 2.9 s PA = PB = .5

WA = 206.5 Hz WB = 211.7 Hz

^{1}(s)	k(s^{-1})	Residuals
1.196	2.628	.081725
1.198	2.623	.081716
1.200	2.619	.081715
1.202	2.615	.081721

Hence for spectrum A at 294.1K using chloroform-d_1 as solvent the rate of rotation is k = 2.619 $\pm$ .005 rad s^{-1}.

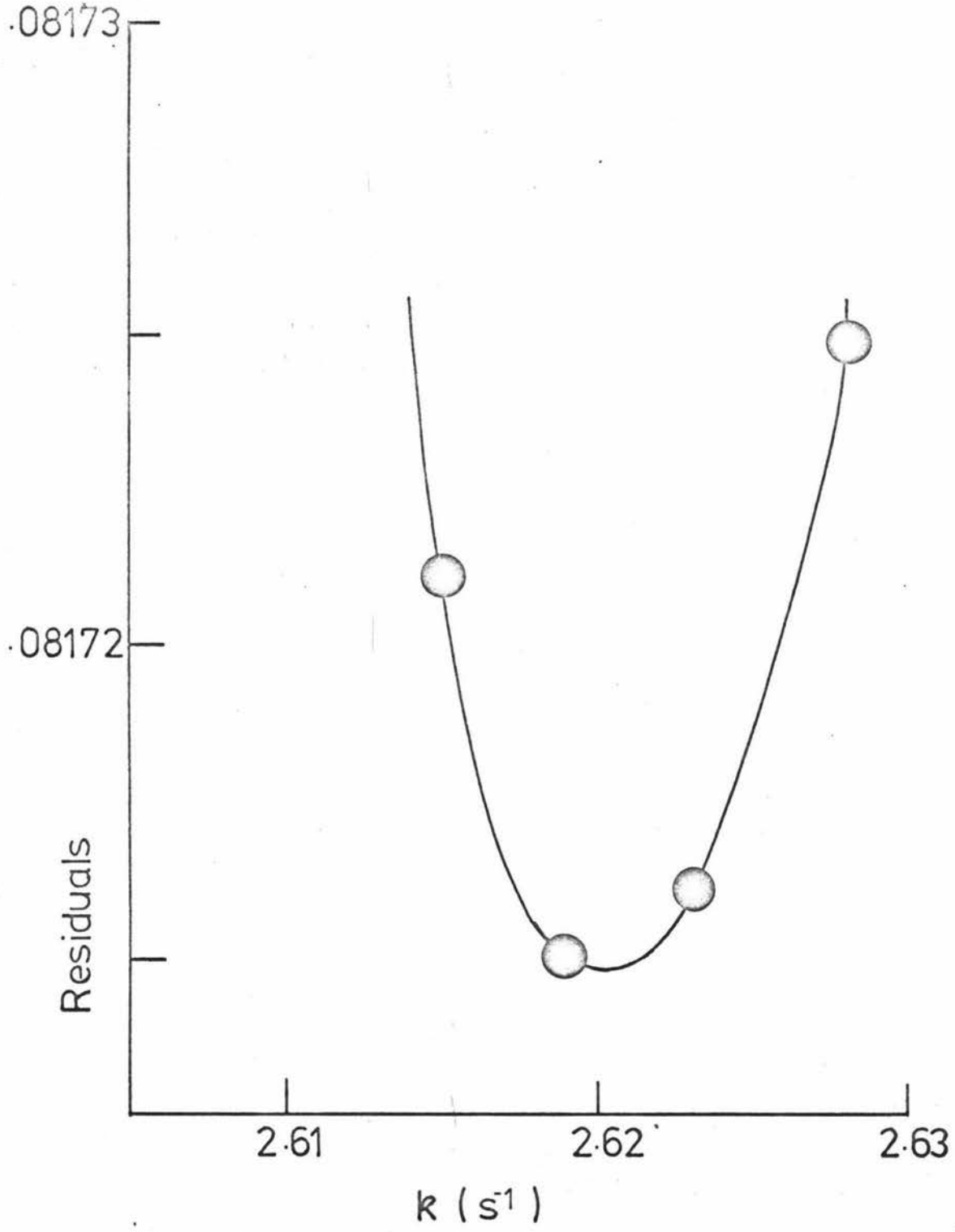

Figure 3-3: Residuals versus rate constant at 294 K for TTD in Chloroform

The variation of $\Delta\omega$ has however a very large drawback when used above the coalescence temperature. Below the coalescence temperature as the minimum in Residuals is pursued the peak separation $\Delta\omega$ = WB - WA rarely varies by more than twice the statistical error from the mean value of $\Delta\omega$. This can be demonstrated with chloroform-d_1 where $\Delta\omega$ = 5.1 $\pm$ .1 Hz and the individual measurements from which $\Delta\omega$ was calculated usually by between 5.0 - 5.2 Hz and never outside 4.9 - 5.3 Hz.

Unfortunately if the minimum in Residuals is pursued above coalescence temperature the value given WB - WA will not correspond so closely to the mean value of $\Delta\omega$, and the magnitude of τ^1 (and k) no longer is related to the temperature. In Table 3-12 and Figure 3-4, if k was an exponential function of temperature, the curve for k versus T would be a simple upward curve. Once such results as are given in Table 3-12 had been found for several solvents it was realised that the difference, WB - WA, in peak position was no longer influential in determining the best fit of theoretical and experimental lineshapes but that the mean of WA and WB, $(WA + WB)/2$, was now the parameter which most affected Residuals. Above coalescence the peak separation, WB - WA, was held constant or held to the temperature dependent equation but was moved along the frequency range e.g. 206.8, 211.9; 206.9, 212.0; 207.0, 212.1. The change in the results above coalescence is remarkable and very satisfactory (Fig. 3-4). The variation in $\Delta\omega$ was now felt to be complete and the same method was applied to the other solvents i.e. below coalescence find the positions WA, WB for which the residuals are lowest but above coalescence hold WB - WA constant and, by varying the midpoint of the frequencies WA and WB, find the lowest residuals consistent with a set value of WB - WA. Using this procedure the difference between the peak positions measured from spectra and those from the computer analyses varied between 0 Hz and 0.4 Hz i.e. within the experimental error of the measurements. (For toluene, the difference was between 0 Hz and 0.6 Hz;

Table 3-12

A. Minimum Residuals Analyses for Acetonitrile

T	ν_A	ν_B	$\Delta\nu$	τ^1	k	Residuals
K	Hz	Hz	Hz	s	rad s^{-1}	
289.2	202.7	206.3	3.6	3.772	0.8330	0.105295
293.6	202.6	206.4	3.8	1.628	1.930	0.054845
296.1	202.7	206.6	3.9	0.963	3.261	0.071396
300.3	202.7	206.5	3.8	0.663	4.735	0.081403
	202.6	206.4	3.8	0.721	4.358	0.049617
302.1	202.7	206.7	4.0	0.588	5.338	0.044250
303.5	202.6	206.9	4.3	0.466	6.741	0.062423
	202.8	206.7	3.9	0.559	5.612	0.062854
306.0	202.7	207.7	5.0	0.278	11.28	0.041412
308.9	202.7	208.0	5.3	0.244	12.83	0.032084
315.4	201.6	208.6	7.0	0.126	24.77	0.062307
322.2	202.6	206.9	4.3	0.156	20.11	0.087430
324.0	203.4	206.3	2.9	0.304	10.30	0.055834

B. Standardised Values for $\Delta\nu$ above the Coalescence Temperature

T	ν_A	ν_B	$\Delta\nu$	τ^1	k	Residuals
K	Hz	Hz	Hz	s	rad s^{-1}	
306.0	203.2	207.3	4.1	0.400	7.857	0.099563
308.9	203.3	207.4	4.1	0.394	7.970	0.109750
315.4	203.1	207.3	4.2	0.318	9.88	0.143353
322.2	202.6	206.9	4.3	0.156	20.11	0.087430
324.0	202.7	207.0	4.3	0.141	22.15	0.064558

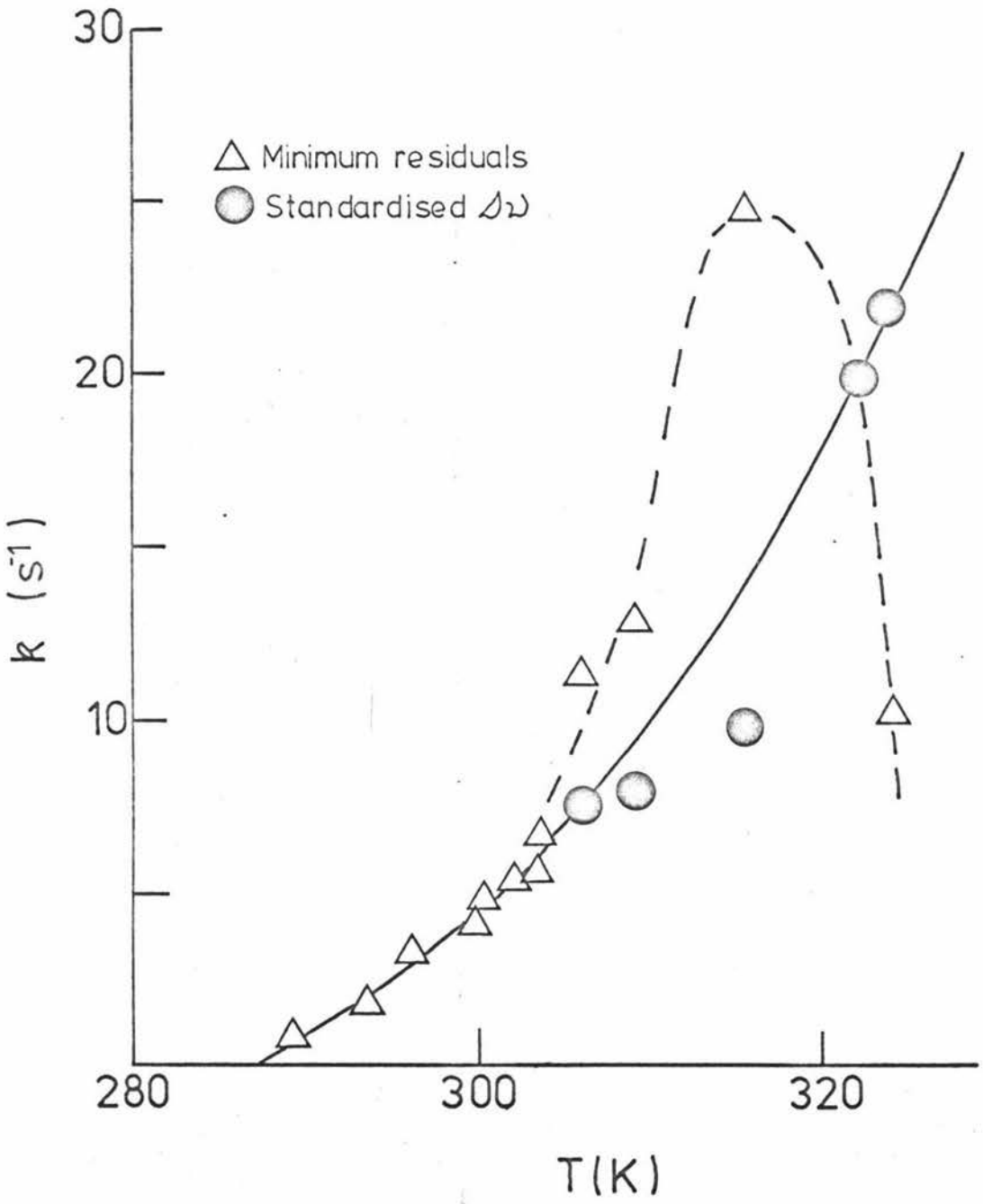

Figure 3-4: Changes in k with temperature and methods of computer analysis

however this was within the experimental error for the lower frequency expansion used in these studies.)

3.4.3 Variation in T_2^1

Once the methods for varying $\Delta\omega$ had been systematised the treatment of the other solvent systems was much more straightforward but knowing that T_2^1 was an experimentally determined parameter with a large percentage error (10%) it was decided, for chloroform, to select four temperatures, set T_2^1 to its value at the error limits as well as the mean and observe any changes in τ^1. From the data presented in Table 3-13, at a given temperature τ^1 decreases in magnitude as T_2^1 is increased. Further analysis must be done to discover if the change in T_2^1 alters anything other than the intercept in an Arrhenius equation plot.

3.5 RESULTS

Using the procedure described in Section 3.4.2 and the slow exchange parameters in Table 3-14, the best-fit values for τ^1 and k were calculated and are summarised in Tables 3-15 to 3-21. Plots of $\log_{10}k$ versus T for each solvent system are shown in Figures 3-5 to 3-11. The data for each system could be fitted by a straight line and appear to obey the empirical Arrhenius equation (Eqn. 1-18) which, in logarithmic form, becomes:

$$\log_{10}k = \log_{10}A - E_a/2.30RT \qquad 3\text{-}4$$

in which E_a, the activation energy for the rotation about the C-N bond, does not vary with temperature. The Eyring equation, derived from transition state theory was given as Equation 1-19 and can also be written as

$$\log_{10}k = \log (k_BT/h) - G^{\neq}/2.303RT \qquad 3\text{-}5$$

where k_B is the Boltzmann constant

T is the absolute temperature

R is the gas constant

h is Planck's constant

Table 3-13

Variation of T_2^{-1} for TTD in Chloroform

T_2^{-1}	T	ν_A	ν_B	$\Delta\nu$	τ^{-1}	k	Residuals
s	K	Hz	Hz	Hz	s	s^{-1}	
2.6	294.1	206.6	211.6	5.0	1.328	2.366	0.068173
	300.0	206.1	211.1	5.0	0.618	5.079	0.073393
	312.2	205.9	211.0	5.1	0.162	19.34	0.066078
	320.8	205.4	210.5	5.1	0.064	48.35	0.057552
2.9	294.1	206.6	211.7	5.1	1.184	2.654	0.068834
	300.0	206.1	211.1	5.0	0.599	5.24	0.073417
	312.2	205.9	211.0	5.1	0.166	18.90	0.063447
	320.8	205.4	210.5	5.1	0.069	44.9	0.057424
3.2	294.1	206.5	211.7	5.2	1.067	2.943	0.068672
	300.0	206.0	211.0	5.0	0.583	5.400	0.085992
	312.2	205.9	211.0	5.1	0.169	18.49	0.061206
	320.8	205.4	210.5	5.1	0.74	41.90	0.057446

Table 3-14

Slow Exchange Parameters

Solvent	$\Delta\omega$ Hz	T_2^{-1} s^{-1}
Acetone	1.4 ± 0.1	2.9 ± 0.3
Acetonitrile	0.726 + 0.011 (± 0.002)T	3.4 ± 0.2
Chloroform	5.1 ± 0.1	2.9 ± 0.3
DMSO-water	2.5 ± 0.2	1.7 ± 0.2
DMSO-water + $NaClO_4$	2.5 ± 0.1	1.8 ± 0.2
Pyridine	19.712 - 0.033 (± 0.002)T	2.7 ± 0.3
Toluene	41.490 - 0.084 (± 0.003)T	6.7 ± 0.2

Table 3-15

Kinetic Data for TTD in Acetone

A. 7.8 w/v% TTD in Acetone

T K	k s^{-1}	$10^3\ T^{-1}$ K^{-1}	$\log_{10}k$
279.9	0.126 ± .002	3.572	-0.900 ± .007
283.5	0.199 ± .001	3.528	-0.701 ± .002
287.9	0.871 ± .003	3.473	-0.060 ± .002
294.1	2.88	3.400	0.459
300.3	7.89	3.330	0.897
300.3	10.61	3.330	1.026
300.3	5.99	3.330	0.777
303.7	7.15	3.293	0.854

Regression line $\log_{10}k = 24.4 - 7.1\ (\pm\ 0.6)\ \frac{1}{T}$

B. 3.6 w/v% TTD in Acetone

T K	k s^{-1}	$10^3\ T^{-1}$ K^{-1}	$\log_{10}k$
278.5	0.065 ± .002	3.591	-1.19 ± .02
287.9	0.970 ± .002	3.473	-0.0132 ± .0009
294.1	2.912	3.400	0.464
300.3	7.86	3.330	0.895
303.7	9.26	3.293	0.967

Regression line $\log_{10}k = 25.2 - 7.3\ (\pm\ 0.7)\ \frac{1}{T}$

Regression line from A and B $\log_{10}k = 24.7 - 7.2\ (\pm\ 0.4)\ \frac{1}{T}$

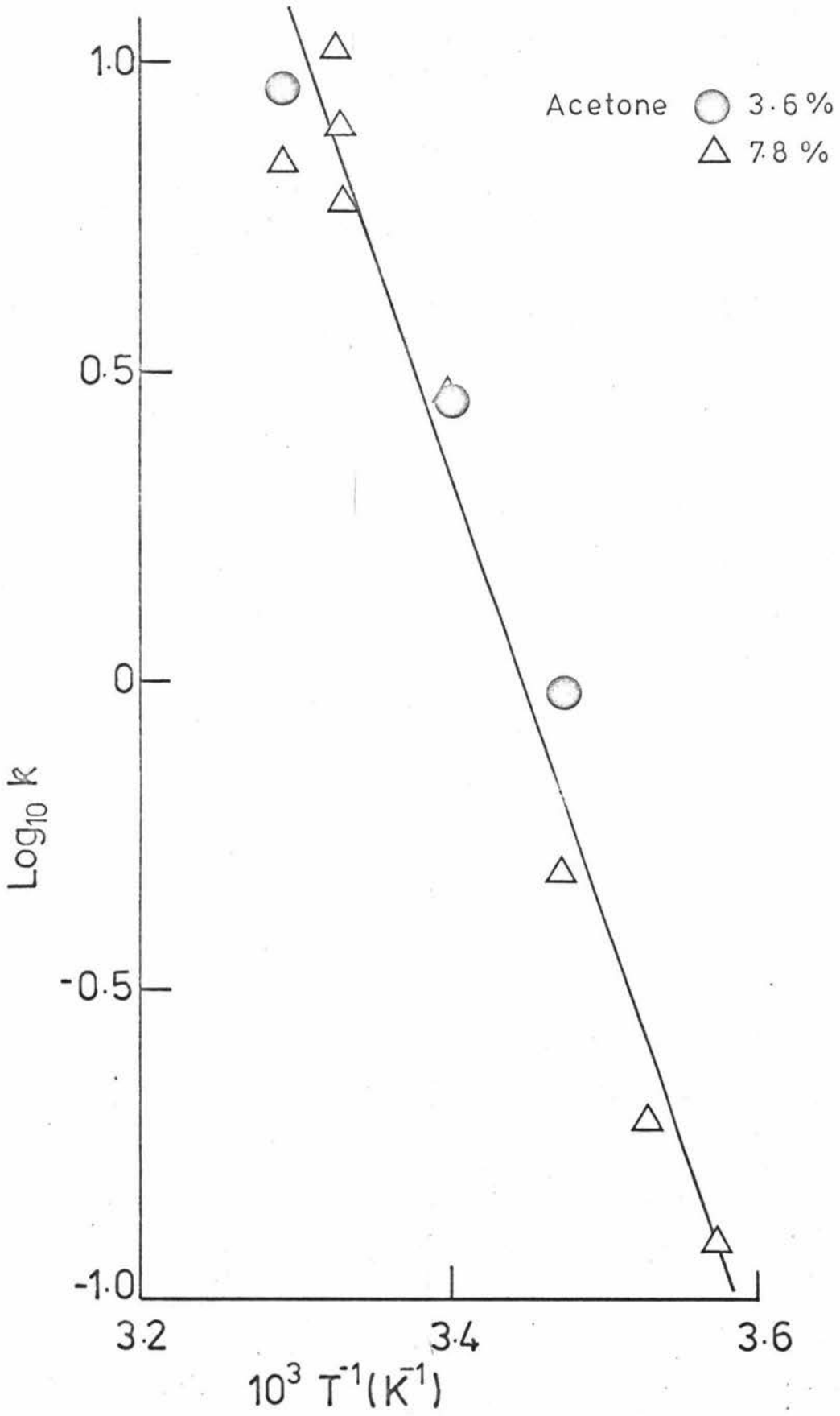

Figure 3-5: $Log_{10} k$ versus T^{-1} for TTD in Acetone

Table 3-16

Kinetic Data for TTD in Acetonitrile

T K	k s^{-1}	$10^3\ T^{-1}$ K^{-1}	$\log_{10}k$
289.2	0.834 ± .003	3.4578	-0.079 ± .002
293.6	1.929 ± .003	3.4059	0.2853 ± .0007
296.1	3.260 ± .005	3.3772	0.5132 ± .0007
300.3	4.738 ± .006	3.3330	0.6756 ± .0007
300.3	3.358 ± .005	3.3330	0.5260 ± .0007
302.1	5.334 ± .006	3.3101	0.7270 ± .0005
303.5	6.740 ± .005	3.2948	0.8287 ± .0004
303.5	5.613 ± .005	3.2948	0.7492 ± .0004
306.0	7.86	3.2679	0.895
308.9	7.97	3.2372	0.902
315.4	9.88	3.1705	0.995
322.2	20.1	3.1055	1.301
324.0	22.1	3.0864	1.345

Regression line $\log_{10}k = 11.9 - 3.4\ (\pm\ 0.4)\ \frac{1}{T}$

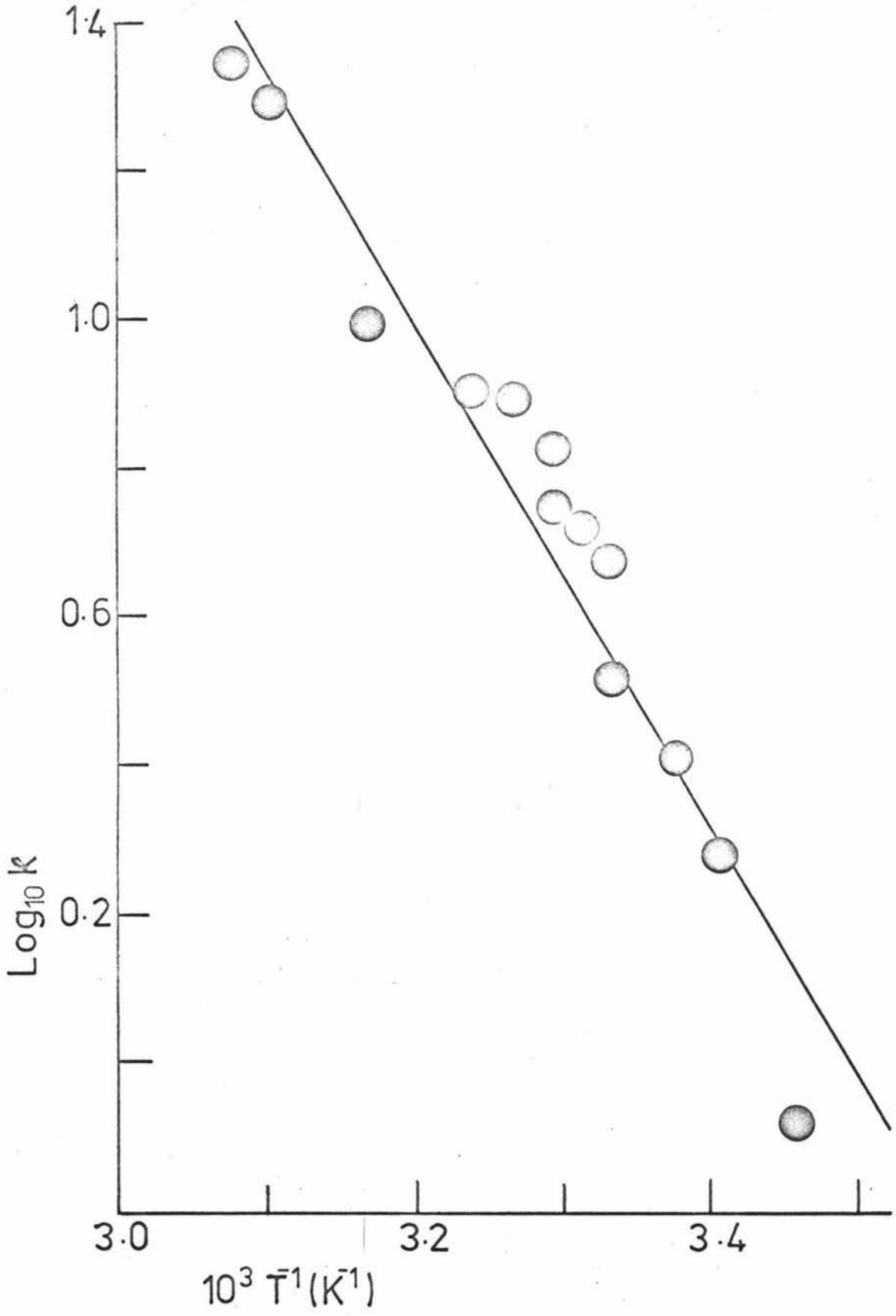

Figure 3-6: $Log_{10} k$ versus T^{-1} for TTD in Acetonitrile

Table 3-17

Kinetic Data for TTD in Chloroform

T K	k s^{-1}	$10^3\ T^{-1}$ K^{-1}	$\log_{10}k$
288.1	1.042 ± .002	3.471	0.0178 ± .0009
294.1	2.619 ± .005	3.400	0.418 ± .001
294.1	2.654 ± .006	3.400	0.424 ± .001
300.0	5.24 ± .02	3.333	0.719 ± .002
300.0	5.23 ± .01	3.333	0.7185 ± .0008
303.7	6.78 ± .01	3.293	0.8312 ± .0007
310.6	15.24	3.220	1.183
310.6	14.70	3.220	1.167
312.2	18.90	3.203	1.277
315.1	22.86	3.174	1.359
320.8	44.9	3.117	1.652

Regression line $\log_{10}k = 15.4 - 4.4\ (\pm\ 0.1)\ \frac{1}{T}$

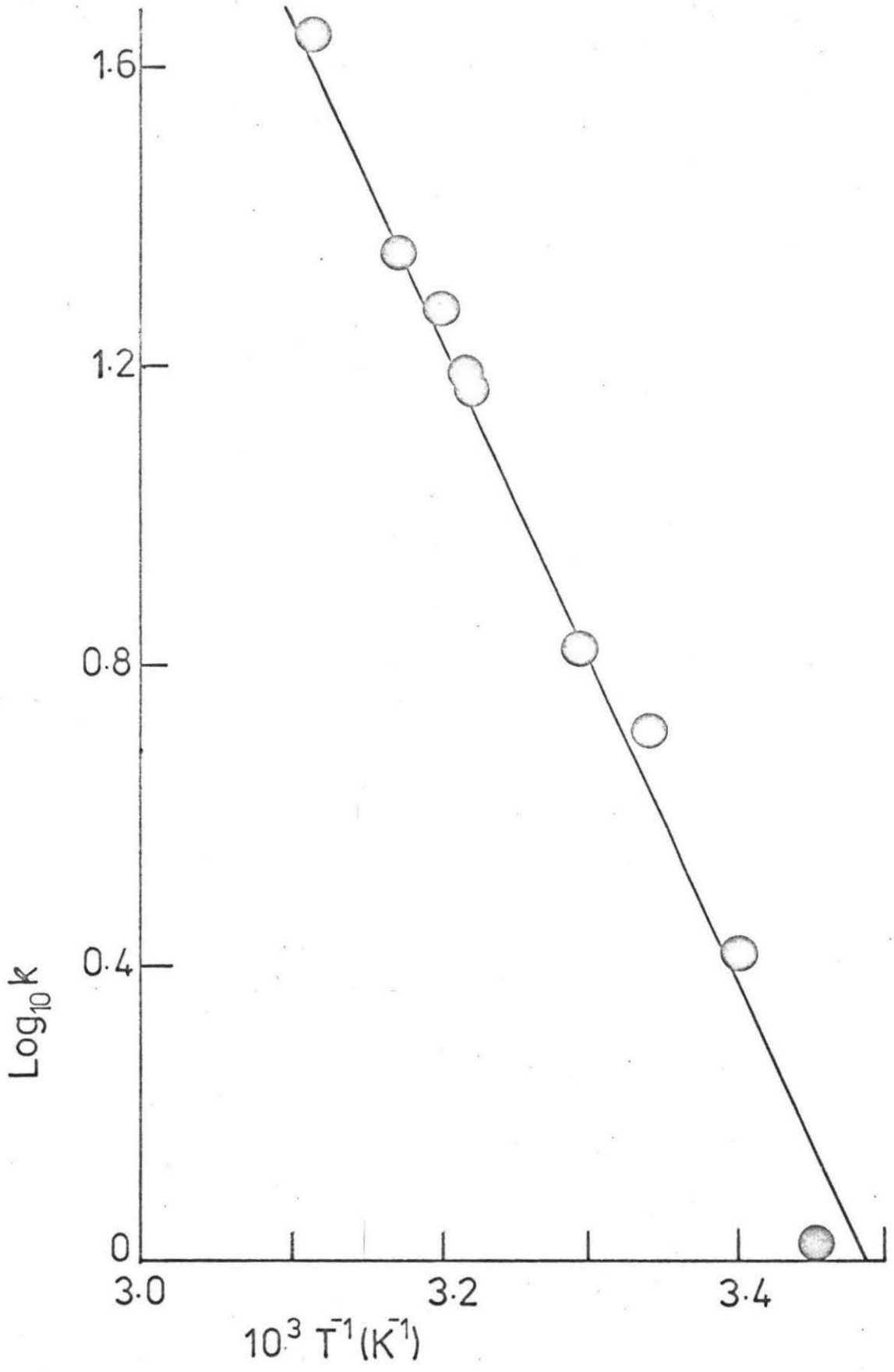

Figure 3-7: $Log_{10} k$ versus T^{-1} for TTD in Chloroform

Table 3-18

Kinetic Data for TTD in DMSO-Water

T K	k s^{-1}	$10^3\ T^{-1}$ K^{-1}	$\log_{10}k$
300.5	0.699 ± .002	3.3277	-0.155 ± .002
302.1	2.080 ± .006	3.3101	0.318 ± .002
303.7	1.202 ± .004	3.2927	0.080 ± .002
305.1	1.704 ± .004	3.2776	0.231 ± .002
308.0	2.805 ± .005	3.2467	0.448 ± .001
310.1	3.300 ± .004	3.2247	0.5185 ± .0005
312.6	5.13	3.1989	0.710
317.0	6.59	3.1545	0.819
319.2	11.47	3.1328	1.060
322.2	9.004	3.1055	0.9544

Regression line $\log_{10}k = 16.0 - 4.8\ (\pm\ .5)\ \frac{1}{T}$

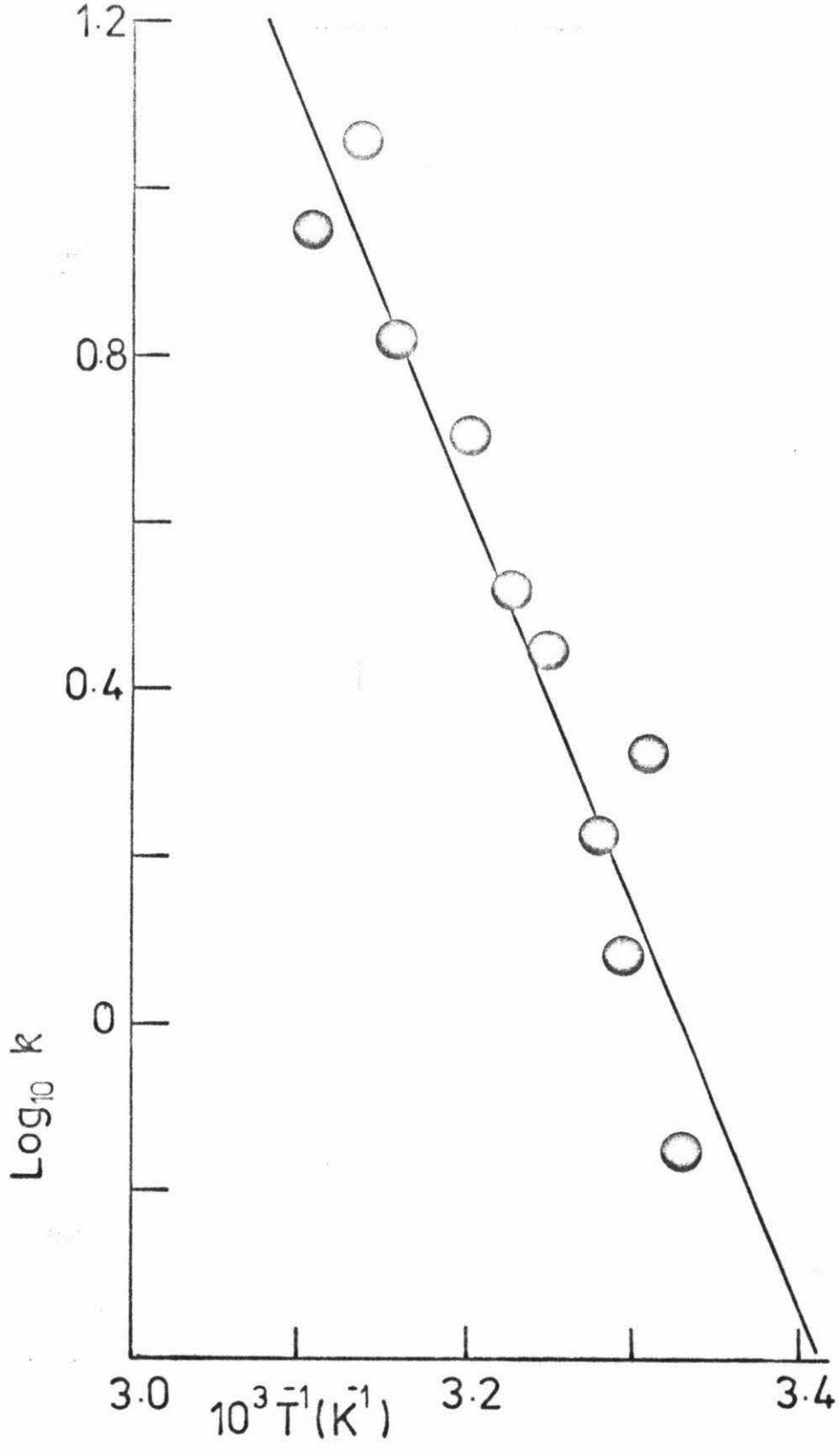

Figure 3-8: $Log_{10}k$ versus T^{-1} for TTD in DMSO-d_6-D_2O

Table 3-19

Kinetic Data for TTD in DMSO-Water and $NaClO_4$

T K	k s^{-1}	$10^3\ T^{-1}$ K^{-1}	$\log_{10}k$
294.7	.468 ± .003	3.3932	- .330 ± .003
300.5	1.212 ± .003	3.3277	+ .0845 ± .0002
301.2	.982 ± .002	3.3200	- .008 ± .001
303.4	1.16 ± .01	3.2959	+ .065 ± .004
304.8	1.688 ± .003	3.2808	.2274 ± .0008
308.2	3.361 ± .007	3.2446	.5264 ± .0009
310.3	2.643 ± .007	3.2226	.422 ± .001
312.4	5.15	3.2010	.712 ± .002
316.9	7.98	3.1555	.901 ± .002
317.2	7.80	3.1525	.892 ± .002
317.2	8.16	3.1525	.912 ± .002
319.5	9.06	3.1298	.957 ± .002
322.0	15.2	3.1055	1.182 ± .003

Regression line $\log_{10}k = 17.3 - 5.2\ (\pm\ .2)\ \frac{1}{T}$

Combined Regression line for both DMSO-water solutions

$$\log_{10}k = 16.6 - 5.0\ (\pm\ .2)\ \frac{1}{T}$$

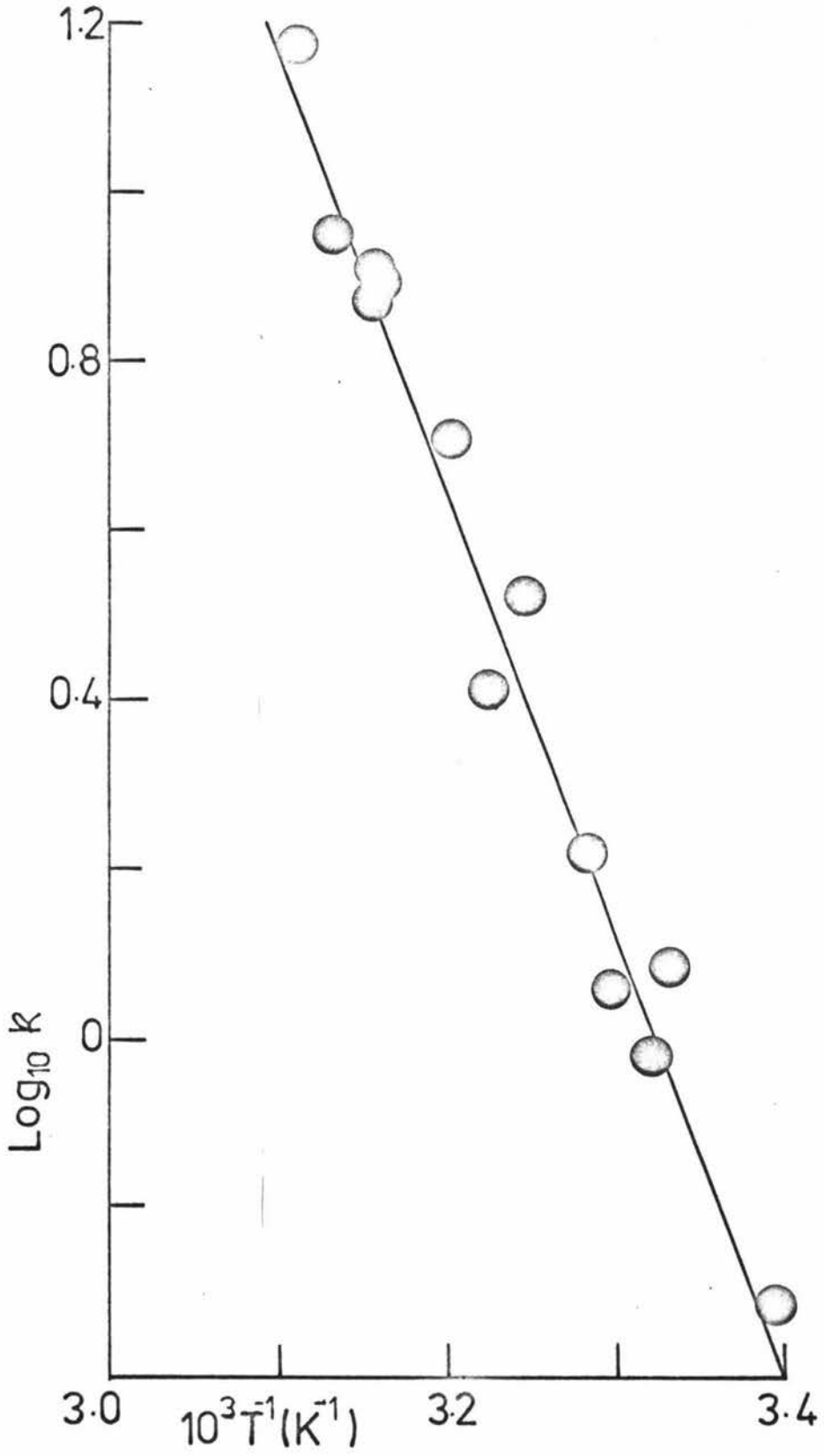

Figure 3-9: $\log_{10} k$ versus T^{-1} for TTD in DMSO-d_6-D_2O + $NaClO_4$

Table 3-20

Kinetic Data for TTD in Pyridine

T K	k s^{-1}	$10^3\ T^{-1}$ K^{-1}	$\log_{10} k$
288.1	.925 ± .003	3.471	- .034 ± .002
300.0	4.580 ± .008	3.333	.6609 ± .0008
300.0	5.42 ± .02	3.333	.734 ± .002
303.7	6.808 ± .005	3.293	.8330 ± .0003
310.1	13.11 ± .02	3.225	1.1176 ± .0008
315.1	18.82 ± .08	3.173	1.275 ± .003
320.8	31.4	3.117	1.497
327.6	57.1	3.053	1.757
333.9	107.4	2.995	2.031

Regression line $\log_{10} k = 14.3 - 4.1\ (\pm\ 0.1)\ \frac{1}{T}$

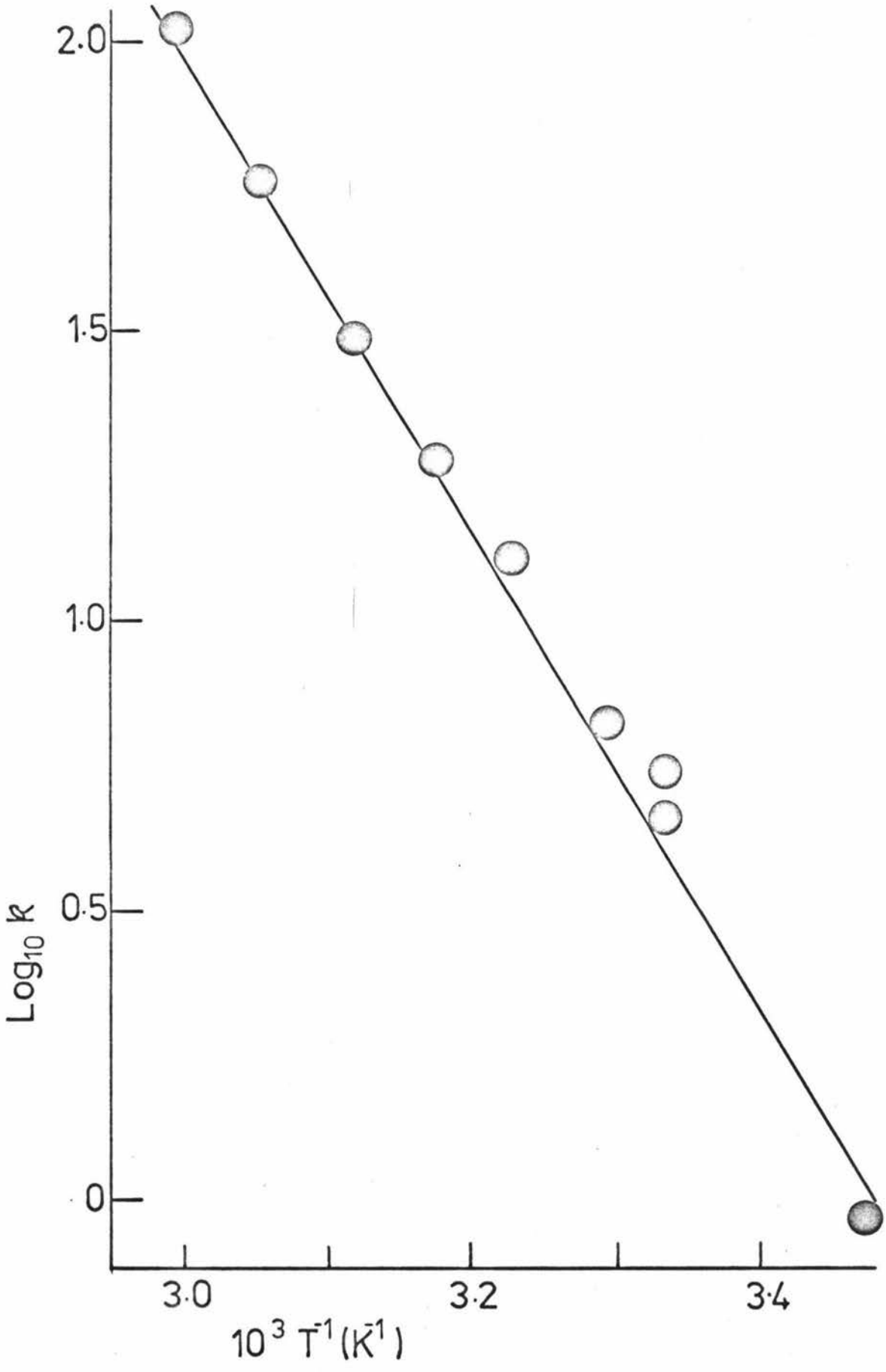

Figure 3-10: $Log_{10}k$ versus T^{-1} for TTD in Pyridine

Table 3-21

Kinetic Data for TTD in Toluene

T K	k s^{-1}	$10^3\ T^{-1}$ K^{-1}	$\log_{10}k$
294.8	13.19 ± .03	3.392	1.120 ± .001
297.9	17.80 ± .02	3.357	1.250 ± .005
300.2	24.9 ± .2	3.331	1.396 ± .003
300.2	24.9 ± .1	3.3201	1.367 ± .002
308.0	45.7	3.247	1.660
313.8	78.6	3.187	1.895
322.5	103.9	3.101	2.017
325.9	110.8	3.068	2.043
330.0	165.4	3.030	2.219

Regression line $\log_{10}k = 11.0 - 2.9\ (\pm\ .2)\ \frac{1}{T}$

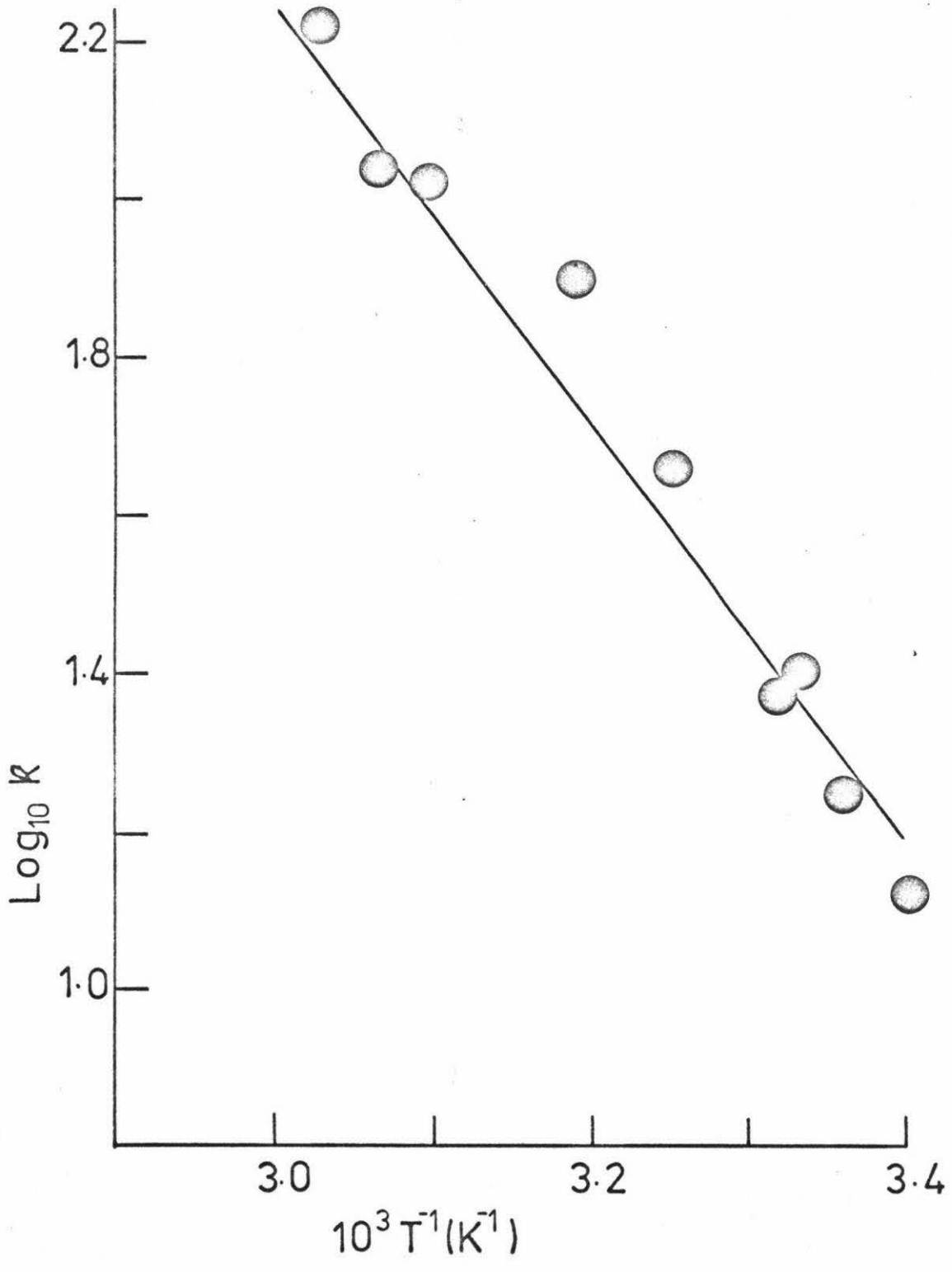

Figure 3-11: $Log_{10}\, k$ versus T^{-1} for TTD in Toluene

Since $E_a = H^{\neq} + RT$ 3-6

and $G^{\neq} = H^{\neq} - T^{\neq}$ 3-7

all the thermodynamic parameters can be found from a plot of $\log_{10}k$ versus 1/T. The best fit for the data can be obtained by carrying out regression analysis on the plot of $\log_{10}k$ versus 1/T.

3.6 DISCUSSION

In the NMR spectra of N,N,N',N'-tetramethylthiodicarbonic diamide at low temperatures, there are only two methyl peaks which coalesce, as the temperature rises, to a single peak so the carbon-nitrogen bonds (and both sets of methyl groups) have been assumed to be equivalent and the equations describing two site exchange have been used as described in Section 3.4 to fit the spectra.

3.6.1 Changes in Spectra and Solutions

In acetone and toluene solutions some changes with time occurred in the NMR samples. Thus in both solutions of acetone the colour of the solution visibly darkened with time but the sample which contained less TTD remained paler than the more concentrated sample. Despite these colour changes there was no perceptible change in the NMR spectra of TTD in acetone; the only difference between the spectra for the two concentrations of TTD in acetone was a lessening in methyl peak intensity for the more dilute solution although the colour difference would have suggested major alterations in the spectrum. The colouration could be explained by decomposition to a product with a high extinction, the equilibrium for which lies well towards the original compound, or by some form of solvent association with TTD. No mention of such changes has been previously reported[45].

Initially the spectra for TTD in toluene showed the familiar pattern for the methyl peaks of two separate peaks at low temperatures which coalesced to a single peak at higher temperatures but after a month two

new small peaks had developed in the low temperature spectra. These peaks, which also coalesced and affected the lineshapes obtained in the intermediate exchange region, appeared as satellites on the original methyl peaks. To obtain spectra to which the two site exchange model could be fitted, a fresh sample of TTD in toluene was prepared and the spectra were run within two days as described in Section 3.2. The changes in the NMR spectra, however, were not accompanied by a colour change similar to those observed in acetone.

In both acetone and toluene the major methyl peak positions were unaltered by such effects and were the same whether measured for a freshly prepared sample or one that had begun to exhibit colour or spectral changes.

In contrast to the apparent instability of TTD in acetone and toluene, the spectra and samples for solutions of TTD in acetonitrile, pyridine, chloroform and DMSO-water were unchanged after three months. Considering the reactivity of these solvents and the general inertness of toluene, this stability is surprising.

3.6.2 Errors in Temperature Measurement

As discussed in Section 2.2.2 the temperature gradients in the NMR probe range from 0.2 K cm^{-1} at 303 K to 0.6 K cm^{-1} at 343 K when the ambient temperature is 300 K, so similar gradients would be expected at correspondingly low temperatures. However, such temperature variations in the probe should not greatly affect the temperature measurements since these are made under the same conditions for both sample and standard by an immovable receiver coil which registers the absorption signals from a very small volume of sample. It seems therefore that an error limit of $\pm$ 0.7 K (quoted in Section 2.2.3) is reasonable.

3.6.3 Changes in $\Delta\nu$ and T_2^{-1}

In Table 3-14, the slow exchange parameters for solutions of TTD have been listed. The largest changes with temperature in $\Delta\nu$ (the methyl

Table 3-22

Kinetic Data for TTD in Chloroform when T_2^{-1} is Varied

T_2^{-1} / s	T / K	k / s^{-1}	$10^3\ T^{-1}$ / K^{-1}	$\log_{10} k$
2.6	294.1	2.366 ± 0.006	3.400	0.374 ± 0.001
	300.0	5.08 ± 0.01	3.333	0.706 ± 0.001
	312.2	19.34	3.203	1.286
2.9	294.1	2.654 ± 0.006	3.400	0.424 ± 0.001
	300.0	5.24 ± 0.02	3.333	0.719 ± 0.002
	312.2	18.90	3.203	1.277
	320.8	44.90	3.117	1.652
3.2	294.1	2.943 ± 0.006	3.400	0.469 ± 0.001
	300.0	5.40 ± 0.02	3.333	0.732 ± 0.001
	312.2	18.49	3.203	1.267
	320.8	41.90	3.117	1.622

Table 3-23

Thermodynamic Parameters for TTD in Chloroform at Various Values for T_2^1

T_2^1 s	E_a kJ mol^{-1}	$\Delta G^{\neq}_{298}$ kJ mol^{-1}	$\Delta H^{\neq}_{298}$ kJ mol^{-1}	$\Delta S^{\neq}_{298}$ JK^{-1} mol^{-1}
2.6	88.1 ± 1.1	69.6	85.6 ± 1.1	53.5 ± 3.8
2.9	82.9 ± 0.2	69.4	80.4 ± 0.2	36.9 ± 0.8
3.2	78.1 ± 0.6	69.5	75.6 ± 0.6	20.4 ± 1.9

peak separation) occurred in the solvents pyridine and toluene, and, in both cases, $\Delta\omega$ decreased significantly with increasing temperature. In other solvents, except for acetonitrile where $\Delta\omega$ showed a small increase as temperature increased, $\Delta\omega$ was effectively constant. Wilson reported a very small increase in the peak separation of TTD in chloroform solutions as temperature increased[44] although these measurements were made using a 100 MHz NMR spectrometer. It is interesting that major changes in $\Delta\omega$ are associated with the aromatic solvents and suggests that specific solvent-solute interactions are occurring in these solvents.

It has been reported[23,46] that inaccurate values of T_2^{-1} can lead to larger values for $\Delta S^{\neq}$. To test this effect the thermodynamic parameters for TTD in chloroform were calculated for a range of values of T_2^{-1} (Tables 3-22, 3-23). It can be seen that a decrease in T_2^{-1} resulted in a significant increase in both $\Delta H^{\neq}_{298}$ and $\Delta S^{\neq}_{298}$ but left $\Delta G^{\neq}_{298}$ virtually unaltered.

3.6.4 Comparison with Previous Results

The only previous lineshape study of N,N,N',N'-tetramethylthiodicarbonic diamide[44] was carried out in chloroform as solvent and the values determined for the thermodynamic parameters are given below with those determined in this study.

Table 3-24

Ref	E_a kJ mol^{-1}	log A	$\Delta G^{\neq}$ kJ mol^{-1}	$\Delta H^{\neq}$ kJ mol^{-1}	$\Delta S^{\neq}$ J K^{-1} mol^{-1}
44[a]	69.0 ± 1.7	12.9	66.9 ± 0.4	66.5 ± 1.7	- 1.9 ± 8.4
Our results[b]	84.2 ± 1.9	15.4	69.3	81.7 ± 1.9	+42.0 ± 8.0

[a] $\Delta G^{\neq}$, $\Delta H^{\neq}$ and $\Delta S^{\neq}$ are calculated at 302 K

[b] $\Delta G^{\neq}$, $\Delta H^{\neq}$ and $\Delta S^{\neq}$ calculated at 298 K

The two sets of values in Table 3-24 differ significantly. The 2.4 kJ mol^{-1} difference for $\Delta G^{\neq}$ is particularly surprising since it is outside

the expected experimental error. In order to demonstrate the validity of the experimental procedures used and that errors were not produced by the input calculations for the theoretical lineshape an NMR analysis was carried out on the well-studied system, N,N-dimethylcarbamic chloride [47,48,49]; as described in Section 4-3 , excellent agreement was obtained with the best literature values[48,49], a result that provides confidence in the methods used in the studies on TTD.

Wilson reports a value of 0.354s for T_2 (i.e. $T_2^1/2$) which is slightly less than our value of 0.461s while the separation of the methyl peaks is given as 0.081 ppm compared to the separation of 0.085 ppm which we measured. As discussed earlier a lower value of T_2 (and hence T_2^1) could give rise to significantly larger values of $\Delta H^{\neq}$ and $\Delta S^{\neq}$. However the direction of the effect is the reverse of that required to explain the difference between the results of the present study and those obtained by Wilson.

Although there is a good deal of error involved in such a procedure, when the data from the $\log_{10}k$ versus 1/T plot in the paper by Wilson is replotted and the slope calculated larger values of E_a (74.6 kJ mol^{-1}) and $\Delta H^{\neq}$ (72.1 kJ mol^{-1}) are obtained. Insufficient data are provided in the paper by Wilson to allow the best fit values of τ to be recalculated from first principles and the reason for the difference between the two sets of results for chloroform as solvent remains unknown.

3.6.5 Solvent Effect Studies

In previous studies on solvent effects (Table 3-25), only small changes in the magnitude of the thermodynamic parameters have been observed. Furness[50] used toluene, chloroform and acetone in a study on N,N-dialkyl-4-nitrosoanilines and found a variation of 4.0 kJ mol^{-1} in $\Delta G^{\neq}_{298}$ and E_a while $\Delta S^{\neq}_{298}$ was almost constant. In the amide-solvent systems examined by Drakenberg[24] N,N-dimethylacetamide showed a variation of 2.3 kJ mol^{-1} in E_a, 5.0 kJ mol^{-1} in $\Delta G^{\neq}_{298}$ (with peak separations in

Table 3-25

Solvent Effect Studies

Compound	Solvent	E_a kJ mol^{-1}	$\Delta G^{\neq}_{298}$ kJ mol^{-1}	$\Delta H^{\neq}_{298}$ kJ mol^{-1}	$\Delta S^{\neq}_{298}$ JK^{-1} mol^{-1}
N,N-dimethyl-4-nitrosoaniline[50]	$(CD_3)_2CO$	61.8 ± 1.6	52.5 ± 0.2	59.4 ± 1.6	23 ± 6
	$CDCl_3$	63.6 ± 1.6	53.6 ± 0.2	61.1 ± 1.6	25 ± 6
N,N-diethyl-4-nitrosoaniline[50]	$(CD_3)_2CO$	63.0 ± 1.6	54.5 ± 0.2	60.5 ± 1.6	20 ± 6
	$CDCl_3$	64.4 ± 1.6	55.8 ± 0.2	61.9 ± 1.6	20 ± 6
	$C_6D_5CD_3$	66.0 ± 1.6	52.1 ± 0.2	63.5 ± 1.6	38 ± 6
N-benzyl-N-methoxy-N-methylamine	n-hexane[51]	54.0			- 8.1
	CS_2[51]	51.9			-10.0
	$CDCl_3$[51]	49.0			-27.3
	CH_2Cl_2[51]	39.0			-61.7
	$(CD_3)_2CO$[52]	34.7	41.4		-43
1,2,2-Trimethylaziridine[53]	neat (60 MHz)	100.7 ± 1.9	74.9		72 ± 18
	neat (100 MHz)	98.4 ± 2.4	74.1		66 ± 16
	C_6D_6	97.8 ± 3.1	76.1		59 ± 13
	$CDCl_3$	136.0 ± 5.8	79.1		160 ± 30
	$(CD_3)_2CO$	101.0 ± 2.2	76.6		65 ± 14

Table 3-25 (continued)

Solvent Effect Studies

Compound	Solvent	E_a kJ mol^{-1}	$\Delta G^{\neq}_{298}$ kJ mol^{-1}	$\Delta H^{\neq}_{298}$ kJ mol^{-1}	$\Delta S^{\neq}_{298}$ JK^{-1} mol^{-1}
N,N-dimethylformamide[24]	neat	89.1 ± 0.4	85.7 ± 0.4	87.4 ± 0.4	- 6 ± 4
	C_2Cl_4	90.4 ± 1.3	86.6 ± 0.4	87.0 ± 1.3	2 ± 8
	decalin	85.4 ± 1.3	84.9 ± 0.4	82.0 ± 1.3	-10 ± 8
N,N-dimethylacetamide[24]	neat	79.5 ± 0.4	75.7 ± 0.4	76.6 ± 0.4	3 ± 4
	$(CD_3)_2CO$	82.0 ± 1.3	75.3 ± 0.4	79.5 ± 1.3	13 ± 8
	D_2O	82.8 ± 0.4	80.8 ± 0.4	79.9 ± 0.4	- 3 ± 4
N,N-dimethyl-1-methoxy-thioformamide	neat[42]	60.7 ± 1.7	72.8	58.2	49
	neat[51]	56.9 ± 2.5	75.3		63 ± 2
	$CDCl_3$[51]	58.2 ± 1.3	74.1		54 ± 8
	C_6H_{12}[42]	59.4 ± 1.7	71.5	56.9	49
	C_6H_5Cl[41]	54.4	59.0		-23

the range 9.3 - 10.7 Hz) while for N,N-dimethylformamide the change in E_a was 5 kJ mol^{-1} and $\Delta G^{\neq}_{298}$ varied by 1.6 kJ mol^{-1} ($\Delta\nu$ varied between 4.3 Hz and 9.4 Hz). The methoxythioformamide showed similarly small ranges in E_a and $\Delta G^{\neq}_{298}$ as did 1,2,2-trimethyl aziridine (except for the chloroform solution in which the atypical behaviour has been accounted for by postulating that the chloroform molecules are hydrogen-bonded to the aziridinyl nitrogen).

For N-benzyl-N-methoxy-N-methylamine in Table 3-25 the value for the activation energy, E_a, decreased by 20 kJ mol^{-1} when the solvent was changed from n-hexane to acetone. For solvents of higher dielectric constant than acetone (ε = 20.7D) the rate of nitrogen inversion occurs too fast for NMR observation; this suggests significant solvent-solute interaction.

3.6.6 Studies of TTD in Selected Solvents

Before discussing the solvent dependence of the rotational barrier in TTD it should be noted that the variation in concentration of the TTD in acetone does not affect the thermodynamic parameters in any significant way (Table 3-26). Those variations which have occurred are well within the experimental error so henceforth the data from both concentrations will be considered together. Also, because the data obtained using dimethylsulphoxide-water as solvent with sodium 3-(trimethylsilyl-) propanesulphonate as reference and for this same solution with .24M sodium perchlorate added are compatible within the error limits (Table 3-26), they will be treated together as data for the dimethylsulphoxide-water (DMSO-water) system.

The thermodynamic parameters derived from the regression lines and equations 3-4, 3-5 and 3-6, are given in Table 3-27. When the peak separation $\Delta\nu$ is compared with the activation energy, E_a, it is found that the larger values of $\Delta\nu$ are associated with the smaller values of E_a but this inverse relationship is very approximate. The range of values

Table 3-26

Solvent	E_a kJ mol^{-1}	$\Delta G^{\neq}_{298}$ kJ mol^{-1}	$\Delta H^{\neq}_{298}$ kJ mol^{-1}	$\Delta S^{\neq}_{298}$ J K^{-1} mol^{-1}
Acetone 7.8 w/v%	136 ± 11	69.7	133 ± 11	210 ± 30
3.6 w/v%	140 ± 13	69.8	137 ± 13	230 ± 50
combined	138 ± 8	69.8	135 ± 8	220 ± 30
DMSO-water	92 ± 10	73.0	89 ± 10	50 ± 30
DMSO-water-$NaClO_4$	100 ± 4	71.7	97 ± 4	80 ± 10
DMSO-water combined	96 ± 4	72.8	93 ± 4	60 ± 10

Table 3-27

Thermodynamic Parameters for the Rotational Barrier of N,N,N',N'-Tetramethylthiodicarbonic Diamide in Selected Solvents

Solvent	E_a kJ mol^{-1}	$G^{\neq}_{298}$ kJ mol^{-1}	$H^{\neq}_{298}$ kJ mol^{-1}	$\Delta S^{\neq}_{298}$ J K^{-1} mol^{-1}
Acetone	137.9 ± 7.7	69.8	135.4 ± 7.7	220 ± 30
DMSO-water	95.7 ± 3.8	72.8	93.2 ± 3.8	60 ± 10
Chloroform	84.2 ± 1.9	69.3	81.7 ± 1.9	42 ± 8
Pyridine	78.5 ± 1.9	69.3	76.0 ± 1.9	19 ± 6
Acetonitrile	65.1 ± 7.7	70.7	62.6 ± 7.7	-25 ± 25
Toluene	55.5 ± 3.8	65.8	53.0 ± 3.8	-40 ± 10

for E_a is so large that the experimental errors cover only a small proportion of the variation in E_a between solvents which is therefore both real and significant.

Though the largest values of $\Delta H^{\neq}_{298}$ and $\Delta S^{\neq}_{298}$ are for acetone as solvent, which, for the reasons discussed in Section 3.3.4, have the largest errors, the range of values for the activation parameters in other solvents still show a variation of 40 kJ mol^{-1} for $\Delta H^{\neq}_{298}$ and 100 J K^{-1} mol^{-1} for $\Delta S^{\neq}_{298}$. These variations are at least twice as large as those previously reported (Section 3.5.5 and Table 3-25).

In Figure 3-12 a plot of $\Delta H^{\neq}_{298}$ versus $\Delta S^{\neq}_{298}$ is shown. The data can be fitted by a line with a least-squares slope of 308.9 and an error in the slope of $\pm$ 20. The pitfalls in the use of such correlations are well-known[55]: in this case the variations in $\Delta H^{\neq}_{298}$ and $\Delta S^{\neq}_{298}$ are much greater than the experimental errors so the correlation is significant. The range of values of $\Delta H^{\neq}_{298}$ and $\Delta S^{\neq}_{298}$ is much greater than that of $\Delta G^{\neq}_{298}$ and such correlations of $\Delta H^{\neq}_{298}$ with $\Delta S^{\neq}_{298}$ leading to largely compensating contributions to $\Delta G^{\neq}$ are often found associated with solvation effects[55]. For this study, in which the only variable is the solvent, it is not surprising that such a correlation is observed.

In an effort to determine which properties of the solvent might be significant in effecting such variation in $\Delta H^{\neq}_{298}$ and $\Delta S^{\neq}_{298}$, an attempt was made to correlate the activation parameters with solvent properties such as melting point, dipole moment and refractive index. In Table 3-28, the solvents are arranged in order of decreasing $\Delta G^{\neq}_{298}$ and are shown with various solvent properties, together with E_a. No correlation was obtained for any solvent property with E_a (and hence $\Delta H^{\neq}_{298}$, and also $\Delta S^{\neq}_{298}$, do not correlate with these solvent properties). However, several properties, namely the dielectric constant, the dipole moment, the Hildebrand solubility parameter, δ, and the empirical polarity parameters, E_T and Z, do correlate with $\Delta G^{\neq}_{298}$. This correlation of $\Delta G^{\neq}_{298}$ for TTD

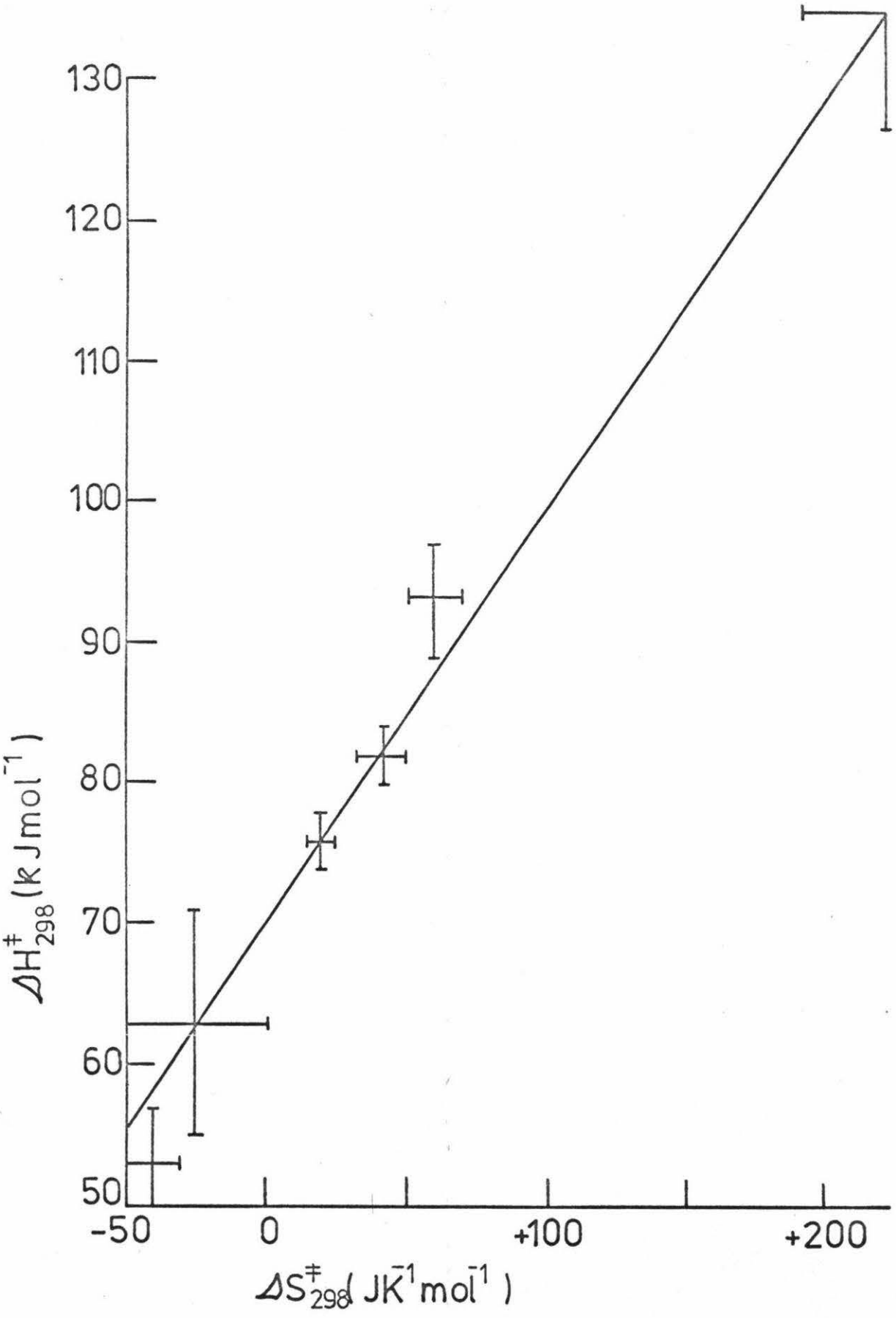

Figure 3-12: $\Delta H^{\ddagger}_{298}$ versus $\Delta S^{\ddagger}_{298}$

Table 3-28

Correlations between $\Delta G^{\neq}_{298}$ for TTD in Selected Solvents and Solvent Parameters[a,37]

Solvent	$\Delta G^{\neq}_{298}$ kJ mol^{-1}	E_a kJ mol^{-1}	MP °C	BP °C	n_D^{20}	ΔH_v kJ mol^{-1}	ϱ/η
DMSO-water	72.8	95.7					.36
Acetonitrile	70.7	65.1	-46	82	1.34	34.2	2.25
Acetone	69.8	137.9	-95	56	1.36	32.0	2.48
Pyridine	69.3	78.5	-42	116	1.51	40.4	1.04
Chloroform	69.3	84.2	-63	62	1.44	31.4	2.61
Toluene	65.8	55.5	-95	111	1.50	36.0	1.57

Solvent	$G^{\neq}_{298}$ kJ mol^{-1}	E_a kJ mol^{-1}	μ_{25} D	ε_{25}	δ	E_T kJ mol^{-1}	Z kJ mol^{-1}
DMSO-water	72.8	95.7		62			
Acetonitrile	70.7	65.1	3.92	36.7	11.9	192	298
Acetone	69.8	137.9	2.88	20.7		177	275
Pyridine	69.3	78.5	2.19	12.3	10.7	168	268
Chloroform	69.3	84.2	1.87	4.7	9.3	164	264
Toluene	65.8	55.5	.36	2.3	8.9	142	

a n_D^{20} = Refractive index for Na D-line at 20°C; ΔH_v = Enthalpy of evaporation

ϱ/η = Fluidity at 25°C in g cm^{-3} cP^{-1}; μ_{25} = Dipole moment at 25°C

ε_{25} = Dielectric constant at 25°C; δ = Hildebrand solubility parameter

E_T, Z = Solvent polarity parameters[56]

with properties related to solvent polarity suggests that the effect of the solvent on $\Delta G^{\neq}_{298}$ is closely related to the bulk solvent properties.

A summary of the literature data on the extensive range of solvents used for N,N-dimethylacetamide (DMA) lineshape studies are listed in Table 1-1. These have been rearranged in order of decreasing $\Delta G^{\neq}$ in Table 3-29 and some solvent parameters have also been given. For DMA, unlike TTD, the decrease in $\Delta G^{\neq}_{298}$ closely follows the order for decreasing E_a. The only solvent parameter which correlates with $\Delta G^{\neq}$ is the dielectric constant (except for 1,2-dichlorobenzene); the other parameters are completely random. Since the exception to this relationship is the only aromatic solvent, the interactions between the aromatic molecule and DMA are rather different to those interactions occurring in the remainder of the solvents. Similarly anomalous behaviour of $\Delta\nu$ for TTD in toluene and pyridine was observed ($\Delta\nu$ is very large with a marked decrease in $\Delta\nu$ as the temperature increases). It would seem that aromatic solvents interact with the solute in different ways to the other solvents. The most likely variation would be the formation of molecular complexes between aromatic solvents and their solutes, although the observed barriers to rotation for TTD in toluene and pyridine at the lower end of the range would seem to refute this suggestion.

As acetone and dimethylsulphoxide, both dipolar aprotic solvents containing oxygen, have the highest values of $\Delta H^{\neq}_{298}$ and $\Delta S^{\neq}_{298}$ while, as mentioned previously, toluene and pyridine have lower values for both parameters perhaps these parameters reflect the strength of solvent-solute binding. The nitrogen-containing dipolar aprotic solvent acetonitrile also has low values for $\Delta H^{\neq}_{298}$ and $\Delta S^{\neq}_{298}$. It is perhaps interesting to note that TTD was insoluble in low dielectric non-polar solvents such as carbon tetrachloride (see Table 3-2). However no simple rationalisation, in terms of the chemical properties of the solvents, of the variation in $\Delta H^{\neq}_{298}$ and $\Delta S^{\neq}_{298}$ seems possible.

Table 3-29

Free Energy Changes for Rotation in N,N-Dimethylacetamide and Solvent Parameters

Solvent	$\Delta G^{\neq}$ kJ mol^{-1}	ε_{25}	μ D	E_T kJ mol^{-1}	Z kJ mol^{-1}
Formamide	78.7 - 81.2	112.6	3.73	237	349
D_2O	80.8	77.9	1.86	264	396
DMSO	77.4	46.6	3.96	188	297
1,2-Dichlorobenzene	77.4	9.93	2.50		
Neat	76.1, 75.7	37.8	3.81		280
Acetone	75.3	20.7	2.88	177	275
CCl_4	72.5	2.23	0	136	
Iso octane	72.4	1.9	0		251

SECTION 4

THE PRELIMINARY INVESTIGATIONS INTO ROTAMERIC SYSTEMS

4.1 INTRODUCTION

Various compounds which should show rotational effects in their NMR spectrum were either prepared or bought, then their spectra were recorded for the neat compound or for a solution made with a deuterated solvent. In most cases the study of these systems was not carried beyond the initial variable-temperature spectra. Since computer programs for the two-site Bloch lineshape and the four-site density matrix analysis were available, the systems which were considered were usually two- or four-site interchanges.

4.2 PREPARATION OF COMPOUNDS

In this section the preparation of those compounds which were made in this laboratory and any purification of commercially-available compounds are described.

4.2.1 Preparation of 1 H-(4-nitrobenzoyl)-pyrrole

The method of preparation was that of Menger and Donohue[57]. 13.2 g (0.100 mole) of 2,5-dimethoxytetrahydrofuran (Aldrich) and 16.6 g (0.100 mole) of 4-nitrobenzamide (BDH) were dissolved in 100cm³ glacial acetic acid and heated gently for 2 hours. The acetic acid was removed under reduced pressure leaving a dark granular residue which was extracted with 500cm³ of diethyl ether in small portions. To determine that this was the product a small sample was analysed by the mass spectrometer and this confirmed that the product was 1 H-(4-nitrobenzoyl)-pyrrole.

4.2.2 Preparation of Dimethyl-4-nitrosophenol

Both 2,6-dimethyl-4-nitrosophenol and 3,5-dimethyl-4-nitrosophenol were prepared by the same method. 2.95 g (0.025 mole) of dimethylphenol

(Kochlight) was suspended in 150cm³ water and solid sodium hydroxide was added until the dimethylphenol dissolved. The solution was made up to 250cm³ (0.1M in dimethylphenol) with water, then cooled to 0°C in a salted ice-bath at which stage 2.55 g (0.15M) sodium nitrite was added. For the next hour, 1.5M sulphuric acid was added slowly until precipitation had finished and the solution was acidic. The precipitate was collected, dissolved in aqueous sodium carbonate, filtered and reprecipitated with dilute acid. The 2,6-dimethyl-4-nitrosophenol reprecipitated almost at once and was recrystallized from benzene but the 3,5-dimethyl-4-nitrosophenol took 48 hours to reprecipitate completely and was recrystallized from 1,4-dioxan.

4.2.3 Preparation of N-Benzyl-N-methoxy-N-methylamine

In the paper by Griffith[51] the preparation of N-benzyl-N-methoxy-N-methylamine (BMM) was summarised as the alkylation of N-methoxy-N-methylamine with benzyl chloride.

Following the standard method of preparation 1.5 g (0.015 mole) of N-methoxy-N-methylamine and 2.25cm³ (0.02 mole) of benzyl chloride in 15cm³ of toluene with 2.6 g of anhydrous potassium carbonate were refluxed for 24 hours. No product was obtained.

To ensure a basic environment the solvent was changed to pyridine. 2.9 g (0.03 mole) of N-methoxy-N-methylamine was dissolved in 50cm³ of pyridine to which 3.4cm³ (0.03 mole) of benzyl chloride was added. The mixture stood for 10 minutes then most of the pyridine was removed on the rotary evaporator to leave about 10cm³ of yellow oil. The oil was dissolved in 30cm³ chloroform and washed three times with 30cm³ of distilled water. Most of the chloroform was removed on the rotary evaporator leaving a brown liquid, presumably the product. An NMR spectrum was run which showed three proton peaks near the TMS reference signal in the ratio 2.2 : 3.0 : 3.1 (the expected ratio for the product) and complex aromatic peaks.

This method was repeated using 6.8 g N-methoxy-N-methylamine and

8cm³ benzyl chloride in 100cm³ pyridine, refluxing this mixture for 15 minutes then dissolving the oil remaining after the pyridine has been removed in 60cm³ of chloroform which was washed with six portions of 30cm³ of water. When the chloroform was removed there was none of the expected product left.

The next preparation used 0.98 g N-methoxy-N-methylamine and 1.2cm³ benzyl chloride in 17cm³ pyridine which was refluxed for 90 minutes on an oilbath then washed with 34cm³ of a saturated solution of sodium bicarbonate (M & B). The pyridine mixture dissolved. When a little sodium hydroxide-pyridine solution was added to 15cm³ of the pyridine-sodium bicarbonate mixture, two layers separated out so this sample was combined with the larger portion and a thin second layer appeared. A pellet of sodium hydroxide was added and the second (upper) layer grew larger and the colour deepened from yellow to orange. When separated this layer (35cm³) was distilled to remove the pyridine. The residual oil was dissolved in chloroform, washed with water and the chloroform was removed on the rotary evaporator but none of the required product was obtained.

To determine if the amine itself was strongly basic in water, 0.0807 g (8.2×10^{-4} mole) of N-methoxy-N-methylamine was dissolved in water and half-neutralised with 4.14cm³ of 0.1M sodium hydroxide. The pH of the solution (measured twice) was 4.73 ± 0.02 so, since at half neutralisation $pH = pK_a$ then $pK_a = 4.73 \pm 0.02$.

Since the pK_a of N-methoxy-N-methylamine is near that of pyridine ($pK_a = 5.25$), a new solvent was used. 0.98 g of N-methoxy-N-methylamine and 1.2cm³ benzyl chloride was dissolved in 20cm³ of 2,6-dimethylpyridine ($pK_a = 6.57$) and refluxed on an oilbath for 24 hours. The resulting oil was washed with sodium bicarbonate-sodium hydroxide solution then, after separation of the dimethyl-pyridine layer, the solvent was partly removed by the rotary evaporator. Distillation on a microscale removed the remainder of the dimethyl-pyridine. A small amount of residue was obtained

which was not the expected product.

4.2.4 Purification of N,N-Dimethylcarbamic Chloride

The N,N-dimethylcarbamic chloride (Fluka) was vacuum distilled using a water pump at a constant temperature of 62°C. Only the middle cut was kept and stored over a molecular sieve (Ajax 4A) in the dark. A neat sample of N,N-dimethylcarbamic chloride, with only TMS added, was degassed on the vacuum line before being sealed in an NMR tube.

4.3 DESCRIPTION OF VARIABLE TEMPERATURE SPECTRA FOR ROTAMERIC SYSTEMS

The variable temperature spectra hereafter described were recorded as described in Sections 2.2.3 and 2.3.5.

4.3.1 3-Methyl-1-(4-methylphenyl)-triazene

After surveying the literature on rotameric compounds, the triazenes were considered possible subjects for variable-temperature studies so without further purification samples of 3-methyl-1-(4-methylphenyl)-triazene (WBL) in deuteroacetone (4 w/v%) and deuterochloroform (3 w/v%) were prepared.

The spectrum of 3-methyl-1-(4-methylphenyl)-triazene (MMT) in chloroform was recorded at several temperatures; at room temperature, the N-methyl peak appears as a singlet which at -22°C has broadened and at -30°C has separated into two unequal peaks with a shoulder on the larger peak.

When the low field portion of the room (about 27°C) temperature spectrum was expanded it became apparent that the aryl peaks were split in a complex pattern with an adjacent very flat hump which was tentatively identified as the proton attached to the nitrogen. At -52°C the proton peak had sharpened reflecting the lower mobility of this tautomeric nucleus which can migrate along the triazene chain.

The aryl peaks show some variation in intensity but this alteration is very small for so large a temperature change. The aryl peaks were unsuitable for variable temperature analysis because of the lack of variation while the methyl peak was unsuitable because of the complications introduced by the mobile proton.

A solution of MMT in acetone was recorded at various temperatures. An expansion of the aryl region from the room (~ 27°C) temperature spectrum (Fig. 4-1) showed a complex broadened set of peaks which were virtually unchanged when re-examined at -44°C. The methyl portion of the spectrum showed, at room temperature a pair of coalescing unequal peaks with a third peak to the high field side of the coalescing pair which was assigned to the aromatic methyl but at -44°C,m though the high field peak was unchanged, the broader high field peak of the pair was stationary and sharper while the low field peak had moved to lower field and a small sharp peak had appeared between them.

A spectrum recorded six weeks later at room temperature showed the same peaks with the intensities of the "coalescing" pair reversed. Under the same conditions a spectrum run after another two weeks showed an extra set of peaks so a series of spectra at various temperatures were run but the only change was the inclusion of the new peaks to the low field side of the "coalescing" pair (in which the low field peak was even less intense and broader than before).

A new solution of MMT in acetone was prepared but spectra run within three hours of sample preparation showed a second new peak and low temperature (-44°C) spectra were rather complex so this system was abandoned.

4.3.2 1-Acylpyrroles

Since a four-site density-matrix program was available, the 1-acylpyrroles were considered possible subjects for study. Lineshape analyses

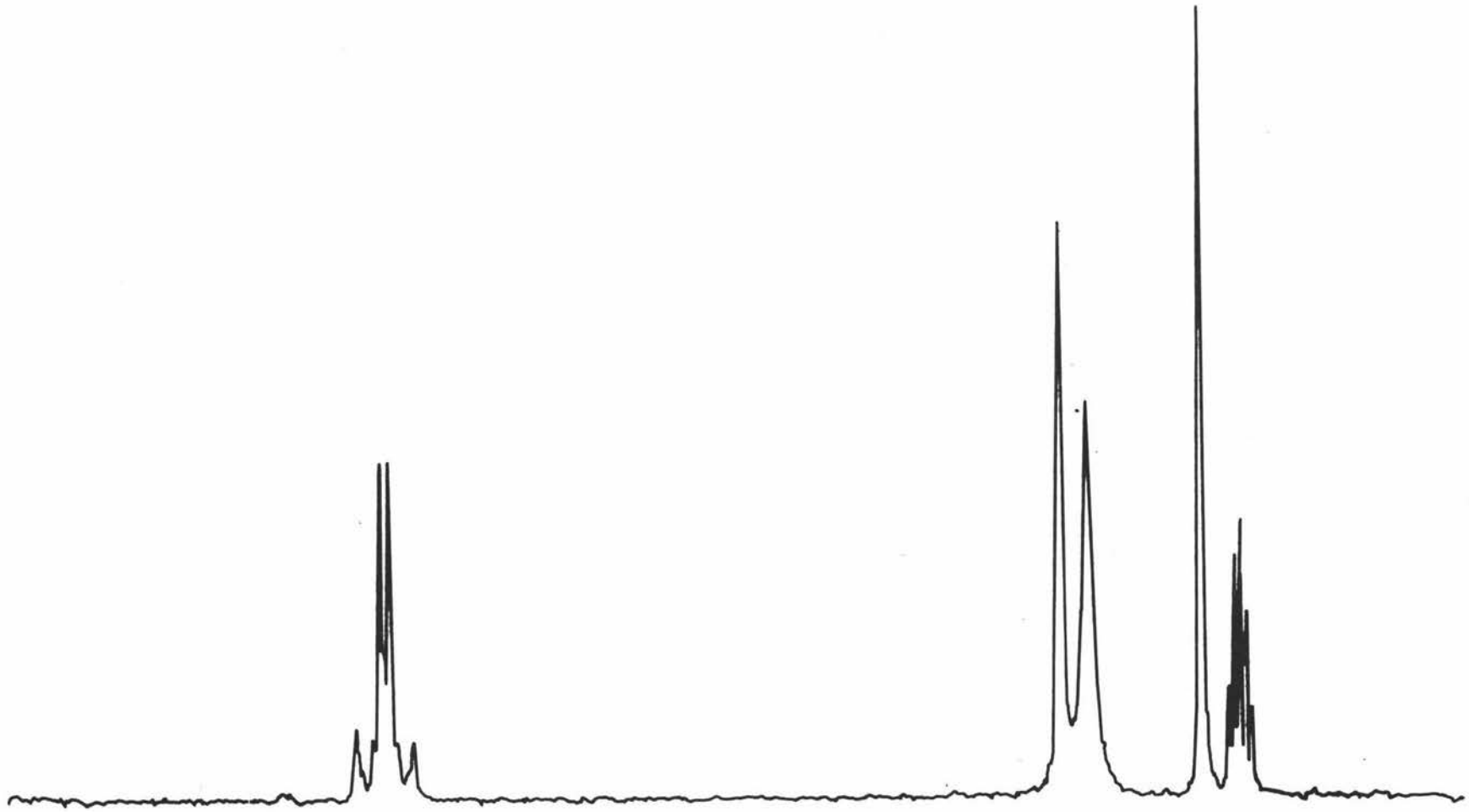

Figure 4-1 3-Methyl-1-(4-methylphenyl)-Triazene in acetone-d_6 at 30°C.

of rotation in 1-acetylpyrrole[58], 3,4-dimethyl-1-acetylpyrrole[59] and barrier-height estimations for 1-benzoyl-pyrroles[59] seemed to indicate that 1H(4-nitrobenzoyl)pyrrole would be a good candidate for lineshape analysis with two unrelated 4-spin systems which should show rotational effects. Such a study should add to the knowledge of rotation in pyrrole-based compounds.

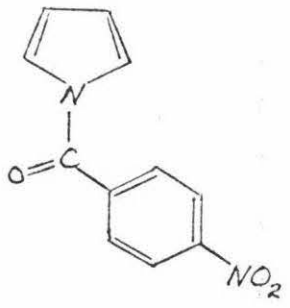

I

1H(4-nitrobenzoyl)pyrrole was prepared as described in Section 4.2.1 and the spectrum of a solution of 1H(4-nitrobenzoyl)pyrrole in deuteracetone was recorded at various temperatures between room temperature and -84°C. At room temperature the aromatic region even at an expansion of 1.5 Hz/cm showed only two peaks with irregularities which could be incipient peaks. At -31°C with the same expansion the two largest peaks had moved apart and were now surrounded by small peaks while at -40°C, there were no new peaks (Fig. 4-2) but all the peaks present had spread over a larger frequency range even though the peaks were sharper. As the temperature dropped the peaks spread coalesced and changed in a fashion not easily disentangled since these were overlapping peaks from the two aromatic regions. Even at -84°C (Fig. 4-3), changes were still occurring so reaching the slow exchange region would not be possible in this solvent (which freezes at -95°C).

4.3.3 4-Acetylpyridine

By analogy with the 1-acyl-pyrroles which had recently been analysed by lineshape methods[58,59], it was thought that 4-acyl-pyridine might be

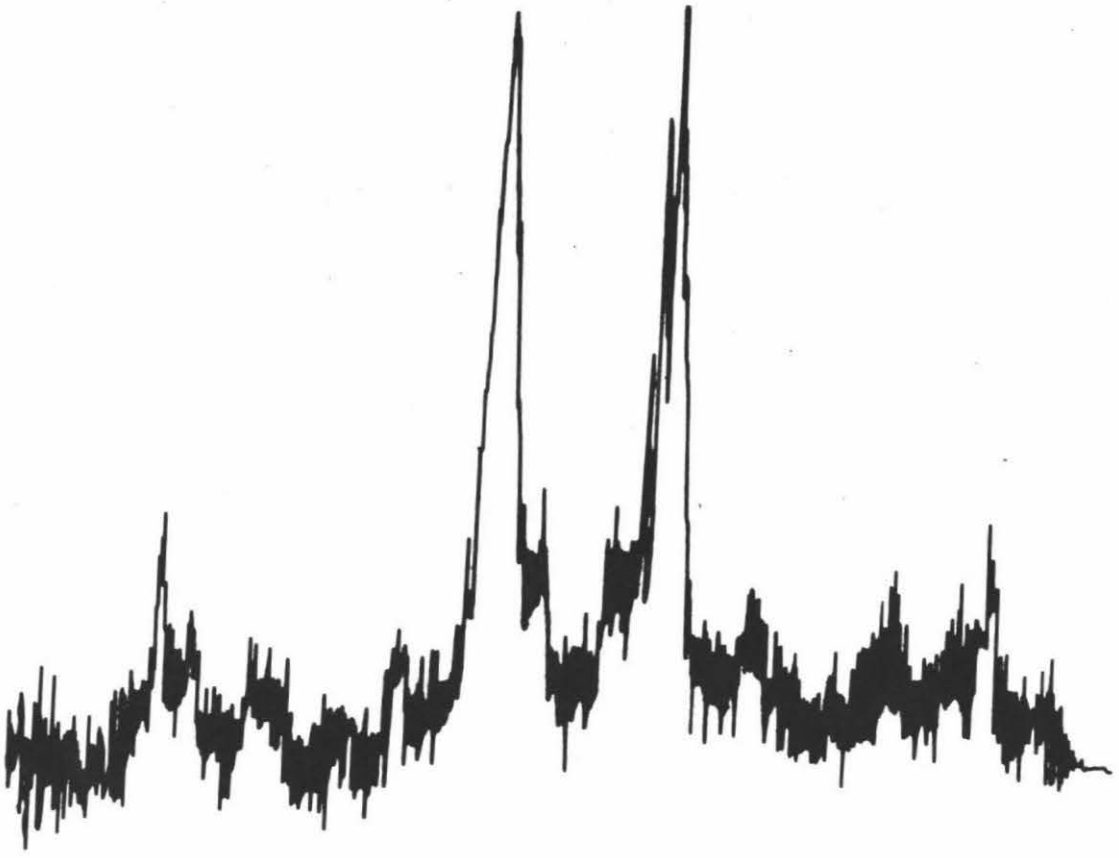

Figure 4-2 1H-(4-nitrobenzoyl)-pyrrole in acetone-d_6 at —40°C.

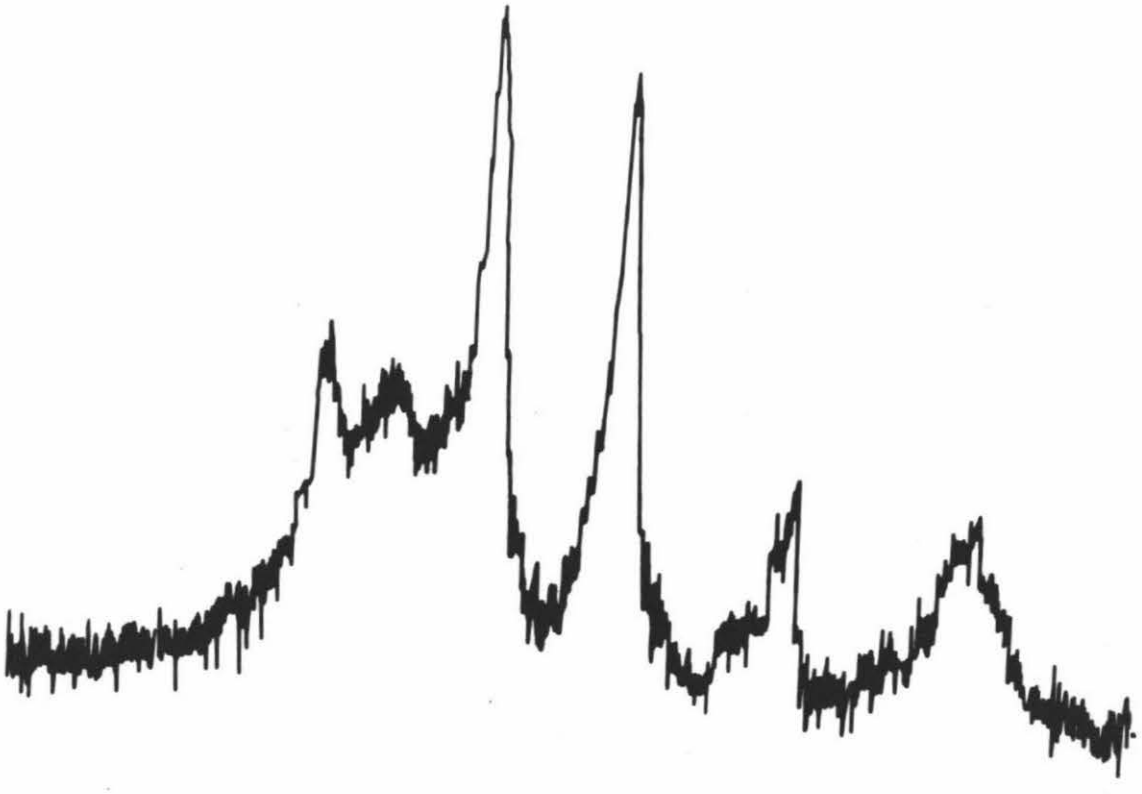

Figure 4-3 1H-(4-nitrobenzoyl)-pyrrole in acetone-d_6 at —84°C.

a suitable four-site system. The spectrum of 4-acetyl-pyridine (BDH) was run in a concentrated sulphuric acid - methanol mixture at 27°C, -13°C, -58°C and -79°C. Since the solvent mixture was undeuterated there were many intense peaks in the spectrum but the aromatic region was fortunately free of interference so only the low field spectra were considered below room temperature. The sample was insoluble in methanol at low temperatures in the absence of acid.

The chemical shift altered very slightly over the temperature range but the appearance of the spectrum altered dramatically as the temperature dropped. At room temperature, there are two sets of complex peaks in the aromatic region (Fig. 4-4) which slowly coalesce as the temperature decreases so that, at -58°C, the aromatic signals consist of two coalescing doublets and, at -79°C, these have become a pair of broad smooth peaks. The complex spectrum at room temperature would be due to the methyl group coupling with the aromatic protons so, at the slow-exchange limit, the spectrum would be even more complex. In this solvent the slow-exchange limit was not reached at -79°C but, if a suitable solvent could be found, this would be a promising system.

4.3.4 Dimethyl-4-nitrosophenols

The 4-spin system of the anion of 4-nitrosophenol has been examined[60] since, in the anion, the rotation of the nitroso group is slowed down by the possibility of the formation of the quinone monoxime form shown below

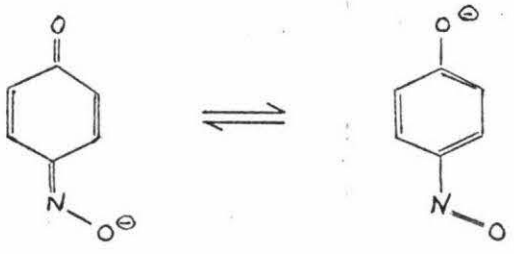

To slow the rotational rate without forming the anion, the most obvious method is to physically hinder the nitroso group with substituents at the

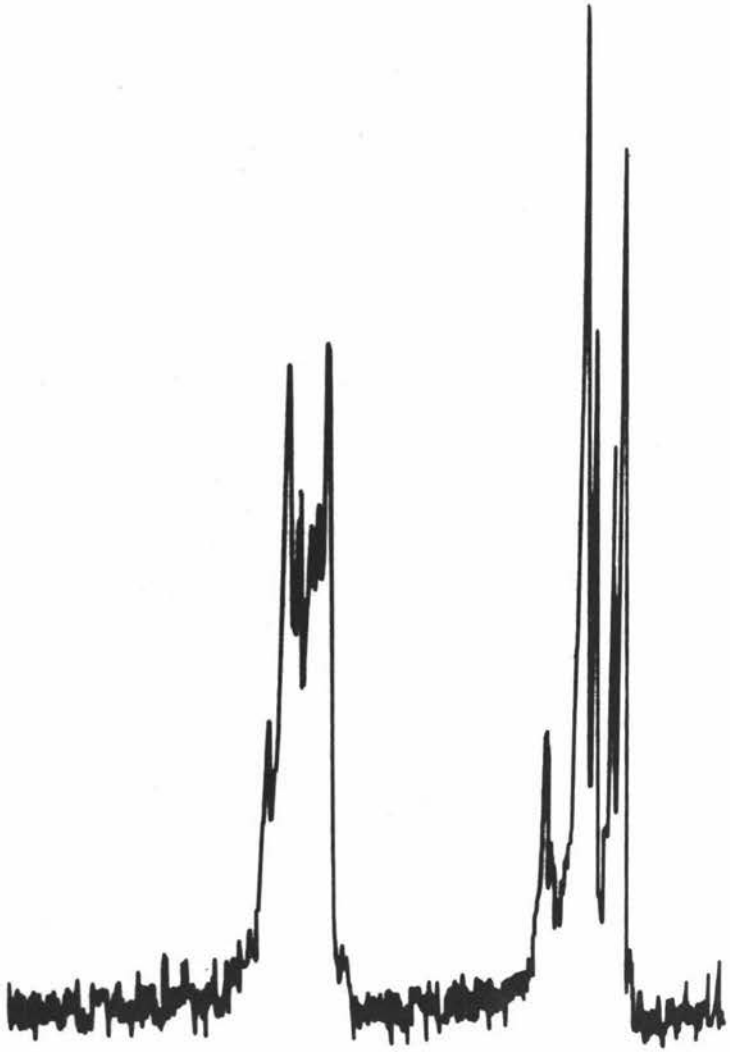

Figure 4-4 4-Acetyl pyridine at 27°C.

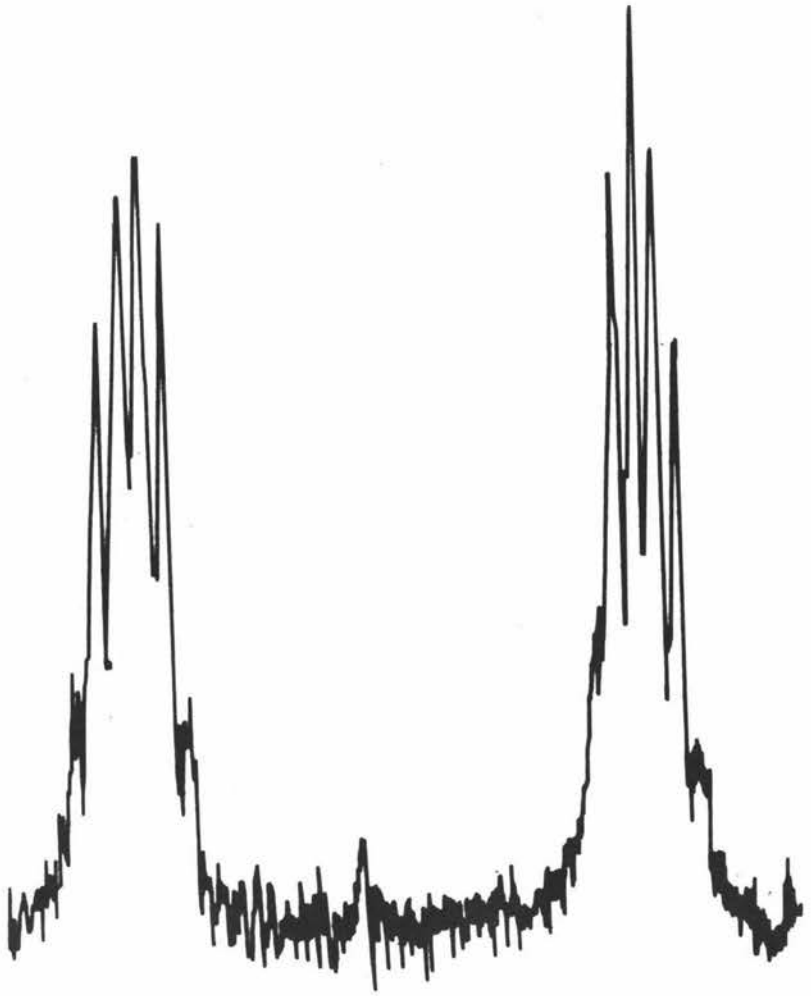

Figure 4-5 2,6-Dimethyl-4-nitrosophenol in acetone-d_6 at —15°C.

2,6 positions on the benzene ring. If two symmetrically-placed methyl groups on the benzene ring hinder the rotation of the nitroso group then the spectrum of dimethyl-4-nitrosophenols should show, at low temperatures, two aryl proton and two methyl group peaks, both pairs (or either pair) coalescing at higher temperatures. If this occurred then the two site Bloch program could be used to analyse the spectra observed.

A solution of 2,6-dimethyl-4-nitrosophenol (2.6 w/v%) in deuteromethanol (BDH) gave a spectrum in which (at room temperature) there is a slight disturbance in the aromatic region and the methyl peaks are single, widely separated and sharp.

In deuteroacetone (9 w/v%), 2,6-dimethyl-4-nitrosophenol shows a very broad single peak in the aromatic region which, as the temperature decreases, separates into two broad featureless peaks (at 0°C). When the temperature reaches -15°C, the spectrum shows a pair of sextets with an internal splitting of 1.3 Hz (Fig. 4-5). The splitting of the two aromatic peaks is probably due to coupling with the methyl groups.

The solution of 2,6-dimethyl-4-nitrosophenol in D_2O, with sodium 3-(trimethyl silyl)-propanesulfonate as reference, showed a pair of broad peaks in the aromatic region at 9 ppm sweep width. When the sweep width was expanded (to 1.8 ppm) the signals were found to be a pair of asymmetric quartets (with a separation of 8 Hz between the quartets) as though the slow-exchange limit was at room temperature (27°C) but when the temperature was increased to + 74°C the spectrum was unchanged. At both temperatures there were two separate sharp methyl peaks.

As a contrast the 3,5-dimethyl-4-nitrosophenol in deuteromethanol showed only a very small broad peak for the aromatic protons but since this compound has very low solubility in deuteromethanol and in 1,4-dioxan, no further spectra from these solutions were recorded.

4.3.5 N,N-Dimethylcarbamic Chloride

A neat sample of N,N-dimethylcarbamic chloride (DCC) with TMS added had spectra recorded for the range -3°C to + 17°C to determine the low temperature parameters. At this point the peak heights were unequal but improvements in resolution and stability did not change the disparity in height. The variation in intensity could not be explained by different populations and under statistical analysis both peaks had the same value of T_2^{-1}:

$$\nu_{\frac{1}{2}}(1) = 0.50 \pm 0.05 \text{ Hz}$$

$$\nu_{\frac{1}{2}}(2) = 0.50 \pm 0.05 \text{ Hz}$$

$$\nu_{\frac{1}{2}} = 0.50 \pm 0.05 \text{ Hz}$$

Hence $T_2^{-1} = 2/\nu_{\frac{1}{2}} = 4.0 \pm 0.4$ s

The peak separation appeared to be independent of temperature so the average was taken as the optimum value:

$$\Delta\nu = 6.61 \pm .09 \text{ Hz}$$

The spectra were recorded at an expansion of 0.75 Hz cm^{-1}. The temperature was determined before and after each spectrum with a thermometer. The smallest division on the thermometer was 0.5 K so the error in temperature measurements was taken as 1 K. The recorded spectra were digitised by finding the intensity at intervals of 0.2 Hz to 0.8 Hz along the spectrum. The Bloch lineshape program LMH was used to find the value of τ^{-1} which maximised the fit between the experimental and theoretical spectra (as described in Section 2.4.2, 2.4.3 and 3.4.2). Sample spectra are given in Figures 4-6 to 4-7. The kinetic parameters are plotted in Figure 4-9; the thermodynamic parameters from the regression analysis of the kinetic data are given in Table 4-3 with the data from previous lineshape analyses of neat N,N-dimethylcarbamic chloride.

The agreement of the thermodynamic parameters within the quoted error

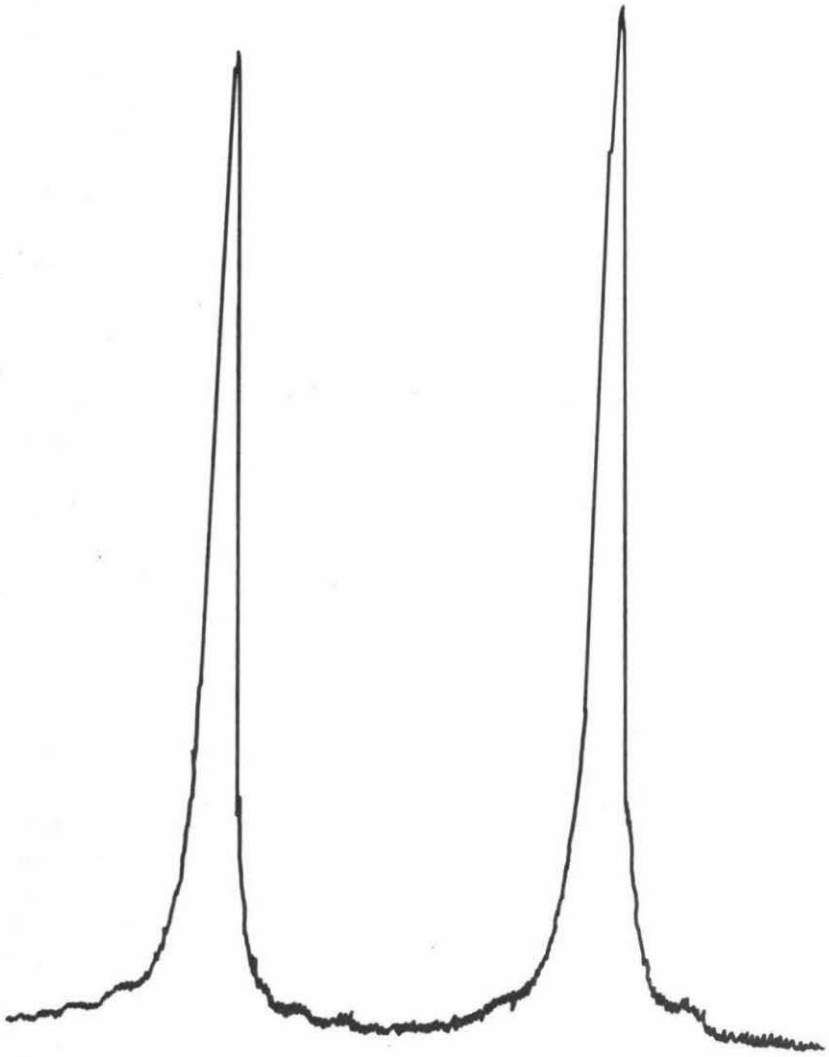

Figure 4-6 N,N-Dimethylcarbamic chloride at 6°C.

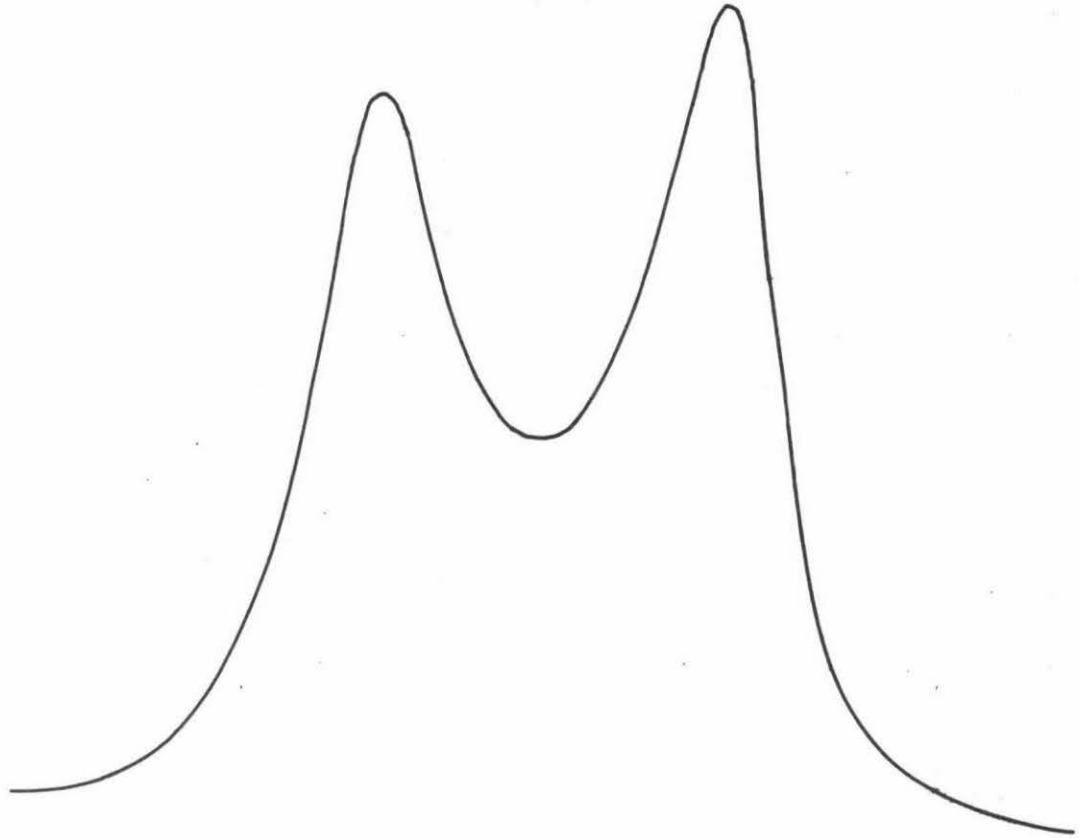

Figure 4-7 N,N-Dimethylcarbamic chloride at 57°C.

Table 4-1

Low Temperature Parameters for DCC

T °C	ν_1 Hz	$\nu_1(1)/2$ Hz	ν_2 Hz	$\nu_1(2)/2$ Hz	$\Delta\nu$ Hz
-3	181.3	.4	187.8	.5	6.5
-3	181.2	.45	187.8	.4	6.6
-3	181.4	.45	188.0	.45	6.6
2	181.0	.5	187.7	.5	6.7
2	181.3	.45	187.7	.45	6.4
6	181.0	.55	187.7	.55	6.7
6	181.0	.55	187.7	.50	6.7
6	181.1	.50	187.8	.50	6.7
6	181.1	.50	187.9	.50	6.8
11	181.1	.55	187.7	.60	6.6
11	181.0	.55	187.6	.55	6.6
11	181.3	.55	187.8	.55	6.5
17	181.0		187.7		6.7
17	181.0		187.6		6.6
17	181.0		187.6		6.6
21	181.0		187.6		6.6
21	181.0		187.6		6.6
21	180.8		187.3		6.5

Table 4-2

Kinetic Parameters for N,N-Dimethylcarbamic Chloride

T K	k s^{-1}	$10^3 T^{-1}$ K^{-1}	$\log_{10} k$
301	2.564 ± 0.003	3.322	0.4089 ± 0.0005
310	6.54 ± 0.01	3.226	0.8156 ± 0.0007
316	13.06	3.165	1.116
323	21.13	3.096	1.325
335	55.26	2.985	1.742

Regression line: $\log_{10} k = 13.4 - 3.9\ (\pm\ 0.2)\ (1/T)$

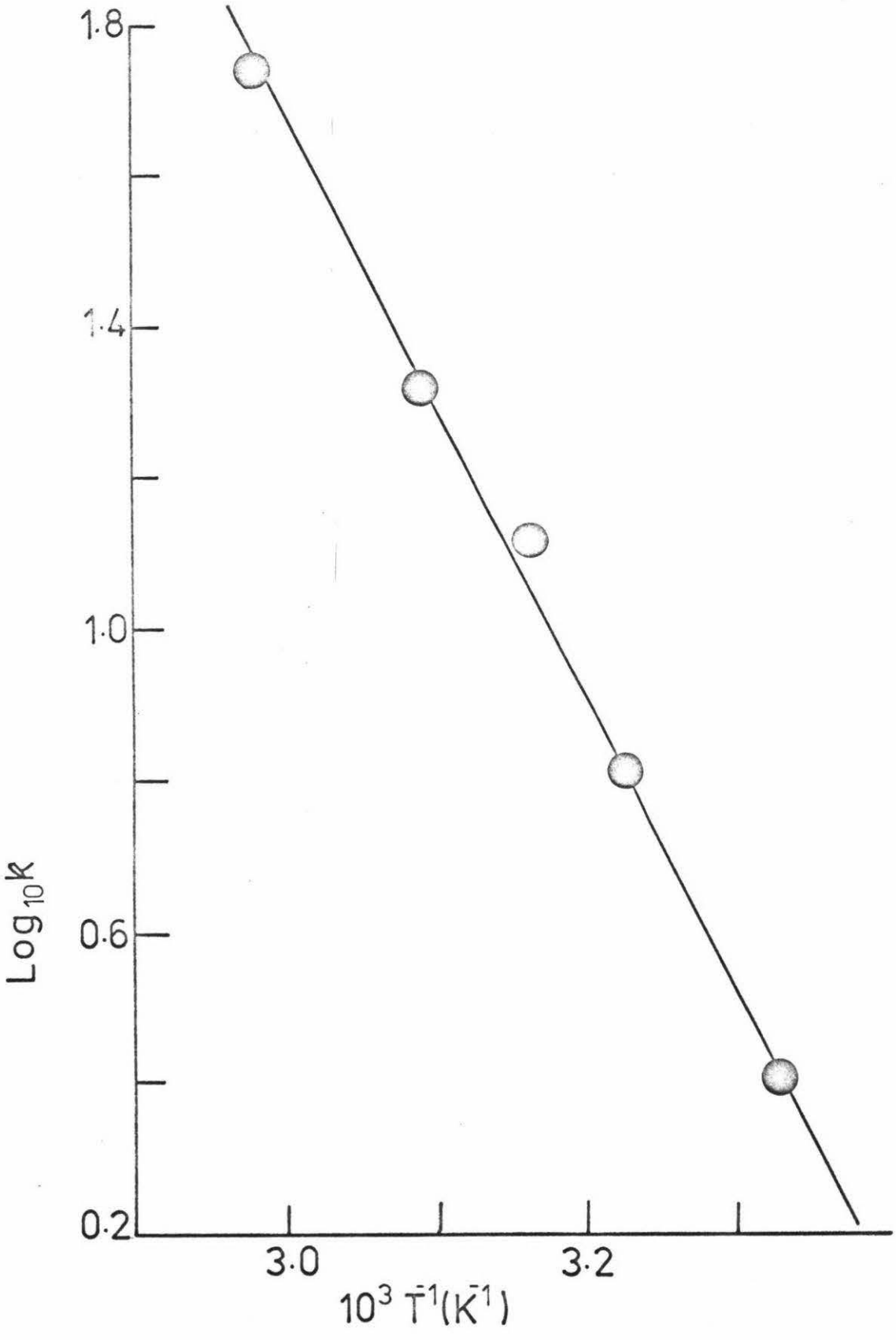

Figure 4-9: $Log_{10}k$ versus T^{-1} for DCC

Table 4-3

Thermodynamic Parameters for the Barrier to Rotation in N,N-Dimethylcarbamic Chloride

Reference	E_a kJ mol^{-1}	$\Delta G^{\neq}_{298}$ kJ mol^{-1}	$\Delta H^{\neq}_{298}$ kJ mol^{-1}	$\Delta S^{\neq}_{298}$ J K^{-1} mol^{-1}
This work	74.7 ± 3.8	71.2 ± 0.6	72.2 ± 3.8	+ 3.2 ± 11.0
47	70.7 ± 2.1	70.3	68.2 ± 2.1	- 6.2 ± 7.7
48	73.6 ± 2.1	70.3 ± 2.1	71.5	+ 3.3 ± 6.7
49	77.2 ± 4.2	70.9 ± 0.8	74.7 ± 4.2	+12.7 ± 16.7

limits (particularly the values for E_a and $\Delta S^{\neq}_{298}$) suggests that the lineshape technique has definitely eliminated those errors due to approximation and has minimised the possibility of systematic error. This consensus of results from different research groups and from ^{1}H and ^{13}C NMR would seem to have finally settled the thermodynamic parameters for DCC. It is interesting that a low number (5) of measurements with relatively inaccurate temperature measurements ($\pm$ 1 K) has given results compatible with those from the most painstaking work. Possibly, when the peak separation of the two signals is not too small (Allan[48] quoted $\Delta\nu$ as 6.8 $\pm$ 0.2 Hz at 60MHz over the temperature range -10°C to 65°C while Neuman[47] used a value of 6.33 Hz at 60MHz), the accuracy of the temperature measurements is no longer the crucial factor which determines the fit of experimental to theoretical spectra. The results are certainly a confirmation of the procedures used for preparing the analysis in this work.

APPENDIX A

The program LMH which was used to obtain the kinetic parameters from digitised spectra is given in this Appendix. The input is the digitized experimental spectrum prefaced by five cards:

Card 1: The number of cases (NCASE) and the title for these cases (NAME).

Card 2: If the program is to iterate, NCON must be 1 or larger; if the program is to plot the results, NPLOT must be 1 or larger; the temperature at which the spectrum was recorded (TEMP).

Card 3: The peak positions WA, WB; the relaxation times for each peak T2A, T2B.

Card 4: The population at each site PA, PB.

Card 5: The estimated lifetime (TOR), the increment for changing the lifetime (TINC) and the limit below which TINC is not effective (TLIM).

```
// FOR
*LIST SOURCE PROGRAM
*ONE WORD INTEGERS
*IOCS(CARD,1132 PRINTER)
*IOCS(PLOTTER)
      DIMENSION V(100),W(100),WINT(100),DIFF(100),NAME(30)
      J=1
C READ IN INPUT DATA
      READ(2,1000) NCASE,NAME
    1 READ(2,1100)NCON,NPLOT,TEMP
      READ(2,1500)WA,WB,T2A,T2B
      READ(2,1500)PA,PB
      READ(2,1500)TOR,TINC,TLIM
      I=0
    2 I=I+1
      READ(2,1500)W(I),WINT(I)
      IF(W(I))3,3,2
    3 NOBS=I-1
      WRITE(3,2500)NAME,J,PA,PB,TEMP
      WRITE(3,2750)WA,WB,T2A,T2B
C SET UP INITIAL CONTROL PARAMETERS
      NIT=0
      NTOR=0
C CALCULATE THEORETICAL INTENSITIES AND NORMALISATION CONSTANT
      SW=(WA-WB)
  100 DO 200 I=1,NOBS
      BW=((WA+WB)/2.)-W(I)
      P=TOR*((1./(T2A*T2B))-BW**2+(SW/2.)**2)+PB/T2B+PA/T2A
      Q=TOR*(BW-(SW/2)*(PA-PB))
      R=BW*(1.+TOR*(1./T2A+1./T2B))+TOR*(SW/2)*(1./T2B-1./T2A)+(SW/2)*(P
     1A-PB)
  200 V(I)-((1.+TOR*(PB/T2A+PA/T2B))*P+Q*R)/(P**2+R**2)
C NORMALISATION OF THEORETICAL INTENSITIES TO EXPERIMENTAL INTENSITIES
      NMAX=MAX(WINT,NOBS)
      CONS=WINT(NMAX)/V(NMAX)
      DO 20 I=1,NOBS
   20 V(I)=V(I)*CONS
C LEAST SQUARES FIT AND CONTROL STATEMENTS
      DIF =0.0
      SUM=0.0
```

```
      DO 30 I=1,NOBS
      DIFF(I)=V(I)-WINT(I)
      DIF =DIF +(V(I)-WINT(I))**2
   30 SUM=SUM+(WINT(I))**2
      SIGM=DIF /SUM
      SIGMA=SQRT(SIGM)
      RTOR=(1./(2.*TOR))*(44./7.)
      IF(NCON)35,35,45
   35 IF(NPLOT)36,36,37
   37 DO 38 I=1,NOBS
   38 W(I)=W(NOBS)-W(I)
      CALL SCALF(0.53,.17,W(1),WINT(1))
      CALL FPLOT(2,W(1),WINT(1))
      DO 39 I=2,NOBS
   39 CALL FPLOT(0,W(I),WINT(I))
      DO 41 I=1,NOBS
      CALL FPLOT(1,W(I),V(I))
      CALL FPLOT(2,W(I),V(I))
   41 CALL POINT(0)
      CALL FGRID(0,-6.,0.,1.,27)
      CALL FCHART(-6.,42.,0.2,0.2,0.)
      WRITE(7,4500)SW
      CALL FCHAR(-6.,28.,0.2,0.2,0.)
      WRITE(7,4700)RTOR
      CALL FCHAR(-6.,22.,0.2,0.2,0.)
      WRITE(7,4800)TEMP
   36 WRITE(3,3000)TOR,RTOR,SIGMA
      DO 40 I=1,NOBS
   40 WRITE(3,3500)W(I),WINT(I),V(I),DIFF(I)
      WRITE(3,3600)NIT
   45 NIT=NIT+1
      IF(NTOR)50,50,60
   50 NTOR=1
   70 TOR=TOR+TINC
      SIG=SIGMA
      GO TO 90
   60 IF(SIGMA-SIG)70,70,80
   80 TINC=-0.5*TINC
      GO TO 70
   90 IF(ABS(TINC)-TLIM)900,150,150
```

```
150 IF(20-NIT)900,100,100
900 IF(NCON)910,910,920
920 TOR=TOR+TINC
    NCON=0
    GO TO 100
910 IF(NCASE-1)110,110,120
120 WRITE(3,4000)J
    J=J+1
    NCASE=NCASE-1
    GO TO 1
110 WRITE(3,4000)J
1000 FORMAT(I2,30A2)
1100 FORMAT(2I2,F8.2)
1500 FORMAT(4F10.3)
2500 FORMAT(1H1,20X,30A2,10X,'CASE NUMBER',I2,//20X,'PA=',F8.2,10X,'PB=
    1',F8.2,10X'TEMP=',F8.2)
2750 FORMAT(  //20X,'WA=',F8.2,10X,'WB=',F8.2,10X,'T2A=',F8.2,10X,'T2B=
    1',F8.2)
3000 FORMAT(//10X,'TOR=',F10.3,'SEC',10X,'RELAXATION RATE=',F10.4,'RAD
    1PER SEC',10X,'RESIDUALS=',F10.6,//12X'FREQUENCY',8X,'EXP INTENSITY
    2',6X'THEOR INTENSITY',7X'INT DIFF')
3500 FORMAT(10X,F10.3, 9X,F10.3, 9X,F10.3,9X,F10.3)
3600 FORMAT(//10X,'NUMBER OF ITERATIONS=',I2)
4000 FORMAT (////40X'END OF CASE',I2)
4500 FORMAT('WA-WB=',F6.2)
4700 FORMAT('RTOR=',F8.2)
4800 FORMAT('TEMP=',F8.2)
     CALL EXIT
     END
```

APPENDIX B

The following spectra are representative of all those spectra from which low temperature and kinetic parameters were derived. These examples were chosen to provide spectra for both a narrow and a wide peak separation. The first series (Figure B1, 2) show the changes in the spectrum of N,N,N',N'-tetramethylthiodicarbonic diamide (TTD) in acetonitrile (the peak separation is temperature-dependent (see Table 3-14) but is about 4.0 Hz) while the second set (Figure B3, 4, 5) show the same compound in pyridine (where the temperature-dependent peak separation ranges from 12.1 Hz to 9.0 Hz).

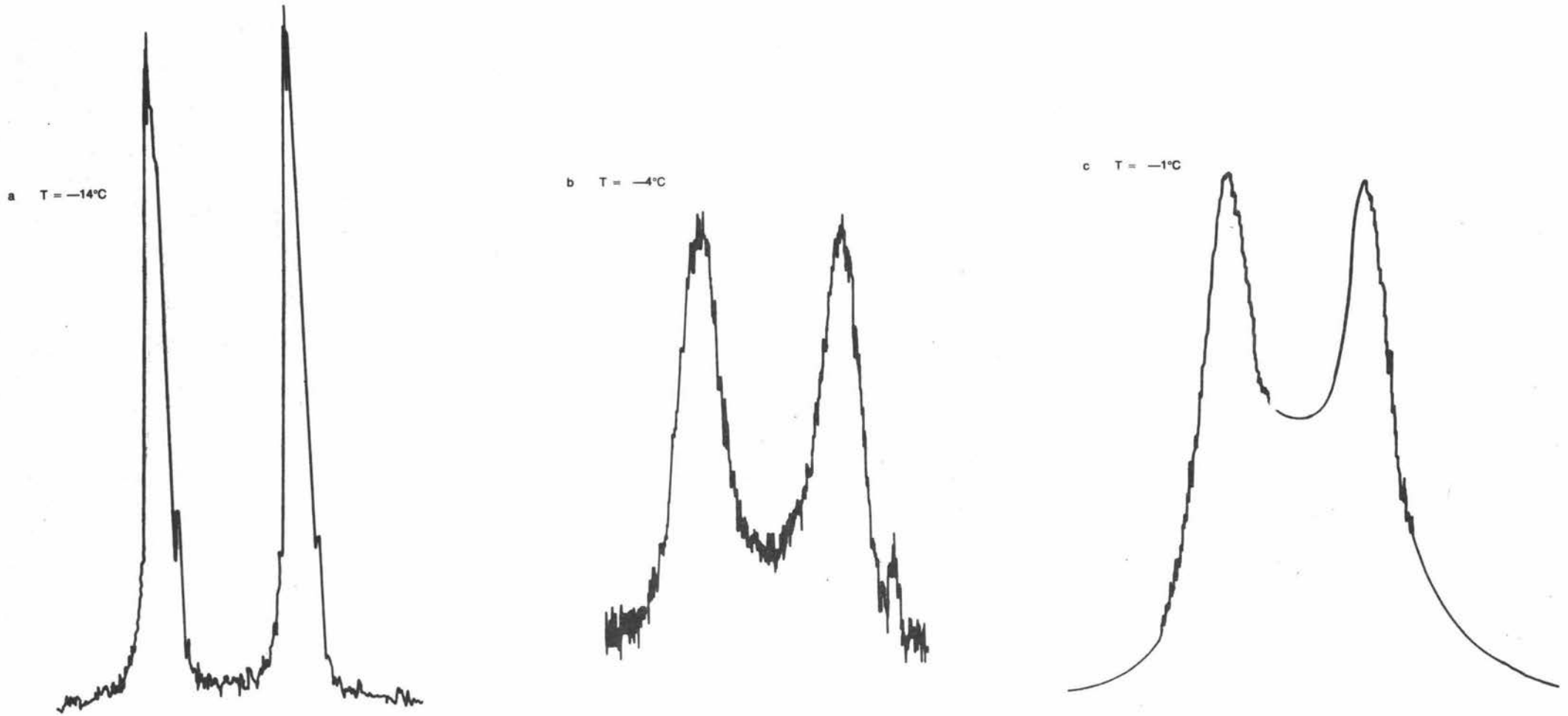

Figure B-1 TTD in acetonitrile-d_3

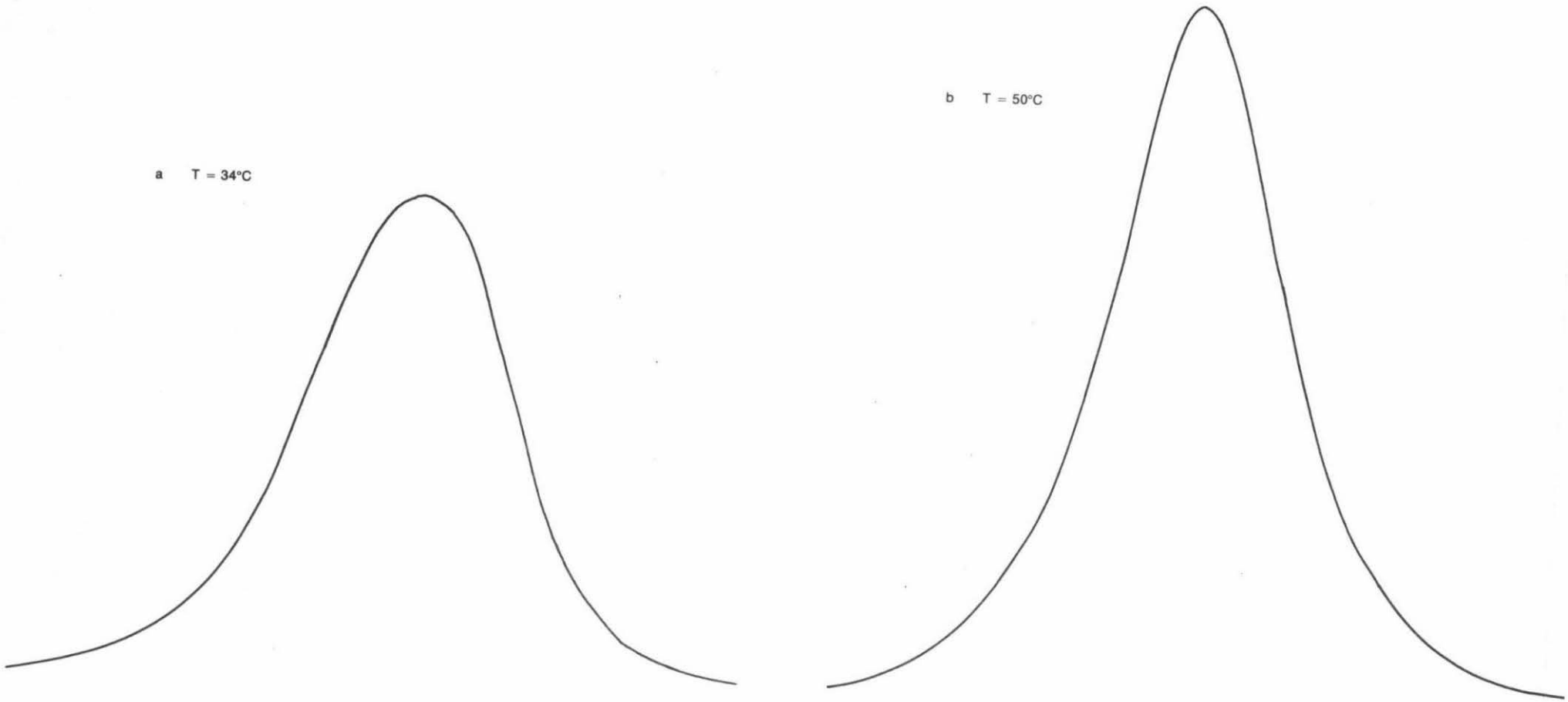

Figure B-2 TTD in acetonitrile-d_3

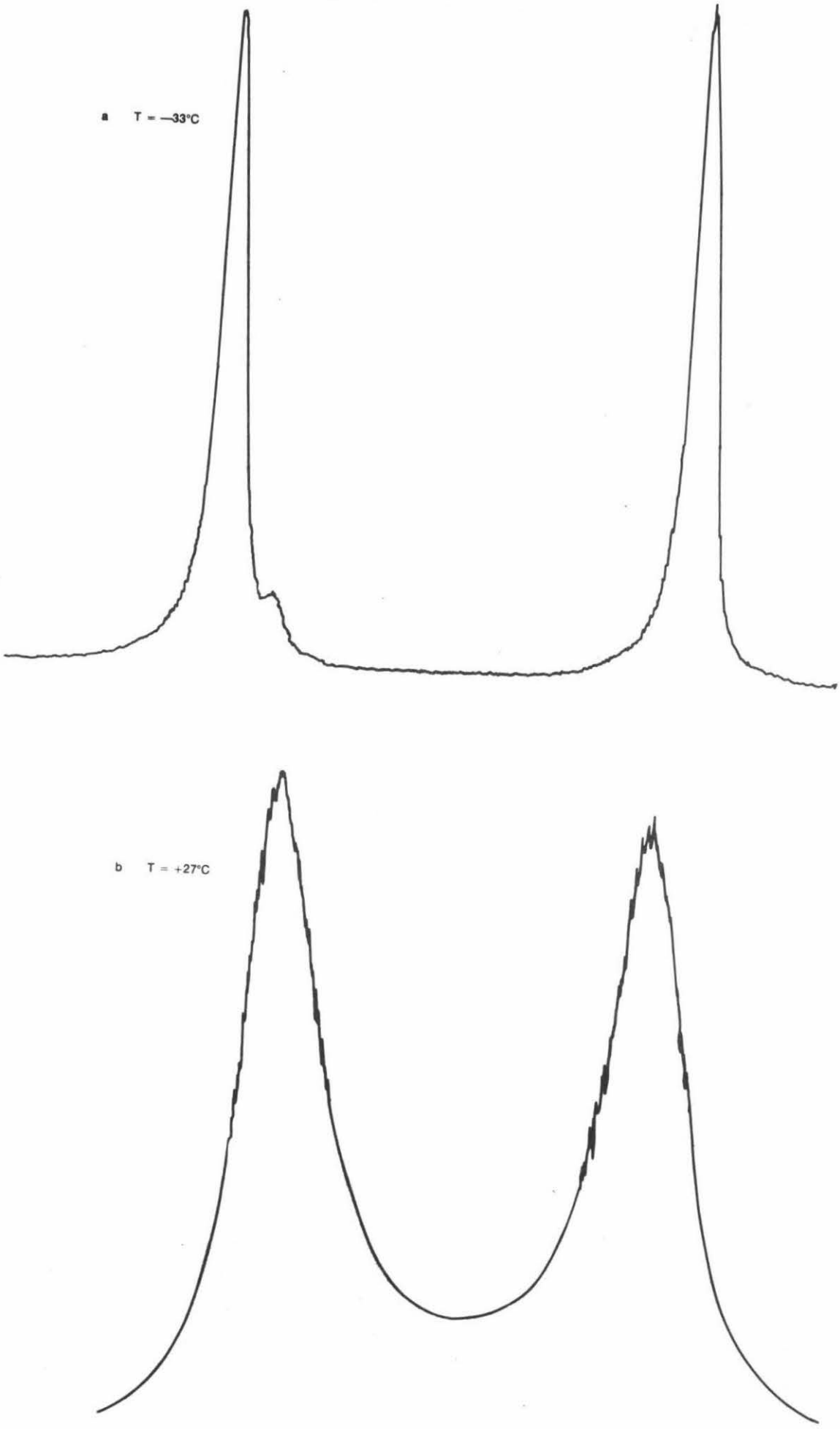

Figure B-3 TTD in pyridine-d_5

a T = 37°C

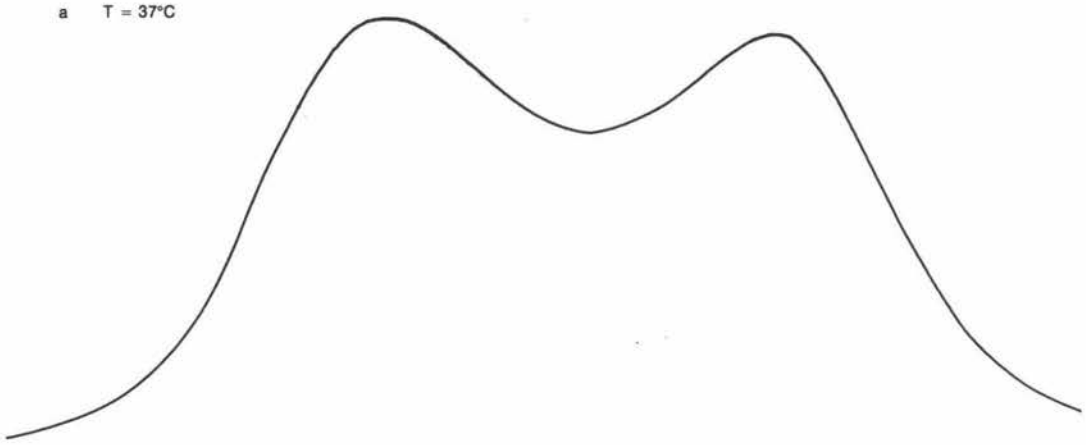

b T = 42°C

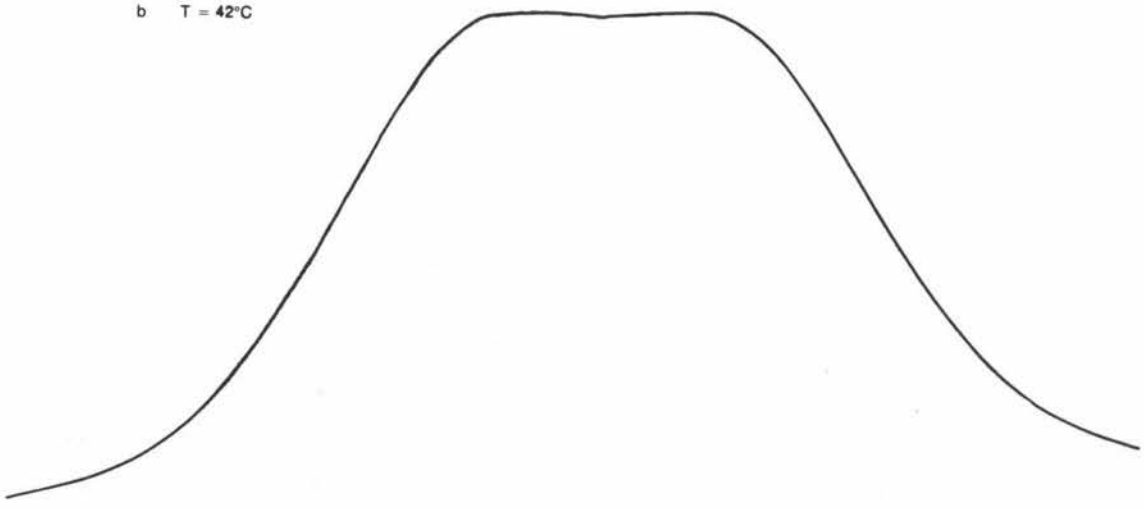

Figure B-4 TTD in pyridine-d_5

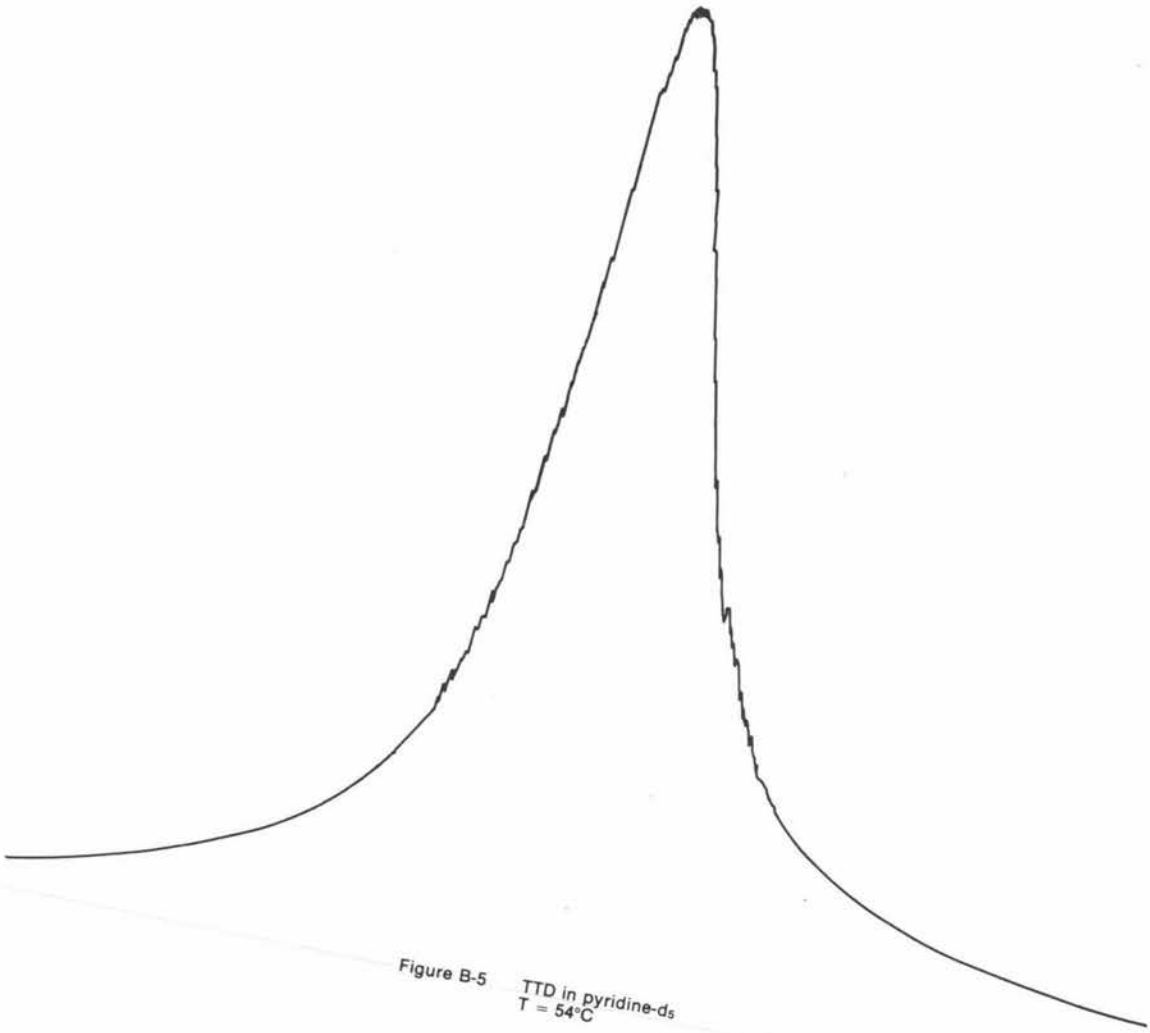

Figure B-5 TTD in pyridine-d_5
$T = 54°C$

APPENDIX C

AN ALTERNATIVE PLOT FROM WHICH TO DETERMINE THE THERMODYNAMIC PARAMETERS

When reporting results for the N,N-dimethylamides, Drakenberg[24] used a variety of the Eyring equation

$$\log_{10}(k/T) = -\Delta G^{\neq}/2.303RT + \log_{10}(k_B/h) \qquad C\text{-}1$$

or $$\log_{10}(k/T) = -\Delta H^{\neq}/2.303RT + \Delta S^{\neq}/2.303R + \log_{10}(k_B/h) \qquad C\text{-}2$$

By plotting $\log_{10}(k/T)$ versus $1/T$ the quantities $\Delta G^{\neq}_{298}$, $\Delta H^{\neq}$ and $\Delta S^{\neq}$ can be found independently of E_a (and without assuming E_a is independent of temperature) and $\log A$. In Table C-1, the kinetic parameters for TTD in chloroform (for the new variables) have been given, together with the regression line for $\log_{10}(k/T)$ versus $(1/T)$, while in Table C-2, the thermodynamic parameters for the two types of plots are compared.

The most interesting point in this comparison is the variation in the value for $\Delta S^{\neq}$. Since this is determined from the intercept when $T = 0$ K, the extrapolation has certainly yielded large errors in $\Delta S^{\neq}$; the noteworthy feature is that the variation, though outside the error limits (which are the standard deviations since random scatter is generally assumed), only involves a factor or two in a very error prone parameter. The remainder of the results are remarkably constant, thus the results reported in Section 3 and Section 4 should be reliable.

Table C-1

Kinetic Parameters for TTD in Chloroform

T	k	T^{-1}	$\log kT^{-1}$
K	s^{-1}	K^{-1}	
288.1	1.042	3.471	-2.435
294.1	2.619	3.400	-2.050
	2.654	3.400	-2.045
300.0	5.24	3.333	-1.758
	5.23	3.333	-1.759
303.7	6.78	3.293	-1.651
310.6	15.24	3.220	-1.309
	14.70	3.220	-1.325
312.2	18.90	3.203	-1.218
315.1	22.86	3.174	-1.139
320.8	44.9	3.117	-0.854

Regression line: $\log_{10}(k/T) = 12.5 - 4.27\ (\pm\ 0.09)(1/T)$

Table C-2

Thermodynamic Parameters for TTD in Chloroform

Method of Analysis	$G^{\neq}_{298}$ kJ mol^{-1}	$H^{\neq}_{298}$ kJ mol^{-1}	$^{\neq}_{298}$ J K^{-1} mol^{-1}
$log_{10}(k/T)$ vs (1/T)	69.6	81.8 ± 1.7	+ 17.7 ± 2.5
$log_{10}k$ vs (1/T)	69.3 ± .2	81.7 ± 1.9	+ 41.5 ± 7.7

BIBLIOGRAPHY

1. Gorter, C.J. and Broer, L.J.F., Physica (Utrecht), 1942, 9, 591.

2. Bloch, F., Hansen, W.W. and Packard, M., Phys. Rev., 1946, 69, 127.

3. Purcell, E.M., Torrey, E.C. and Pound, R.V., Phys. Rev., 1946, 69, 37.

4. Knight, W.D., Phys. Rev., 1949, 76, 1259.

5. Proctor, W.G. and Yu, F.C., Phys. Rev., 1950, 77, 717.

6. Dickinson, W.C., Phys. Rev., 1950, 77, 736.

7. Gutowsky, H.S. and Hoffman, C.J., Phys. Rev., 1950, 80, 110.

8. Hahn, E.L., Phys. Rev., 1950, 80, 50.

9. Gutowsky, H.S. and Saika, A., J. Chem. Phys., 1953, 21, 1688.

10. Lynden-Bell, R.M. and Harris, R.K. "Nuclear Magnetic Resonance Spectroscopy" (Studies in modern chemistry) Nelson, London (1969), Pg. 131-141.

11. Bloch, F., Phys. Rev., 1946, 70, 460.

12. Wangsness, R.K. and Bloch, F., Phys. Rev., 1953, 89, 728.

13. Gutowsky, H.S., McCall, D.W. and Slichter, C.P., J. Chem. Phys., 1953, 21, 279.

14. Gutowsky, H.S. and Holm, C.H., J. Chem. Phys., 1956, 25, 1228.

15. McConnell, H.M. and Berger, S.B., J. Chem. Phys., 1957, 27, 230.

16. Grunwald, E., Loewenstein, A. and Meiboom, S., J. Chem. Phys., 1957, 27, 630, 646.

17. McConnell, H.M., J. Chem. Phys., 1958, 28, 430.

18. Emsley, J.W., Feeney, J. and Sutcliffe, L.H. "High Resolution Nuclear Magnetic Resonance Spectroscopy" Pergamon Press, London (1965), Vol. 1.

19. Rogers, M.T. and Woodbrey, J.C., J. Phys. Chem., 1962, 66, 540.

20. Meiboom, S., Luz, Z. and Gill, D., J. Chem. Phys., 1957, 27, 1411.

21. Sunners, B., Piette, L.H. and Schneider, W.G., Can. J. Chem., 1960, 38, 681.

22. Piette, L.H. and Anderson, W.A., J. Chem. Phys., 1959, 30, 899.

23. Temussi, P.A., Tancredi, T. and Quadrifoglio, F., J. Phys. Chem., 1969, 73, 4227.

24. Drakenberg, T., Dahlqvist, K.-I. and Forsén, S., J. Phys. Chem., 1972, 76, 2178.

25. Johnson, C.S. and Moreland, C.G., J. Chem. Educ., 1973, 50, 477.

26. Buckley, P.D., Jolley, K.W. and Pinder, D.N., Prog. Nucl. Magn. Resonance Spectrosc., 1975, 10, 1.

27. Buckley, P.D., Furness, A.R., Jolley, K.W. and Pinder, D.N., Aust. J. Chem., 1974, 27, 21.

28. Neuman, R.C. and Jonas, V., J. Amer. Chem. Soc., 1968, 90, 1970.

29. Neuman, R.C. and Jonas, V., J. Phys. Chem., 1971, 75, 3532.

30. Reeves, L.W., Shaddick, R.C. and Shaw, K.N., Can. J. Chem., 1971, 49, 3683.

31. Neuman, R.C. and Jonas, V., J. Org. Chem., 1974, 39, 929.

32. Siddall, T.H., Stewart, W.E. and Knight, F.D., J. Phys. Chem., 1970, 74, 3580.

33. Neuman, R.C., Woolfenden, W.R. and Jonas, V., J. Phys. Chem., 1969, 73, 3177.

34. Egan, W., Bull, T.E. and Forsén, S., J. Chem. Soc. Chem. Commun., 1972, 1099.

35. Japan Electron Optics Lab. Co. Ltd., JNM-C-60HL, Nuclear Magnetic Resonance Instrument Instruction Manual (NM 10382-6).

36. Japan Electron Optics Lab. Co. Ltd., JNM-VT-C-60HL, Variable Temperature NMR Detector Instruction Manual (NM-10382-6); JES-VT-3 Temperature Controller Instruction Manual (NM 54722-10).

37. Chemical Rubber Co. Handbook of Chemistry and Physics, 57th Ed., 1976-77.

38. Van Geet, A.L., Anal. Chem., 1968, 40, 2227.

39. Van Geet, A.L., Anal. Chem., 1970, 42, 679.

40. Lemire, A.E. and Thompson, J.C., Can. J. Chem., 1972, 50, 1386.

41. Yoder, C.H., Komoriya, A., Kochanowski, J.E. and Suydam, F.H., J. Amer. Chem. Soc., 1971, 93, 6515.

42. Lemire, A.E. and Thompson, J.C., Can. J. Chem., 1970, 48, 824.

43. Holloway, C.E. and Gitlitz, M.H., Can. J. Chem., 1967, 45, 2659.

44. Wilson, N.K., J. Phys. Chem., 1971, 75, 1067.

45. Thorn, G.C. and Ludwig, R.A. "The Dithiocarbamates and Related Compounds", Elsevier, Amsterdam (1962).

46. Holubec, Z.M. and Jonas, J., J. Amer. Chem. Soc., 1968, 90, 5986.

47. Neuman, R.C., Roark, D.N. and Jonas, V., J. Amer. Chem. Soc., 1967, 89, 3412.

48. Allan, E.A., Hobson, R.F., Reeves, L.W. and Shaw, K.N., J. Amer. Chem. Soc., 1972, 94, 6604.

49. Trotter, C.M. and Jolley, K.W., Aust. J. Chem., 1976, 29, 1623.

50. Furness, A.R., Buckley, P.D. and Jolley, K.W., Aust. J. Chem., 1975, 28, 2303.

51. Griffith, D.L. and Roberts, J.D., J. Amer. Chem. Soc., 1965, 87, 4089.

52. Griffith, D.L., Olson, B.L. and Roberts, J.D., J. Amer. Chem. Soc., 1971, 93, 1648.

53. Jautelat, M., and Roberts, J.D., J. Amer. Chem. Soc., 1969, 91, 642.

54. Inglefield, P.T. and Kaplan, S., Can. J. Chem., 1972, 50, 1594.

55. Leffler, J.E. and Grunwald, E. "Rates and Equilibria of Organic Reactions", Wiley, New York, 1963; Ritchie, C.D. and Sager, W.F., Progr. Phys. Org. Chem., 1964, 2, 323.

56. Kosower, E.M., "Physical Organic Chemistry", Wiley, New York, 1968.

57. Menger, F.M. and Donohue, J.A., J. Amer. Chem. Soc., 1973, 95, 432.

58. Dahlqvist, K.-I., and Forsén, S., J. Phys. Chem., 1969, 73, 4124.

59. Matsuo, T., Shosenji, H. and Miyamoto, R., Bull. Chem. Soc. Japan, 1973, 46, 1437.

60. Furness, A., Thesis, Ph.D., Massey University, 1975.